Allosteric Modulation of Glucocorticoid Receptor Activity through Key Interactions within the Ligand Binding Pocket

A Dissertation Presented for the
Doctor of Philosophy
Degree
The University of Tennessee, Knoxville

Wesley Benjamin Seaton
December 2024

ACKNOWLEDGEMENTS

I want to start by thanking Dr. Shawn Campagna for all that he has done to help me throughout my time at UT. I've been fortunate enough to work on projects I enjoy and develop a wide range of skills while maintaining a healthy work-life balance. I can imagine that not all PIs are as understanding about things like bringing infants/toddlers to group meetings, but in the end, I believe that I have been able to be more productive at work because of this flexibility. He has challenged and inspired me to think critically, and I am sincerely grateful to have had the opportunity to complete my PhD as a member of his lab. I would also like to thank Dr. Elizabeth Fozo for allowing me to collaborate on multiple projects with her and for always being willing to take time to discuss both research and life. Additionally, I want to thank my committee members, Dr. Fozo, Dr. Michael Best, and Dr. Konstantinos Vogiatzis, for their advice, scientific insight, and guidance during my graduate career.

My group members have played a key role in my success over the past five years. I am grateful to several of my other mentors including Dr. Alex Fisch, Dr. Ashley Starck, Dr. Amanda May, and Dr. Hector Castro for training me, working through problems I wasn't sure could be solved, and helping me manage my anxiety at key moments by simply talking through challenges. I know that without all of these people, I could not have grown into the scientist I am today. I am very grateful to the rest of my group members, including Dr. Katarina Jones, Dr. Courtney Christopher, Dr. Brittni Woodall, Lindsay Brown, Zane Vickery, Alex Walls, Maliha Tabassumand, Opeyemi Tade, Imanche Joshua Moses, Qudus Sarumi, Blessing Abiodun, Will Schilletter, Nick Orlando, and Tobi Ogungbe. Katarina and Courtney have both been supportive as I work through analytical projects and try to navigate my career following graduate school. Zane Vickery and Lindsay Brown entered at the same time as me, and the three of us have become good friends since then, sharing in the normal struggles and triumphs of grad school like submitting papers and passing examinations, and well as some not-so-normal challenges, like raising a child while trying to complete your PhD. I'm confident that both of them will find exciting careers that bring them joy. Lastly, I want to thank Opeyemi, Joshua, and Will. I have consistently felt supported by each of them both in

and outside of the lab. They are the kindest and most thoughtful group individuals to work with.

Most importantly, I want to acknowledge and thank my family. My wife Jessica has shared in my highs and lows throughout this program and has been a constant source of reassurance and joy. She has supported me mentally, spiritually, and, upon her own graduation, financially. Neither of us fully understood what this program would entail, but she has been the first to celebrate with me in my achievements and comfort me in trying moments. I must thank my parents for all of their sacrifices and love. In many ways they made this accomplishment possible, and I hope I can continue to make them proud. Finally, I want to thank the real brains behind all of this work, Emma. You are so wonderful.

ABSTRACT

The glucocorticoid receptor (GR) is a transcription factor that influences thousands of genes throughout the body. Activated by steroidal hormones known as glucocorticoids (GCs), the GR-GC complex suppresses inflammation and treats autoimmune diseases and cancer. However, long-term GC use is associated with deleterious effects such as hypertension, osteoporosis, and diabetes. As a result, there is an urgent need for the development of a GC capable of selectively modulating the GR. Unfortunately, much is still unknown regarding how GR conformation is influenced upon ligand binding. To this end, a series of GC analogues were designed, synthesized, and biologically evaluated through testing with both luciferase and gene expression assays. Their resulting activity was explained by docking ligands of interest and probing their impact on GR conformation using molecular dynamic simulations and free-energy calculations. In the first study, **DX1,** an analogue of dexamethasone with a C21 substituted mercaptobenzothiazole moiety, maintained 90% of the anti-inflammatory potential of its parent molecule, while simultaneously exhibiting a reduced toxicity profile. Additionally, **DX4** and **PN4** displayed comparable mRNA expression in the attomolar region to dexamethasone at nanomolar concentrations. Molecular dynamic (MD) simulations revealed that this potency results from the formation of an unoccupied channel near the A-ring of each compound. The flexibility of the GR was further probed in the second study through the systematic derivatization of hydrocortisone. Aryl pyrazole addition to the A-ring alone produced compounds **6** and **7** which both exhibited expression of *Sgk1* mRNA abundance by nearly 20-fold over control each. Furthermore, these compounds were not selective for any other nuclear receptor than the GR, making them unlikely to produce as many side effects. Finally, a GR dimer, comprising DNA binding domains, hinge regions, and ligand binding domains, was constructed *in silico* and docked with a variety of both GR agonists and antagonists. Subsequent MD simulations revealed, for the first time, that agonists consistently produce unique interdomain contacts, while antagonists allosterically drive the dimer complex apart. Together, this research offers enhanced alternatives to current GC therapies and

establishes a platform for more deeply understanding how different ligands influence GR activity.

TABLE OF CONTENTS

LIST OF TABLES

LIST OF FIGURES

INTRODUCTION

The human genome has the remarkable ability to generate over 20,000 proteins, ranging from enzymes that drive biochemical reactions to carrier proteins such as hemoglobin, which transports oxygen throughout the body.[1] Furthermore, individual proteins can have multiple functions, which may be beneficial, harmful or a combination of both for their host.[2] These activates are closely linked with a protein's structure, dynamics, and interactions with ligands.[3] Upon ligand binding, proteins undergo a conformational change which produces chemical signals responsible for dictating their function. Predicting and controlling this conformational change is a challenge that has the potential to improve treatment for a variety of illnesses.

The glucocorticoid receptor (GR) is a multidomain protein first identified in 1966 as the primary receptor responsible for the anti-inflammatory activity induced by cortisone therapy.[4, 5] Rumors during World War II suggested that cortisone may relieve hypoxia in German Luftwaffe pilots which led to a national effort in the United States for its production.[5] While this rumor proved false, Nobel Laureate Dr. Tadeus Reichstein successfully synthesized cortisone's precursor, cortin, and observed that administering it to adrenalectomized animals prolonged their lives. Subsequently, glucocorticoids (GCs), such as cortisone, were shown by co-laureates Drs. Edward Kendall and Philip Hench to be naturally secreted by the cortex of the adrenal gland in response to emotional and physical stress and could be used to treat rheumatoid arthritis.[4] Since this initial discovery, a continually growing number of synthetic GCs have been synthesized. Making up a 10-billion-dollar market annually, GCs are used to treat diseases caused by inflammation like asthma, multiple sclerosis, and Crohn's disease, as well as autoimmune disorders like lupus.[6-8] Despite their beneficial properties, chronic GC use or excess endogenous cortisol production can lead to serious adverse effects such as diabetes and Cushing syndrome.[9-11]

The usefulness of GCs is, in part, a result of the GRs ubiquity throughout the body.[4] Several selective glucocorticoid receptor modulators (SGRMs) have been synthesized in recent years in an effort to bias the GR to induce specific therapeutic activity with diminished side effects. While this has been met with some success, no

SGRMs are currently on the market and many questions remain surrounding how GC ligands influence GR conformation and activity.[12, 13]

The GR is a nuclear receptor (NR) consisting of a highly disordered N-terminal domain (NTD), a DNA binding domain (DBD), and a hinge region (HR) connected to a ligand binding domain (LBD).[14] Biologically, GC agonists act by binding the GR, translocating to the nucleus, and function as either a monomer or dimer complex to transcriptionally activate or repress gene-expression (**Figure 1**).[4] The GC-GR monomer is largely responsible for the anti-inflammatory activity of the system. These monomers inhibit pro-inflammatory cytokines, such as IL-1β, through protein-protein interactions.[15, 16] Furthermore, as a dimer, the GC-GR complex binds to a variety of genomic glucocorticoid binding sequences (GBS) to exert its transactivation (TA) function that's believed to induce insulin resistance.[17] Each half of the dimer's DBD makes contact in a head-to-tail fashion with 5 amino acids in a segment known as the D-loop.[4, 18] A single point mutation (A458T) to this D-loop in mice resulted in diminished TA and inflammation, suggesting that dimerization is not the primary mechanism behind the therapeutic activity of the GR.[19] However, more recent literature has demonstrated that multiple anti-inflammatory genes are upregulated in response to GR action, highlighting the complex nature of this system.[20, 21] Despite this, there is still strong evidence to suggest that a GC agonist capable of selectively modulating the GR to prevent dimerization may result in a steroid with an improved therapeutic profile.

To date, several promising SGRMs have been synthesized.[13] Alternative approaches to increase the efficacy of GCs have focused on increasing the potency of GC agonists in order to access a "dosage window", wherein concentrations are low enough to induce transrepression (TR) but not TA. This unique approach to selectively modulating GR activity has resulted in the production of compounds like deacylcortivazol (DAC) and VSGC12, both of which occupy distinctive hydrophobic cavities within the ligand binding pocket (LBP) of the GR.[22, 23]

By contrast, GR antagonists, such as mifepristone, bind to the same active site and prevent GR signaling.[24, 25] Interestingly, mifepristone, like other GR agonists and

Figure 1 – General mechanism of action for the glucocorticoid receptor in response to agonists and antagonists.

antagonists, not only targets the GR but also interacts with additional NRs, including the progesterone receptor.[11] This lack of specificity among GR ligands is likely responsible for many of the complications associated with GC treatment that cannot be addressed through GR modulation alone. With small modifications to GC ligands resulting in dramatically different selectivity and transcriptional activity, it seems prudent to begin questioning the impact of each ligand on the entire protein conformation. The task of developing a GC with retained anti-inflammatory activity, reduced TA, and high selectivity for the GR over other NRs has so far proved challenging. However, the problem is not hopeless. With the development of new computational, biological, and synthetic tools and methodologies, probing the structure-activity relationship between proteins and ligands is now more accessible than ever before.

OUTLINE OF DISSERTATION

Herein, the LBP of the GR was probed though the derivatization of the most commonly prescribed GCs. In brief, chapter 1 builds upon existing work by synthesizing 24 GC analogues with mercaptobenzothiazole, thiomethyl, and furoyl ester moieties. All compounds were evaluated using a series of biological assays that measure their capacity to induce both transactivation and transrepression. Furthermore, the size of the LBP in response the top compounds was assessed utilizing molecular dynamic simulations. Chapter 2 probes this space through the systematic derivatization of hydrocortisone. Expansion of the A-ring, followed by the addition of the same moieties used in chapter 1, tests the flexible nature of the GR. Additionally, the free-binding energy between the ligands and amino acids within the active site is determined to understand how more nuanced interactions drive activity. Finally, chapter 3 employs AI software to construct a more comprehensive model of the GR and examines how its conformation changes in response to both GR agonists and antagonists.

CHAPTER 1: CHANNEL EXPANSION IN THE LIGAND BINDING DOMAIN OF THE GLUCOCORTICOID RECEPTOR CONTRIBUTES TO THE ACTIVITY OF HIGHLY POTENT GLUCOCORTICOID ANALOGUES

A version of this chapter was originally published by Seaton W. B., et al.:
Seaton, W.B.; Burke, S.J.; Fisch, A.R.; Schilletter, W.A.; Beck, M.G.A.; Cassagne, G.A.; Harvey, I.; Fontenot, M.S.; Collier, J.J.; Campagna, S.R. Channel Expansion in the Ligand-Binding Domain of the Glucocorticoid Receptor Contributes to the Activity of Highly Potent Glucocorticoid Analogues. *Molecules* **2024**, 29, 1546. https://doi.org/10.3390/molecules29071546
Contributions:

Conceptualization, W.B.S., J.J.C. and S.R.C.; methodology, W.B.S., S.J.B., J.J.C. and S.R.C.; validation, W.B.S., S.J.B. and S.R.C.; formal analysis, W.B.S., S.J.B., J.J.C. and S.R.C.; investigation, W.B.S., S.J.B., A.R.F., W.A.S., M.G.A.B., G.A.C., I.H. and M.S.F.; resources, J.J.C. and S.R.C.; writing—original draft preparation, W.B.S. and S.J.B.; writing—review and editing, J.J.C. and S.R.C.; visualization, W.B.S. and S.J.B.; supervision, J.J.C. and S.R.C.; funding acquisition, J.J.C. and S.R.C.

1.1 - ABSTRACT

Glucocorticoids (GCs) act through the glucocorticoid receptor (GR) and are commonly used as anti-inflammatory and immunosuppressant medications. Chronic GC use has been linked with unwanted complications such as steroid-induced diabetes mellitus (SIDM), although the mechanisms for these effects are not completely understood. Modification of six GC parent molecules with 2-mercaptobenzothiazole resulted in consistently less promoter activity in transcriptional activation assays using a 3xGRE reporter construct while constantly reducing inflammatory pathway activity. The most selective candidate, **DX1**, demonstrated a significant reduction (87%) in transactivation compared to commercially available dexamethasone. **DX1** also maintained 90% of the anti-inflammatory potential of dexamethasone while simultaneously displaying a reduced toxicity profile. Additionally, two novel and highly potent compounds, **DX4** and **PN4**, were developed and shown to elicit similar mRNA expression at attomolar concentrations that dexamethasone exhibits at nanomolar dosages. To further explain these results, Molecular Dynamic (MD) simulations were performed to examine structural changes in the ligand binding domain of the glucocorticoid receptor in response to docking with the top ligands. Differing interactions with the transcriptional activation function 2 (AF-2) region of the GR may be responsible for lower transactivation capacity in **DX1**. **DX4** and **PN4** lose contact with Arg611 due to a key interaction changing from a stronger hydrophilic to a weaker hydrophobic one, which leads to the formation of an unoccupied channel at the location of the deacylcortivazol (**DAC)** expanded binding pocket. These findings provide insights into the structure-function relationships important for regulating anti-inflammatory activity, which has implications for clinical utility.

1.2 - INTRODUCTION

Glucocorticoids (GCs) are a class of anti-inflammatory and immunosuppressive steroid ligands that reduce or attenuate the immune response and are thus used to treat various diseases of inflammation.[26] Physiologically, these ligands are synthesized and released from the adrenal cortex and function by binding to the glucocorticoid receptor (GR; NR3C1).[27, 28] Commonly prescribed GCs, such as dexamethasone (**DX**) and

hydrocortisone (**HC**), are used pharmacologically in clinical settings despite their risk to induce cardiovascular diseases, obesity, osteoporosis, and diabetes when used long term.[29] Chronic GC use can lead to steroid-induced diabetes mellitus (SIDM), and therefore discovery of a GC capable of reducing these side effects is highly desired.[29] Around 1.2% of the US population use GCs for approximately 1,600 days.[30] This clinically prescribed chronic steroid use enhances the risk of developing SIDM. For example, 40% of prednisolone-treated renal transplant patients develop post-transplant diabetes mellitus (PTDM).[31] Possible mechanisms for diabetes onset include GCs enhancing the gluconeogenesis pathway in the liver, which increases the synthesis of glucose.[32] Additionally, excess GC promotes insulin resistance in liver, white adipose tissue, and skeletal muscle. Attenuating immunosuppression by limiting GC administration has proven difficult due to an increased risk of graft rejection and thus, GC therapy continues to be one of the best options for transplant patients.[33]

The activated GR-GC complex has two main modes of action after translocating to the nucleus. First, GR homodimers that form following ligand binding selectively associate with glucocorticoid-responsive genomic elements (GREs) in the nucleus and regulate gene transcription through transactivation (TA).[1] Furthermore, TA also induces genes that code for phosphoenolpyruvate carboxykinase (PCK1) which helps maintain glucose homeostasis via gluconeogenesis. [32] The second mode, thought to be responsible for part of the anti-inflammatory activity of GCs is termed transrepression (TR) and results from the interaction of the monomer ligand-bound GR complex with transcription factors (TFs) that normally respond to inflammatory cytokines such as IL-1β.[19] TR can lead to direct anti-inflammatory activity. However, this paradigm is more nuanced as TA of genes such as *Dusp1/Mkp1*, *Rgs2* and *Tsc22d3* have positive therapeutic impact inducing broncho protection and decreased CCL2 expression, respectively.[20, 34, 35]

Despite the structural diversity of commercially available GCs, none are presently capable of dissociating the two modes of transcription. However, a significant effort has been made with the aim of developing such a selective glucocorticoid receptor modulator (SGRM). For example, substitution of the C-21 hydroxyl group on **HC** with 2-mercaptobenzothiazole (MBT) has been shown to reduce impact on islet β-cell insulin

secretion while maintaining anti-inflammatory activity.[36] Interestingly, further modification of this compound through esterification of C-17 with 2-furoyl chloride decreased selectivity due to enhanced TA. This result was expected as furoate ester has proven to dramatically increase potency of several GCs used in treating asthma such as fluticasone furoate (**FF**), mometasone furoate (**MF**), and drug candidates such as VSGC12.[23] Specifically, VSGC12 induced TR activity at one-fourth the concentration of **FF** while reducing insulin resistance. Accessing this "dosage window", wherein concentrations are low enough to induce TR but not TA, is a unique approach to selectively modulate the GR. Thus, a specific combination of these functional groups has the potential to produce a powerful SGRM.

Herein, a total of 24 compounds were synthesized by derivatizing seven common GC scaffolds currently prescribed for human inflammatory conditions. To understand how these structural modifications altered activity, a series of biological assays were performed to evaluate promoter activity, gene expression, and cellular toxicity. Molecular dynamic (MD) simulations and subsequent computational analyses were performed on the top structures to understand their structure-activity relationships (SARs) within the GR ligand-binding domain. Importantly, a highly selective GC, **DX1**, demonstrated a significant reduction (87%) in TA compared to commercially available **DX** while maintaining TR capacity. Furthermore, two novel, highly potent GCs, **DX4** and **PN4** elicited GR activity in the attomolar range similar to that of their parent scaffolds, **DX** and **PN**, at the nanomolar and micromolar ranges, respectively. Possible explanations for their altered activity were provided by molecular docking and dynamic simulations. Collectively, these compounds and their unique modes of action could prove useful in understanding how to improve GC-based therapies.

1.3 – SYNTHETIC METHODS

Compounds **1** – **4** were synthesized with slight modifications to previously published methods (**Figure 1.1**).[36-38] Six different GCs **(Figure 1.1**) were chosen to be derivatized with MBT and both MBT and furoyl to explore how these modifications to the steroidal core impact activity (series **1** and **2**). Unfortunately, addition of furoyl moiety alone proved synthetically difficult due to cleavage of the furoyl moiety upon

Figure 0.1 – (**A**) Starting glucocorticoid structures. (**B**) Synthetic route for benzothiazole analogues **1** and **2**. Reagents and conditions: (i) methanesulfonyl chloride, DIPEA, CH_2Cl_2, 0 °C to rt, 15 h, (ii) 2-mercaptobenzothiazole, K_2CO_3, acetone, reflux, (iii) furoyl chloride, DMAP, CH_2Cl_2, 0 °C to rt. (**C**) Synthetic route for thiomethyl analogues **3** and **4**. Reagents and conditions: (i) diisopropyl azodicarboxylate, PPh_3, thiobenzoic acid, THF, 0 °C to rt, 2.5 h, (ii) 1 N NaOH, iodomethane, MeOH, 3.5 h, (iii) furoyl chloride, DMAP, CH_2Cl_2, 0 °C to rt. (**D**) Synthetic route for desonide and budesonide analogues 1. Reagents and conditions: (i) methanesulfonyl chloride, DIPEA, CH_2Cl_2, 0 °C to rt, 15 h, (ii) 2-mercaptobenzothiazole, K_2CO_3, acetone, reflux.

removal of C-21 protecting groups, which is potentially promoted by the unmasked oxygen on the side chain that is five atoms away from the furoyl ester carbonyl. Therefore, to investigate the impact of furoyl ester alone, a thiomethyl (SMe) group was introduced at C21 on **HC**, **DX**, **BM**, **PN** and **FM**, affording series **3**. Subsequent furoylation of these analogues yielded (series **4**). **DX5** – **DX8** were synthesized with the appropriate mercapto reagent using the same procedure as series **1**. Complete synthetic procedures and characterizations for all compounds can be found in SI, sections 1 and 2.

1.4 – BIOLOGICAL ASSAYS

All in vitro assays were performed using the 832/13 rat insulinoma cell line, which was confirmed to be free of mycoplasma.[39] Cells were cultured in either 12 or 24-well plates, and treated at 80-95% confluence. 832/13 cells were exposed to the steroidal compounds for 24 h at concentrations indicated in the figure legends. Using both 3-(4,5-dimethylthiazol-2-yl)-5-(3-carboxymethoxyphenyl)-2-(4-sulfophenyl)-2H-tetrazolium (MTS) and adenylate kinase (ADK) assays, cell viability was assessed as described previously.[40] The ability of compounds to repress IL-1β mediated increases in pro-inflammatory promoter activity were examined using the previously reported CCL2-promoter luciferase plasmid construct (CCL2-Luc).[20] 832/13 cells were transfected with the CCL2-Luc plasmid. 24 h post-transfection, cells were treated with the concentrations of each compound shown in the figure legends for 1 h, followed by stimulation with 1 ng/mL IL-1β for 4 h. Furthermore, transactivation activity of the synthesized compounds was determined using plasmid constructs containing three copies of a glucocorticoid responsive element (3xGRE-Luc).[36] The 832/13 cells were transfected with the 3xGRE luciferase reporter plasmid. 24 h post-transfection, the cells were exposed to each synthetic compound at the concentrations shown in the figure legends for 4 h. At the end of each respective treatment period, the cells were harvested using passive lysis buffer (Promega, Madison, WI) and luciferase activity measured in a Glomax luminometer (Promega, Madison, WI). Luciferase activity was normalized to total protein to account for differences in cell numbers between experiments. The ability of each compound to suppress transcription induced by IL-1β was also assessed by examining gene expression of *Ccl2* and *Ccl20*, two distinct chemokine genes known to be upregulated in mouse and

human islets exposed to cytokines.[41] 832/13 cells were cultured in 12 well plates and were treated for 1 h with each compound, then stimulated for a further 3 h with 1 ng/mL IL-1β. To investigate expression of GR target genes, 832/13 cells were treated with each compound for 6 h. Cells were lysed with TRI Reagent (Sigma, St. Louis, MO) and RNA extracted, cDNA synthesized, and mRNA expression levels were determined as previously described.[42] Transcript levels were normalized to the housekeeping gene, Ribosomal S9 (*Rs9*). Primer sequences of *Rs9*, *Ccl2*, *Ccl20*, *Rgs2*, and *Sgk1* are available upon request. Parental compounds were purchased from Sigma Aldrich (St. Louis, MO). For low dose experiments, Dexamethasone and Prednisolone were purchased from two vendors (Sigma Aldrich and Selleck Chemicals LLC; Houston, Tx) and an equal number of replicates were performed with compounds from each vendor.

1.5 – COMPUTATIONAL EXPERIMENTS

1.5.1 – MOLECULAR DOCKING AND PDB RATIONAL

Computational experiments and analysis tools were used to probe the interactions between the top 3 ligands, **DX1**, **DX4**, and **PN4** and the GR. Using the GR LBD bound to **FF** (PDB ID: 7prv), molecular docking was performed. This crystal structure was chosen because its native ligand, **FF**, is highly similar to two of the three compounds of interest, **DX4** and **PN4**. **FF**, **DX4** and **PN4** all have three atoms after the C-18 carbonyl, and all possess the furoate ester group branching off C-17. Together, this increased the accuracy of docking results. Furthermore, 7prv is one of the newest crystal structures of the GR and is the first to show the quaternary structure of the GR.[14] The first LBD (LBD1) of this structure was isolated in PyMol (Schrödinger) and used for molecular docking (residues 528-776).[43] Docking was performed using AutoDock Vina (The Scripps Research Institute).[44] Excess water molecules and the starting compound were removed from the GR LBD1 in order to prepare the complex for the docking study. The energy of the ligands was optimized in Chem3D (PerkinElmer) prior to docking between the flexible ligand and the rigid 7prv LBD1 protein. LigPlot+ (European Molecular Biology Laboratory) was used to analyze and compare ligand-residue interactions.[45] This procedure was repeated with **DAC** in its native receptor (PDB ID: 3bqd) and initial docking results of native ligands, **FF** and **DAC**, in LBD1 and 3bqd, respectively,

validated the docking procedure as the ligands maintained their position within the receptor.

1.5.2 – MOLECULAR DYNAMIC SIMULATIONS

Our previous efforts used AutoDock Vina (The Scripps Research Institute) exclusively.[44] However, AutoDock Vina only allows movement of ligand position and atoms inside a static protein. This resulted in relatively weak and potentially unrealistic positioning and low binding affinities of **DX1** due to an inability to accommodate the added steric bulk. Therefore, AutoDock Vina was only used to insert the ligands into the receptor and to calculate binding energies before and after MD simulations, while GROMACS[46] was used to obtain more accurate models. To obtain an optimally positioned ligand within the GR, **DX1**, **DX4**, and **PN4** protein-ligand complexes underwent 100 ns molecular dynamic (MD) simulations using GROMACS software version 2021.5-gcc and CHARMM36 force field.[46, 47] **FF** and **DAC** were also simulated in their native receptors (PDB ID: 7prv and 3bqd, respectively) in order to validate results and draw conclusions. Only LBD1 of 7prv was used for the simulations of synthesized ligands and **FF**. The hinge region (residues 489-527) is unresolved and connectivity between each LBD and DBD of the crystal structure 7prv is based on proximity alone.[14] Between generating force fields for unresolved amino acids, assuming connectivity between domains, and allocating the required amount of computational resources required to simulate the entire structure, we elected to use only this single LBD for analysis. Additionally, full protein changes were out of scope due to interest primarily in the ligand-protein active site and ligand binding pocket (LBP).

Simulations allowed for the evaluation of the various complexes' thermodynamic and structural stability in the presence of salts and solvents. After preparation of the ligand and protein topology, a cubic box was defined as the unit cell and the complex was placed at least 1 nm distance from its edges. The system was solvated with TIP3P water model and Na^+ or Cl^- ions were added to maintain neutrality.[48] Energy minimization was achieved on the system after it was subjected to 50,000 steps and was stopped when a maximum force of 10.0 kJ/mol was achieved. Following this, NVT (amount of substance, volume, and temperature) and NPT (amount of substance, pressure, and temperature)

equilibration were run for 50,000 steps each. Temperature and pressure were kept constant at 300 K and 1 bar, respectively. Finally, a 100 ns MD simulation was performed to optimize the structure of each complex. Stability of the system was analyzed and ensured using time vs RMSD (root-mean square deviation) plots (**Appendix Figure 1.65**). The resulting trajectories were clustered based on the protein active site. This active site was identified as all protein residues within 10 Angstroms of the starting position of each ligand in VMD.[46, 49, 50] Gromos clustering was used based on the RMSD of the C-alpha atoms within the active site and the most central member of the most populated cluster was chosen for 2D analysis in LigPlot+ (European Molecular Biological Laboratory).[45] **FF** was subjected to the same procedure and analysis as the top ligands to validate these methods. The clustered frame of **FF** in 7prv LBD1 retained all hydrogen bonding interactions with Asn564, Gln570, and Arg611, as well as 8 of the 11 hydrophobic interactions described in existing literature.[51] Finally, pocket volume calculations were performed on the clustered frame of each ligand-protein complex using CASTp default parameters and a 1.4 Å radius probe.[52]

1.6 – RESULTS

1.6.1 – BIOLOGICAL EVALUATION

A promoter-luciferase construct containing three copies of the glucocorticoid-response element (3xGRE-Luc) was transfected into 832/13 rat insulinoma cells to assess TA of each compound. Concurrently, the ability of all compounds to repress IL-1β-mediated activation of a promoter luciferase construct containing 3.6kb of the CCL2 promoter (CCL2-Luc), was investigated to determine the TR capability of each compound. pIC_{50} and pEC_{50} values were calculated for all compounds that exhibited a dose-dependent response (**Table 1.1**). The most selective compound, **DX1**, showed only 13% transcriptional activity of the 3xGRE-Luc when compared with **DX** while maintaining 90% of its TR activity (**Table 1.1**). However, furoylation to **DX2** restored 50% TA response in 3xGRE-Luc when compared to **DX**. Repression of IL-1β induced CCL2 promoter activity by **DX2** was virtually unchanged when compared with **DX1**. Diminished TA of the 3xGRE-Luc and greater discrimination between TR and TA was noted across all steroid scaffolds in series **1** (**Figure 1.2B**). For example, at 100 nM **BM**

and **BM1** reduced IL-1β response by 88.7% and 85.7%, respectively (**Figure 1.2C**) while only **BM1** selectively reduced 3xGRE activation by 4.6-fold when compared with **BM** (**Figure 1.2D**). **PN1** displayed similar selectivity but did lose overall potency in the CCL2-Luc assay with only a 75% response at 100 nM. Furoylation reinstated TA potential across all series **2** compounds, giving them similar activity to their parent steroidal compounds (**Figure 1.2E** and **Figure 1.2F**).

The addition of a SMe group to the parent steroids instead of MBT led to analogues in series **3**. These served to illuminate the isolating effects sulfur has on potency in the absence of benzothiazole. Furthermore, the addition of this smaller, less nucleophilic group at C-21 allowed for further investigation into the properties of the furoyl group in series **4**. All SMe analogs in series **3** demonstrated a moderate decrease in anti-inflammatory potential when compared with their parent molecules, and the impact on TA potential was negligible in most cases (**Table 1.1**). For example, **DX3** induced only 84% suppression of the CCL2-Luc when compared with **DX** while maintaining 94% of its TA activity in 3xGRE-Luc. Trends between series **3** and **4** were not as consistent as anticipated based on the activity of compounds from series **1** and **2**. Some compounds were more active in both luciferase assays with **DX4** and **PN4** both inducing more TR and TA when compared with **DX3** and **PN3,** respectively. Specific compounds showed an increase in anti-inflammatory activity and decrease in potential side effects upon furoylation of the SMe derivate. For example, at 0.1nM the CCL2-Luc assays of **PN4** and **DX4** showed a 74% and 81% anti-inflammatory response, respectively, along with a lowering of the pIC_{50} to greater than 10. For comparison, at the same concentration **PN** and **DX** elicited only 13% and 45% response with pIC_{50}'s of 8.4 and 8.3, respectively (**Table 1.1**). Additionally, **PN4** displayed reduced activation with an E_{max} of 5.4 in the 3xGRE-Luc assay compared to **PN** with an E_{max} of 10 (**Table 1.1**).

Intrigued by these results, **DX4** and **PN4** were further diluted to 10^{-18} M (1aM) and tested in both CCL2 and 3xGRE luciferase assays and compared with their parent compounds, **DX** and **PN (Figure 1.3A)**. **DX** and **PN** induced little to no significant

Figure 0.2 – Bioassay data showing relative steroid activity of selected series **1** and **2** compounds. (**A**) Structure of compounds **DX1**, **BM1**, and **PN1**. (**B**) GR-ligand activity in CCL2-Luc (TR) and 3xGRE-Luc (TA) assays as a percent response against dexamethasone at 100 nM for selected compounds. (**C**) CCL2-promoter-luciferase-reporter activity assay (**D**) 3xGRE-promoter-luciferase-reporter activity assay. (**E**) CCL2-promoter-luciferase-reporter activity assay. (**F**) 3xGRE-promoter-luciferase-reporter activity assay.

Table 0.1 – General Biological Analysis of CCL2 (TR) and 3xGRE (TA) Promoter Activity

	CCL2			3xGRE		
Compd	pIC_{50}	E_{max}	[b]%DX	pEC_{50}	E_{max}	[b]%DX
DX	8.3	88.6	100.0	6.8	7.9	100.0
[a]HC1	6.9	77.0	94.0	5.3	1.8	24.6
[a]HC2	6.2	72.8	82.2	7.4	8.2	104.8
HC3	NDR	37.1	41.8	NDR	1.4	17.2
HC4	7.1	78.6	88.7	AAC	3.6	45.9
DX1	7.2	80.0	90.3	NDR	1.0	12.6
DX2	8.3	89.7	101.3	6.7	4.9	62.2
DX3	AAC	75.1	84.7	NDR	7.4	94.4
DX4	AAC	84.7	95.6	AAC	8.9	113.0
BM	8.3	88.7	100.1	9.8	10.3	131.3
BM1	7.2	85.7	96.7	7.2	2.2	28.0
BM2	7.8	83.3	94.0	7.8	4.7	59.9
BM3	8.9	83.5	94.3	7.3	4.8	60.6
BM4	7.2	81.6	92.1	7.5	4.9	62.0
PN	8.4	85.1	96.1	9.4	10.0	127.2
PN1	5.9	75.0	84.7	6.1	2.4	30.5
PN2	AAC	90.9	102.6	8.8	7.5	95.9
PN3	7.1	49.6	56.0	6.6	3.4	43.3
PN4	AAC	80.8	91.2	AAC	5.4	69.2
FM	AAC	90.4	102.1	AAC	10.2	129.5
FM1	7.5	85.9	97.0	8.8	4.8	60.4
FM2	AAC	88.3	99.6	7.9	11.7	149.1
FM3	AAC	82.2	92.8	AAC	5.6	71.6
FM4	AAC	75.9	85.7	AAC	4.9	62.6
DN	8.8	83.2	93.9	AAC	9.6	121.7
DN1	7.9	65.6	74.1	7.0	2.5	31.8
BD	AAC	83.4	94.1	AAC	7.0	88.7
BD1	6.6	57.6	65.0	6.0	2.0	25.3

[a]Selected values taken from previously published work.[36]

[b]Values represented as percentage of maximal response of dexamethasone

AAC = Active at all concentration

NDR = No dose-dependent response

Note: All tabulated raw values and standard deviations are available in SI, sections 4 – 9.

reduction in CCL2 promoter activity at 1aM with 29% and 19% anti-inflammatory activity, respectively (**Figure 1.3B**). By contrast, **DX4** and **PN4** maintained consistently high TR capabilities demonstrating an 82% and 68% reduction at the same concentration. Furthermore, **DX4** and **PN4** displayed high potency as they prompted a 6.7 and 3.8-fold increase in the 3xGRE assay at 1 aM (**Figure 1.3C**). Interestingly, **DX4** and **PN4** didn't exhibit a typical dose-dependent response. When plotting TR and TA promoter activity over the concentrations tested, **DX** and **PN** exhibited a gradual increase in activity that was dependent on the concentration, while **DX4** and **PN4** displayed less dependence on concentration.

GCs can promote cellular toxicity in pancreatic β-cells.[53] To determine the impact on cellular viability during exposure to these compounds, ADK release and MTS reduction was measured as previously described.[40] Release of ADK was measured to determine losses in cellular membrane integrity, and MTS reduction measures cellular respiration activity, which could be taken as an index of proliferation, viability, or both. At 100 nM, nearly all modified GCs displayed a reduced toxicity profile in both assays. For example, **DX** generated a 1.6-fold increase in ADK release while **DX1**, **DX2**, and **DX4** produced 1.25, 1.31, and 1.38 increase, respectively, indicating decreased cytotoxicity compared to **DX** (**Figure 1.4A**). Further, **DX** promoted a 37% reduction in the MTS assay, **DX1**, **DX2**, and **DX4** induced only a 7%, 19%, and 19% reduction, respectively (**Figure 1.4B**). No ADK release was detected for **BM4** when compared with the control vehicle DMSO; note that this is a 60.7% improvement over **BM** toxicity. **BM2** outperformed **BM4** in the MTS assay with only 20.3% reduction against **BM4's** 27.6% reduction (**Figure 1.4B**). Only **HC4** and **FM3** showed potential impacts on viability comparable to the parent scaffolds, and these molecules elicited MTS reduction responses within 2.9% and 8.7% of those measured for the unmodified steroids, respectively (Appendix Table 1.8). Finally, **PN** induced the greatest change of all steroids with a 1.72-fold increase in ADK release and 25.4% MTS reduction. In contrast, the addition of MBT to the **PN** structure (**PN1**) reduced ADK release to 1.25-fold and only decreased MTS reduction by 8.3%. To determine GC impact on GR target genes, relative

Figure 0.3 – Dose-response curve of the transcription activities of GCs. (**A**) Structures of highly potent compounds **DX4** and **PN4** and their respective parent compounds. (**B**) CCL2-promoter-luciferase-reporter activity assay. (**C**) 3xGRE-promoter-luciferase-reporter activity assay.

mRNA levels of *Sgk1* and *Rgs2* were measured. Upregulation of serum and glucocorticoid inducible kinase-1 (*Sgk1*) has been linked to GC-mediated impairment of insulin secretion.[54] At 100 nM concentrations, the expression of *Sgk1* is strongly activated by **DX** in 832/13 cells (7.9-fold). By contrast, **DX1** and **DX2** demonstrated no significant induction of *Sgk1* relative mRNA abundance relative to vehicle control (**Figure 1.5A**). The largest activity change between any analogues and their parent molecule was observed for **BM** and **BM1** with *Sgk1* mRNA abundance in **BM** increased by 8-fold and with no induction of *Sgk1* mRNA abundance observed in response to treatment with **BM1** (**Appendix Table 1.10**). The regulator of G-protein signaling 2 (*Rgs2*) gene encodes the *Rgs2* protein and its increased abundance is linked with cardiac hypertrophy.[34] At a concentration of 100 nM, the relative mRNA abundance of *Rgs2* in response to **DX1** treatment was 2.2% that of **DX** (**Figure 1.5B**) and **DX2** prompted 4.3% of the response seen with **DX**. Of note, the most dissociated compound in this assay was **PN1**, demonstrating no significant induction of *Sgk1* mRNA abundance and only 1.9% of the activity when compared with **PN** increases in *Rgs2* transcript levels (**Figure 1.5C** and **Figure 1.5D**).

DX, **DX4**, **PN**, and **PN4** were diluted to 10^{-18} M and tested for their capacity to induce transcription of *Sgk1* and *Rgs2*. At 1 aM concentrations, **DX4** and **PN4** induced *Sgk1* mRNA abundance by 3.7 and 3.4-fold, respectively (**Figure 1.5E**). Significantly, *Rgs2* mRNA abundance was 6.6-fold greater for **DX4** than for **DX** at 1 aM and nearly 75-fold greater for **PN4** than **PN** (**Figure 0.5F**). Clear dose-dependent responses can once again be observed in both TA assays for **DX** and **PN**, while **DX4** and **PN4** gene expression profiles stay relatively constant at all concentrations tested.

Ccl2 and *Ccl20* are both chemokines responsible for recruiting immune cells to sites of inflammation.[20, 41, 55] The ability of each derivatized compound to repress cytokine-induced expression of the *Ccl2* and *Ccl20* genes was therefore evaluated. The IL-1β mediated increase in *Ccl2* mRNA was diminished by all compounds except **HC3** and **PN1** at 100 nM, with **PN2** having the largest impact with an 87% decrease compared to vehicle control **(Figure 1.6A**). In addition to **PN2**, **HC4** was the only compound to

Figure 0.4 – Toxicity assays of 832/13 cells treated with 100 nM concentrations of GC. (**A**) Adenylate kinase release into culture medium after exposure to indicated GC. (**B**) MTS reduction after exposure to indicated GC.

display increased anti-inflammatory activity compared to its parent molecule at this concentration with a 73% reduction in *Ccl2* expression compared with the 31% decrease observed in response to **HC** (**Figure 1.6C**). **DX4** and **PN4** each decreased *Ccl2* mRNA at 100 nM by 79% (**Figure 1.6E**) while **HC3** was the least effective compound reducing *Ccl2* mRNA by only 14%. Furthermore, the effects of all compounds on *Ccl20* transcript levels were also assessed. The chemokine *Ccl20* is of particular interest due to its known upregulation in non-obese diabetic mice (NOD) [56], a T1D model, and db/db mice, a T2D model.[40, 41] **PN2**, **HC4**, and **BM2** all displayed stronger anti-inflammatory activity than their parent molecules by suppressing *Ccl20* mRNA abundance by 81%, 66%, and 79%, respectively, at 100 nM concentrations (**Figure 1.6B** and **Figure 1.6D**). By contrast, **PN**, **HC**, and **BM** only suppressed *Ccl20* mRNA abundance at the same concentration by 68%, 63%, and 21%, respectively. No analogues of **DX** outperformed their parent compounds (**Figure 1.6F**) and, once again, **HC3** displayed significantly reduced potency with only a 9% decrease in *Ccl20* mRNA levels compared to the vehicle control (**Figure 1.6D**).

1.6.2 – COMPUTATIONAL ANALYSIS

In total, **DX1** displayed 13 hydrophobic and 3 polar interactions. The MBT moiety of **DX1** extended into a region between helix 3 (H3), helix 7 (H7), and helix 10 (H10) of the LBD which is not occupied by **DX** (**Figure 1.7A**). Despite entering this new space, many of the interactions previously reported for crystal structures of **DX** were retained by **DX1**.[57, 58] Indeed, when comparing the amino acid interactions of **DX1** with **DX** (PDB ID: 4udc), 13 out of 16 total interactions were identical (**Figure 1.7B**). Interestingly, **DX1** displayed 3 additional hydrophobic interactions with Met745, Met646, and Leu608. Furthermore, residues of H3, helix 4 (H4), and helix 12 (H12) of the LBD together form a mostly hydrophobic area termed the ligand-dependent transcriptional activation function 2 (AF-2) which has been associated with conformational changes in the GR.[59] Within H3, Asn564 stabilizes the AF-2 domain.[60, 61] This interaction is weakened upon addition of MBT as it changes from polar to hydrophobic which may contribute to the improved selectivity in **DX1**.

Figure 0.5 – 832/13 cells treated with 100 nM concentrations of GCs. (**A**) *Sgk1* and (**B**) *Rgs2* gene expression associated with transactivation after exposure to dexamethasone and its analogues. (**C**) *Sgk1* and (**D**) *Rgs2* gene expression associated with transactivation after exposure to prednisolone and its analogues. Dose-response curve of the transcription activities of highly potent GCs. (**E**) *Sgk1* gene expression. (**F**) *Rgs2* gene expression.

Figure 0.6 – 832/13 cells treated with 100 nM concentrations of GCs. (**A**) *Ccl2* and (**B**) *Ccl20* relative mRNA release into medium in response to **PN**-**PN4** versus DMSO (black bar). (**C**) *Ccl2* and (**D**) *Ccl20* relative mRNA release into medium in response to **HC-HC4**. (**E**) Ccl2 and (**F**) *Ccl20* relative mRNA release into medium in response to **DX**-**DX4**.

Because the present results did not fully explain the selective nature of **DX1**, the presence of the MBT moiety was further probed through the synthesis and biological evaluation of 4 additional dexamethasone analogues (**Figure 1.8**). **DX5** – **DX8** were synthesized utilizing mercaptobenzimidazole (MBI), mercaptobenzoxazole (MBO), mercaptoimidazole (MI), and mercaptothiazole (MT). This slight modification proved to generate a wide range of activity in the 3xGRE-luciferase and CCL2-luciferase assays. To begin, **DX5** – **DX8** all displayed reduced anti-inflammatory activity when compared with **DX** and **DX1**. **DX5** and **DX6** exhibited little selectivity inducing TA with an E_{max} of 3.2 and 4.9, respectively (**Table 1.2**). Interestingly, at lower concentrations **DX7** induced TA preferentially over TR with a pIC_{50} of 7.1 and pEC_{50} of 7.7. **DX8** did display discrimination between modes of activity with 30% transcriptional activity of the 3xGRE-Luc when compared with **DX**. However, overall potency of the compound dropped along with the loss of the benzene ring.

DX4 displayed a total of 13 interactions, all of which were hydrophobic. This resulted in a decrease in binding affinity from -12.2 to -10.2 kcal/mol. **PN4** displayed the exact same interactions but with three additional hydrophobic interactions. The furoyl group present in **FF**, **DX4**, and **PN4** expanded the LBP and occupied the hydrophobic cavity as previously described in literature.[23] Furthermore, the interaction with Asn564 changed from hydrophobic to polar with **PN4**. Two of the most common polar interactions among GCs, the 3-keto group with Arg611 and Gln570, are absent for **DX4** and **PN4**. Arg611 rotates away over time in response to **DX4** and **PN4** and the interaction never returns (**Figure 1.8A** and **Figure 1.8B**). As a result, there is a continuous binding pocket channel formed in response to **DX4** and **PN4** that expands beyond what is typical for **FF** (**Figure 1.8A-C**). Indeed, **FF's** calculated solvent-accessible (SA) pocket volume was ~334 $Å^3$, while **DX4** and **PN4** expanded the pocket's volume to ~484 $Å^3$ and ~546 $Å^3$, respectively. Increased potency associated with this type of binding pocket expansion along with loss of polar contact with Arg611 has been previously observed with agonist deacylcortivazol (**DAC**), which exhibited a calculated SA pocket volume of ~463 $Å^3$

Figure 0.7 – (**A**) Molecular docking experiment with **DX1** inserted into LBD1 of 7prv. (**B**) 2D representations of the ligand–receptor interactions. Red half-circles represent hydrophobic interactions, and the green dotted line represents a hydrogen bond.

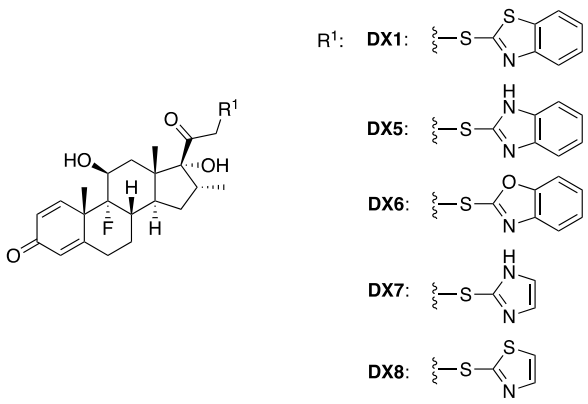

Figure 0.8 – Synthesized analogues of dexamethasone.

Table 0.2 – General Biological Analysis of CCL2 (TR) and 3xGRE (TA) Promoter Activity of DX Analogues

	CCL2			3xGRE		
Compd	pIC_{50}	E_{max}	[b]%DX	pEC_{50}	E_{max}	[b]%DX
DX	8.3	88.6	100.0	6.8	7.9	100.0
DX1	7.2	80.0	90.3	NDR	1.0	12.6
DX5	6.2	67.2	75.8	5.8	3.2	40.5
DX6	7.1	65.0	73.4	7.5	4.9	61.7
DX7	7.1	66.7	75.3	7.7	6.5	82.4
DX8	6.3	54.0	60.9	6.9	2.3	29.5

[a]Values represented as percentage of maximal response of dexamethasone

NDR = No dose-dependent response

(**Figure 1.8D**).[22] The results of these volume calculations are consistent with prior research, although the magnitudes of the pocket volumes are smaller. Differences can be rationalized due to the use of larger radius probes, different software, and lack of manual refinements to the protein structure.

1.7 – DISCUSSION

Glucocorticoids represent a large class of lipophilic steroid molecules frequently used in clinical settings for their anti-inflammatory and immunosuppressive activity.[62] However, their prolonged use leads to a vast array of side effects due to their impact on glucose and lipid homeostasis.[29] A group of MBT-modified glucocorticoids were synthesized and evaluated for their ability to distinguish between TA and TR modes of action. This work reports data for analogues of seven commercially available steroids. All of the MBT compounds, **DX1**, **BM1**, **PN1**, **FM1**, **BD1** and **DN1** displayed greater signs of selectivity with reduced TA activity. The top performing compound, **DX1**, maintained ~90% TR activity of **DX** with only ~13% of the TA activity while simultaneously displaying diminished toxicity in both the MTS and ADK assays.

BM1, **PN1**, **FM1**, **BD1**, and **DN1,** all showed similar, though less profound, distinctions between modes of activity when compared with their parent molecules. Addition of MBT to all parent scaffolds markedly increased their tolerability in both toxicity assays while decreasing their TA potential. Specifically, **PN1** became the second most tolerable compound in the MTS assay and did not induce expression of the *Sgk1* or *Rgs2* genes. Whether a decrease in *Rgs2* mRNA abundance may counteract the therapeutic effects associated with **PN**, such as improved broncho-protection[34], remains to be established. Additionally, the C-16 stereoisomer of **DX1**, **BM1** displayed 96% of the TR activity of **DX** with only ~28% TA, making it a potentially valuable alternative to **DX1**. Interestingly, further modification with a furoyl moiety on all the compounds with a C-17 hydroxyl resulted in decreased discrimination between TA and TR while increasing the TR activity in the CCL2-Luc assays of all compounds, except for **BM2**.

Figure 0.9 – Ligand-binding pocket created in response to GR agonists. Wire represents the protein, and the solid surface represents the ligand-binding pocket area. The red line is placed in the same spot for all structures for scale and reference. (**A**) Ligand-binding pocket and interaction between Arg611 for **DX4** (yellow), (**B**) **PN4** (blue), (**C**) **FF** (purple), and (**D**) **DAC** (green).

The combination of molecular docking and dynamics was used to obtain a more precise picture of ligand-protein interaction between **DX1** and the GR. The MBT moiety expanded into an open region of the GR between H3, H7, and H10 not occupied by **DX**. Despite entering this new space, **DX1** maintained many of the same amino acid interactions as **DX**. However, 2D analysis revealed that **DX1** displayed a hydrophobic interaction with a key amino acid associated with the AF-2 domain, Asn564, while **DX** displays a stronger polar interaction. The weakening of this contact may lower the TA capacity of **DX1** and be partly responsible for changing the ligand activity profile. Further, by synthesizing new analogues and selectively exchanging the various heteroatoms of MBT, as well as removing the benzene ring, we were able to determine that the sulfur in the thiazole ring of **DX1** may help alter modes of action (TA vs TR) while the benzene ring contributes to its anti-inflammatory potential. However, these results would require further testing to prove definitively.

Despite the decrease in efficacy from series **1** to series **2**, the addition of the furoyl moiety increased the efficacy of all compounds when added to series **3** analogues. Specifically, **DX4** and **PN4** displayed the most profound activity as they induced the expression of two separate genes, *Sgk1* and *Rgs2* at attomolar concentrations. To our knowledge, this is the first study to document the uniquely potent transcriptional potential of **DX4** and **PN4**, which, in general, were able to induce the same activity as **DX** at one billion and one million fold lower concentrations, respectively. It is also the first to report a change in the channel formation of the GR LBP in the absence of a bulky group adjacent to the A ring. However, these new findings are supported by previous work that has shown that ligands, such as **DAC**, which expand the binding pocket often show activity greater than endogenous steroidal hormones.[22] For **DX4** and **PN4**, an open channel through the binding pocket near the A ring is observed. This channel, combined with the hydrophobic cavity occupied by the furoyl moiety, allows **DX4** and **PN4** to occupy a greater total volume than both **DAC** and **FF**. Thus, this enhanced agonist activity, combined with a newly proposed mode of action, makes these results potentially useful in developing and designing better GR agonists.

1.8 – CONCLUSION

In summary, all series **1** compounds that were modified with MBT exhibited a decrease in TA with **DX1** showing the most profound selectivity, including retention of ~90% of its anti-inflammatory properties, while reducing transcription of GR target genes, such as *Sgk1*, nearly 8-fold. Series **2** compounds also retained anti-inflammatory activity, but TA potential increased upon furoylation. Finally, while series **3** compounds containing a SMe group lost overall potency, addition of the furoyl moiety in series **4** restored or even increased TR and TA properties at low concentrations for compounds **DX4** and **PN4**.

DX1, DX4, and **PN4** have been identified as anti-inflammatory molecules that have a greater selectivity and increased anti-inflammatory activity when compared with dexamethasone and prednisolone. Additionally, molecular dynamics simulations were performed to determine accurate binding positions of ligands in the GR and revealed an expanded GR LBP in response to **DX4** and **PN4**. Further, this expansion caused an unoccupied channel in the region of the GR LBP similar to that created upon **DAC** binding needed to accommodate the bulk of the arylpyrrazole group. We hypothesize that creation of this channel leads to an overall GR conformation that alters the activity of the protein. Forthcoming *in vivo* studies and further modifications to the various standard of care glucocorticoids will provide a deeper understanding of the mechanism of GC/GR function and improve the understanding of both clinically available anti-inflammatory compounds as well as novel molecules that have improved side effects profiles.

1.9 – METHODS

1.9.1 – MATERIALS

Unless otherwise noted, all reactions were performed in inert atmospheric conditions using dry solvents. All reagents and solvents were obtained from commercial suppliers. ^{1}H NMR and ^{13}C NMR spectra were taken on either a Varian Inova 500 MHz instrument or Bruker 5 mm SmartProbe 500MHz in $CDCl_3$ solutions. Thin-layer chromatography (TLC) was performed with Sorbent Technologies silica G w/UV254 TLC plates. High resolution mass spectrum were performed on an Exactive Plus Orbitrap mass spectrometer with an ESI source operating in positive ionization mode. Specific rotations were taken on a Perkin Elmer 241 Polarimeter and IR were performed on a

Thermo Nicolet IR-1000 FTIR. ^{1}H NMR chemical shifts were recorded in parts per million (ppm). ^{1}H NMR abbreviations are as follows: s = singlet, d = doublet, t = triplet, q = quartet, m = multiplet, dd = doublet of doublets, td = triplet of doublets.

1.9.2 – SYNTHETIC PROCEDURES AND CHARACTERIZATION

General procedure for mercapto derivitization – Steroid (1.34 mmol) was stirred in 25ml of dichloromethane and cooled to 0 ºC. Diisopropylethylamine (DIPEA) (1.3 mL, 10.2 mmol) and mesylchloride (MsCl) (0.16 mL, 2.01 mmol) were then added and the reaction was slowly warmed to room temperature. The reaction was allowed to stir for 15 h until no changed was observed in TLC and then concentrated *in vacuo*. The resulting oil was redissolved in 25 mL DCM and washed with 50 mL saturated bicarbonate. The aqueous layer was extracted with 10 mL DCM. The combined organic layers were washed with brine (25 mL x 2), dried with $MgSO_4$, filtered, and concentrated *in vacuo*. The tan mesylate was carried through crude to the next reaction.

To a solution of steroid mesylate (0.25 g, 0.567 mmol) in acetone (50 mL) was added potassium carbonate (0.784 g, 5.67 mmol) and appropriate mercapto reagent (1.14 mmol) and subjected to reflux for 1 h. The mixture was filtered through a short pad of silica and concentrated *in vacuo*. Purification of the crude product was accomplished using flash chromatography (40% EtOAc in hexanes) to give a white or tan product.

(8S,9R,10S,11S,13S,14S,16R,17R)-17-(2-(benzo[d]thiazol-2-ylthio)acetyl)-9-fluoro-11,17-dihydroxy-10,13,16-trimethyl-6,7,8,9,10,11,12,13,14,15,16,17-dodecahydro-3H-cyclopenta[a]phenanthren-3-one (DX1): white solid obtained in 41% yield; mp 210.7-212 ºC; TLC (Silica G w/UV254) R_f = 0.59, 10:1 CH_2Cl_2:MeOH; $[\alpha]_D^{20}$ = +219.66 (c 0.61, CH_2Cl_2); ^{1}H NMR (500 MHz, $CDCl_3$) δ 7.85 (d, *J* = 8.2 Hz, 1H), 7.73 (d, *J* = 7.9 Hz, 1H), 7.43 (t, *J* = 8.4 Hz, 1H), 7.33 (t, *J* = 8.2 Hz, 1H), 7.21 (s, 1H), 6.34 (d, *J* = 12.1 Hz, 1H), 6.13 (s, 1H), 5.12 (d, *J* = 15.4 Hz, 1H), 4.42 (d, *J* = 7.8 Hz, 1H), 3.31 (d, *J* = 15.4 Hz, 1H), 3.09 – 3.18 (m, 1H), 2.75 (d, *J* = 14.2 Hz, 1H), 2.57 – 2.67 (m, 1H), 2.30 – 2.48 (m, 3H), 2.17 (s, 1H), 1.80 – 1.91 (m, 1H), 1.61 – 1.76 (m, 2H), 1.56 (s, 4H), 1.30 (td, *J* = 8.0, 4.0 Hz, 1H), 1.25 (s, 1H), 1.04 (s, 3H), 0.92 (d, *J* = 7.2 Hz, 3H).;^{13}C NMR (126 MHz, $CDCl_3$) δ 206.02, 186.58, 168.28, 166.14, 152.00, 150.48, 134.31, 129.92, 126.78, 125.23, 121.34, 120.53, 100.78, 99.38, 92.10, 72.48, 48.38,

47.45, 43.65, 37.66, 35.00, 34.40, 32.54, 31.11, 29.29, 27.31, 23.02, 17.27, 15.57; IR (NaCl, thin film) ν_{max} (cm^{-1}): 3344, 2940, 2871, 1658, 1426, 753; HRMS (ESI) m/z: $[M+H]^+$ Calcd for $C_{29}H_{32}FNO_4S_2$, 542.1831; found 542.1833.

(8S,9R,10S,11S,13S,14S,16R,17R)-17-(2-((1H-benzo[d]imidazol-2-yl)thio)acetyl)-9-fluoro-11,17-dihydroxy-10,13,16-trimethyl-6,7,8,9,10,11,12,13,14,15,16,17-dodecahydro-3H-cyclopenta[a]phenanthren-3-one (DX5): white solid obtained in 36.5% yield; mp 181.1-182.1 ºC; TLC (Silica G w/UV254) R_f = 0.37, 10:1 CH_2Cl_2:MeOH; $[\alpha]_D^{20}$ = +94.2 (c 0.54, MeOH); ^{1}H NMR (500 MHz, DMSO) δ 7.41 (s, 1H), 7.33 (d, *J* = 10.2 Hz, 1H), 7.12 (dd, *J* = 6.0, 3.2 Hz, 2H), 6.68 (s, 1H), 6.23 (dd, *J* = 10.1, 2.0 Hz, 1H), 6.02 (s, 1H), 5.40 (d, *J* = 4.9 Hz, 1H), 4.76 (d, *J* = 16.2 Hz, 1H), 4.20 (s, 1H), 3.84 (d, *J* = 16.0 Hz, 1H), 2.91 – 2.99 (m, 1H), 2.63 (td, *J* = 14.0, 6.1 Hz, 1H), 2.31 – 2.44 (m, 3H), 2.18 – 2.26 (m, 1H), 2.08 (s, 1H), 1.76 – 1.84 (m, 1H), 1.64 (t, *J* = 11.8 Hz, 2H), 1.50 (s, 3H), 1.33 – 1.43 (m, 1H), 1.07 – 1.18 (m, 2H), 0.91 (s, 3H), 0.79 (d, *J* = 7.2 Hz, 3H). ^{13}C NMR (126 MHz, DMSO) δ 207.37, 185.78, 167.59, 153.30, 150.92, 129.45, 124.60, 102.44, 101.05, 91.78, 71.16, 70.87, 48.53, 48.35, 47.72, 43.76, 40.59, 40.50, 40.42, 40.33, 40.26, 40.17, 40.09, 40.00, 39.92, 39.83, 39.67, 39.50, 37.22, 36.44, 34.84, 34.13, 33.98, 32.54, 31.16, 30.78, 27.76, 23.48, 23.43, 16.96, 15.87. IR (NaCl, thin film) ν_{max} (cm^{-1}): 3362, 2926, 1655, 1307, 759; HRMS (ESI) m/z: $[M+H]^+$ Calcd for $C_{29}H_{33}FN_2O_4S$, 525.2223; found 525.2213.

(8*S*,9*R*,10*S*,11*S*,13*S*,14*S*,16*R*,17*R*)-17-(2-(benzo[*d*]oxazol-2-ylthio)acetyl)-9-fluoro-11,17-dihydroxy-10,13,16-trimethyl-6,7,8,9,10,11,12,13,14,15,16,17-dodecahydro-3*H*-cyclopenta[*a*]phenanthren-3-one (DX6): white solid obtained in 31% yield; mp 180.9-182.9 ºC; TLC (Silica G w/UV254) R_f = 0.46, 10:1 CH_2Cl_2:MeOH; $[\alpha]_D^{20}$ = +75.3 (c 0.56, CH_2Cl_2); ^{1}H NMR (500 MHz, $CDCl_3$) δ 7.48 (d, *J* = 9.3 Hz, 1H), 7.44 (d, *J* = 7.3 Hz, 1H), 7.27 – 7.30 (m, 2H), 7.20 (d, *J* = 10.2 Hz, 1H), 6.35 (d, *J* = 10.1 Hz, 1H), 6.14 (s, 1H), 5.03 (d, *J* = 15.3 Hz, 1H), 4.43 (d, *J* = 7.6 Hz, 1H), 3.15 (ddd, *J* = 11.0, 7.2, 3.9 Hz, 1H), 3.08 (d, *J* = 15.3 Hz, 1H), 2.78 (d, *J* = 14.0 Hz, 1H), 2.58 – 2.66 (m, 1H), 2.40 – 2.45 (m, 2H), 2.37 (dd, *J* = 16.1, 4.0 Hz, 1H), 1.83 – 1.89 (m, 2H), 1.73 (d, *J* = 12.1 Hz, 1H), 1.63 (dd, *J* = 12.3, 5.4 Hz, 1H), 1.56 (s, 3H), 1.46 (d, *J* = 14.3 Hz, 1H), 1.33 (d, *J* = 4.0 Hz, 2H), 1.04 (s, 3H), 0.93 (d, *J* = 7.1 Hz, 3H). ^{13}C NMR (126 MHz,

$CDCl_3$) δ 206.49, 186.49, 165.87, 165.26, 152.09, 151.69, 140.21, 130.02, 125.23, 124.89, 124.61, 117.77, 110.31, 91.84, 77.26, 77.01, 76.76, 72.50, 72.19, 48.12, 47.39, 43.62, 37.95, 35.02, 34.37, 34.21, 32.55, 31.08, 27.28, 23.04, 17.30, 15.25. IR (NaCl, thin film) ν_{max} (cm^{-1}): 3361, 2927, 1653, 1308, 758; HRMS (ESI) m/z: $[M+H]^+$ Calcd for $C_{29}H_{32}FNO_5S$, 526.2063; found 526.2047.

(8*S*,9*R*,10*S*,11*S*,13*S*,14*S*,16*R*,17*R*)-17-(2-((1*H*-imidazol-2-yl)thio)acetyl)-9-fluoro-11,17-dihydroxy-10,13,16-trimethyl-6,7,8,9,10,11,12,13,14,15,16,17-dodecahydro-3*H*-cyclopenta[*a*]phenanthren-3-one (DX7): white solid obtained in 16.3% yield; mp 240.5-249.0 ºC; TLC (Silica G w/UV254) R_f = 0.34, 10:1 CH_2Cl_2:MeOH; $[\alpha]_D^{20}$ = +82.3 (c 0.55, MeOH); ^{1}H NMR (500 MHz, cd_3od) δ 7.30 – 7.44 (m, 1H), 7.00 (s, 2H), 6.28 (dd, *J* = 10.1, 1.9 Hz, 1H), 6.08 (s, 1H), 4.49 (d, *J* = 16.2 Hz, 1H), 4.25 (d, *J* = 8.9 Hz, 1H), 3.63 (d, *J* = 16.2 Hz, 1H), 3.01 – 3.10 (m, 1H), 2.71 (td, *J* = 14.0, 5.7 Hz, 1H), 2.47 (td, *J* = 12.1, 5.1 Hz, 1H), 2.39 (dt, *J* = 11.9, 3.3 Hz, 3H), 2.25 (td, *J* = 11.9, 8.4 Hz, 1H), 2.15 (s, 1H), 1.88 (dt, *J* = 12.9, 6.0 Hz, 1H), 1.71 (q, *J* = 11.8 Hz, 1H), 1.58 (s, 3H), 1.44 – 1.57 (m, 2H), 1.29 (s, 1H), 1.19 (ddd, *J* = 12.2, 8.1, 4.0 Hz, 1H), 0.95 (s, 3H), 0.82 (d, *J* = 7.2 Hz, 3H). ^{13}C NMR (126 MHz, MeOD) δ 187.64, 169.61, 154.51, 128.40, 123.73, 91.60, 71.66, 71.36, 48.93, 48.74, 48.22, 48.10, 48.05, 47.93, 47.88, 47.76, 47.59, 47.42, 47.25, 47.08, 43.52, 36.29, 34.88, 34.23, 34.07, 32.09, 30.82, 27.40, 22.26, 22.21, 16.04, 14.07. ν_{max} (cm^{-1}): 3361, 2928, 1655, 1306, 757; HRMS (ESI) m/z: $[M+H]^+$ Calcd for $C_{25}H_{31}FN_2O_4S$, 475.2067; found 475.2078.

(8*S*,9*R*,10*S*,11*S*,13*S*,14*S*,16*R*,17*R*)-9-fluoro-11,17-dihydroxy-10,13,16-trimethyl-17-(2-(thiazol-2-ylthio)acetyl)-6,7,8,9,10,11,12,13,14,15,16,17-dodecahydro-3*H*-cyclopenta[*a*]phenanthren-3-one (DX8): white solid obtained in 38.2% yield; ; mp 191.1-191.8 ºC; TLC (Silica G w/UV254) R_f = 0.29, 10:1 CH_2Cl_2:MeOH; $[\alpha]_D^{20}$ = +10.0 (c 0.55, CH_2Cl_2); ^{1}H NMR (500 MHz, $CDCl_3$) δ 7.57 (d, *J* = 3.7 Hz, 1H), 7.27 (s, 1H), 7.21 (d, *J* = 10.1 Hz, 1H), 6.34 (d, *J* = 12.1 Hz, 1H), 6.12 (s, 1H), 5.03 (d, *J* = 15.4 Hz, 1H), 4.41 (d, *J* = 8.2 Hz, 1H), 3.45 (d, *J* = 15.4 Hz, 1H), 3.07 – 3.19 (m, 1H), 2.72 – 2.57 (m, 2H), 2.32 – 2.40 (m, 3H), 1.84 (d, *J* = 6.7 Hz, 1H), 1.70 (d, *J* = 12.1 Hz, 1H), 1.60 (d, *J* = 14.5 Hz, 2H), 1.55 (s, 3H), 1.26 (s, 3H), 1.01 (s, 3H), 0.89 (d, *J* = 7.2 Hz, 3H). ^{13}C NMR (126 MHz, $CDCl_3$) δ 186.51, 165.88, 151.85, 129.95,

125.21, 119.69, 91.79, 77.26, 77.01, 76.76, 72.51, 72.20, 48.32, 48.14, 47.43, 43.72, 37.47, 35.17, 34.41, 34.26, 32.51, 31.06, 29.71, 27.26, 23.03, 22.98, 17.17, 15.06. ν_{max} (cm^{-1}): 3360, 2928, 1655, 1097, 758; HRMS (ESI) m/z: $[M+H]^+$ Calcd for $C_{25}H_{30}FNO_4S_2$, 492.1679; found 492.1665.

(8S,9R,10S,11S,13S,14S,16S,17R)-17-(2-(benzo[d]thiazol-2-ylthio)acetyl)-9-fluoro-11,17-dihydroxy-10,13,16-trimethyl-6,7,8,9,10,11,12,13,14,15,16,17-dodecahydro-3H-cyclopenta[a]phenanthren-3-one (BM1): white solid obtained in 49% yield; mp 202.4-207.8 ºC; TLC (Silica G w/UV254) R_f = 0.52, 10:1 CH_2Cl_2:MeOH; $[\alpha]_D^{20}$ = +80.1 (c 0.8, CH_2Cl_2); ^{1}H NMR (500 MHz, $CDCl_3$) δ 7.73 (dd, *J* = 8.2, 3.9 Hz, 2H), 7.42 (t, *J* = 7.8 Hz, 1H), 7.31 (t, *J* = 7.6 Hz, 1H), 7.20 (d, *J* = 10.1 Hz, 1H), 6.34 (dd, *J* = 10.1, 2.0 Hz, 1H), 6.14 (s, 1H), 4.35 (d, *J* = 9.2 Hz, 1H), 4.21 (d, *J* = 16.4 Hz, 1H), 4.15 (d, *J* = 15.0 Hz, 1H), 2.64 (td, *J* = 13.8, 6.1 Hz, 1H), 2.44 – 2.51 (m, 2H), 2.38 – 2.43 (m, 1H), 2.34 (q, *J* = 8.3 Hz, 1H), 2.26 (td, *J* = 12.3, 6.3 Hz, 1H), 2.17 (s, 1H), 2.09 – 2.16 (m, 1H), 1.89 – 2.94 (m, 1H), 1.67 (td, *J* = 13.3, 5.3 Hz, 1H), 1.56 (s, 3H), 1.40 (d, *J* = 15.4 Hz, 1H), 1.24 – 1.35(m, 1H), 1.20 (s, 3H), 1.15 (d, *J* = 8.4 Hz, 1H), 1.09 (d, *J* = 7.6 Hz, 3H); ^{13}C NMR (126 MHz, $CDCl_3$) δ 186.51, 165.97, 151.96, 129.90, 127.65, 126.08, 125.20, 121.50, 121.12, 119.59, 100.80, 99.39, 90.09, 72.59, 60.40, 48.35, 47.97, 43.37, 37.88, 35.13, 33.95, 33.79, 31.11, 27.54, 23.03, 22.99, 20.00, 17.50, 14.21; IR (NaCl, thin film) ν_{max} (cm^{-1}): 3383, 2933, 2357, 1659, 1428, 889; HRMS (ESI) m/z: $[M+H]^+$ Calcd for $C_{29}H_{32}FNO_4S_2$, 542.1835; found 542.1837.

(8S,9S,10R,11S,13S,14S,17R)-17-(2-(benzo[d]thiazol-2-ylthio)acetyl)-11,17-dihydroxy-10,13-dimethyl-6,7,8,9,10,11,12,13,14,15,16,17-dodecahydro-3H-cyclopenta[a]phenanthren-3-one (PN1): white solid obtained in 38% yield; mp 174.8 – 189.6 ºC; TLC (Silica G w/UV254) R_f = 0.44, 10:1 CH_2Cl_2:MeOH; $[\alpha]_D^{20}$ = +138.84 (c 0.77, CH_2Cl_2); ^{1}H NMR (500 MHz, $CDCl_3$) δ 7.67 – 7.78 (m, 2H), 7.39 (t, *J* = 7.1 Hz, 1H), 7.30 (d, *J* = 7.1 Hz, 1H), 7.27 (s, 1H), 6.27 (d, *J* = 10.0 Hz, 1H), 6.03 (s, 1H), 5.81 (s, 1H), 4.95 (d, *J* = 15.3 Hz, 1H), 4.52 (s, 1H), 3.32 (d, *J* = 15.3 Hz, 1H), 2.81 (t, *J* = 11.6 Hz, 1H), 2.57 (td, *J* = 13.6, 4.6 Hz, 1H), 2.31 – 2.39 (m, 2H), 2.16 (s, 2H), 1.80 – 1.96 (m, 2H), 1.53 – 1.67 (m, 3H), 1.46 (s, 3H), 1.41 – 1.45 (m, 1H), 1.13 – 1.21 (m, 2H), 0.98 (s, 3H); ^{13}C NMR (126 MHz, $CDCl_3$) δ 205.26, 186.66, 170.09, 156.13, 128.10,

127.51, 126.05, 122.67, 122.63, 121.59, 119.96, 90.92, 70.60, 60.54, 55.42, 51.66, 47.31, 44.19, 40.70, 39.85, 35.35, 34.08, 32.21, 31.56, 24.27, 21.29, 17.80, 14.35; IR (NaCl, thin film) ν_{max} (cm^{-1}): 3345, 2936, 2362, 1622, 648; HRMS (ESI) m/z: $[M+H]^+$ Calcd for $C_{28}H_{31}NO_4S_2$, 510.1767; found 510.1774.

(6S,8S,9R,10S,11S,13S,14S,16R,17R)-17-(2-(benzo[d]thiazol-2-ylthio)acetyl)-6,9-difluoro-11,17-dihydroxy-10,13,16-trimethyl-6,7,8,9,10,11,12,13,14,15,16,17-dodecahydro-3H-cyclopenta[a]phenanthren-3-one (FM1): tan solid obtained in 41% yield; mp 210.2-211.8 ºC; TLC (Silica G w/UV254) R_f = 0.59, 10:1 CH_2Cl_2:MeOH; $[\alpha]_D^{20}$ = +138.76 (c 0.51, CH_2Cl_2); ^{1}H NMR (500 MHz, $CDCl_3$) δ 7.79 (d, *J* = 8.2 Hz, 1H), 7.72 (d, *J* = 8.1 Hz, 1H), 7.41 (t, *J* = 7.8 Hz, 1H), 7.29 – 7.35 (m, 1H), 7.13 (d, *J* = 10.4 Hz, 1H), 6.45 (s, 1H), 6.38 (d, *J* = 10.1 Hz, 1H), 5.25 – 5.49 (m, 1H), 5.06 (d, *J* = 15.0 Hz, 1H), 4.44 (d, *J* = 7.7 Hz, 1H), 3.17 (ddd, *J* = 11.0, 7.1, 3.7 Hz, 1H), 3.08 (d, *J* = 15.2 Hz, 1H), 2.81 (d, *J* = 14.5 Hz, 1H), 2.52 – 2.61 (m, 1H), 2.35 – 2.49 (m, 1H), 2.29 (t, *J* = 5.9 Hz, 1H), 1.69 – 1.88 (m, 3H), 1.54 (s, 3H), 1.49 (d, *J* = 13.0 Hz, 1H), 1.33 (s, 1H), 1.25 (s, 1H), 1.03 (s, 3H), 0.91 (d, *J* = 7.1 Hz, 3H); ^{13}C NMR (126 MHz, $CDCl_3$) δ 206.48, 185.61, 167.30, 151.40, 150.51, 134.84, 130.27, 126.50, 124.92, 121.29, 121.08, 120.74, 92.02, 87.40, 87.37, 85.90, 72.24, 71.94, 47.36, 43.29, 37.68, 36.24, 34.88, 33.62, 32.89, 32.35, 23.08, 17.27, 15.56; IR (NaCl, thin film) ν_{max} (cm^{-1}): 3343, 2913, 2363, 1617, 754; HRMS (ESI) m/z: $[M+H]^+$ Calcd for $C_{29}H_{31}F_2NO_4S_2$, 560.1735; found 560.1741.

(6aR,6bS,7S,8aS,8bS,11aR,12aS,12bS)-8b-(2-(benzo[d]thiazol-2-ylthio)acetyl)-7-hydroxy-6a,8a,10,10-tetramethyl-1,2,6a,6b,7,8,8a,8b,11a,12,12a,12b-dodecahydro-4H-naphtho[2',1':4,5]indeno[1,2-d][1,3]dioxol-4-one (DN1): white solid obtained in 32% yield; mp 218.3-230 ºC; TLC (Silica G w/UV254) R_f = 0.54, 10:1 CH_2Cl_2:MeOH; $[\alpha]_D^{20}$ = +118.56 (c 0.84, CH_2Cl_2); ^{1}H NMR (500 MHz, $CDCl_3$) δ 7.86 (d, *J* = 7.2 Hz, 1H), 7.77 (d, *J* = 7.0 Hz, 1H), 7.43 (t, *J* = 7.1 Hz, 1H), 7.34 (t, *J* = 7.0 Hz, 1H), 7.28 (d, *J* = 10.0 Hz, 1H), 6.28 (d, *J* = 10.1 Hz, 1H), 6.03 (s, 1H), 5.04 (d, *J* = 4.6 Hz, 1H), 4.70 (d, *J* = 18.1 Hz, 1H), 4.62 (d, *J* = 18.1 Hz, 1H), 4.55 (s, 1H), 2.51 – 2.59 (m, 1H), 2.33 (d, *J* = 11.2 Hz, 1H), 2.16 (s, 2H), 2.13 (d, *J* = 3.4 Hz, 1H), 2.03 – 2.09 (m, 2H), 1.73 (d, *J* = 7.3 Hz, 1H), 1.56 – 1.63 (m, 2H), 1.46 (s, 6H), 1.22 (s, 3H), 1.14 (t, *J* =

11.7 Hz, 2H), 0.98 (s, 3H); ^{13}C NMR (126 MHz, $CDCl_3$) δ 202.88, 186.59, 156.35, 127.99, 127.88, 126.54, 122.56, 121.55, 119.90, 111.33, 102.24, 98.59, 81.90, 81.18, 70.20, 60.39, 55.33, 50.04, 45.73, 44.17, 39.75, 34.07, 33.97, 31.96, 30.75, 26.59, 25.61, 21.01, 16.80, 14.21; IR (NaCl, thin film) ν_{max} (cm^{-1}): 3383, 2931, 3258, 1654, 755; HRMS (ESI) m/z: $[M+H]^+$ Calcd for $C_{31}H_{35}NO_5S_2$, 566.2029; found 566.2036.

(6aR,6bS,7S,8aS,8bS,12aS,12bS)-8b-(2-(benzo[d]thiazol-2-ylthio)acetyl)-7-hydroxy-6a,8a-dimethyl-10-propyl-1,2,6a,6b,7,8,8a,8b,11a,12,12a,12b-dodecahydro-4H-naphtho[2',1':4,5]indeno[1,2-d][1,3]dioxol-4-one (BD1): white solid obtained in 22% yield; mp 213.5-214.5 ºC; TLC (Silica G w/UV254) R_f = 0.54, 10:1 CH_2Cl_2:MeOH; $[\alpha]_D^{20}$ = +120.16 (c 0.54, CH_2Cl_2); ^{1}H NMR (500 MHz, $CDCl_3$) δ 7.78 (dd, *J* = 22.3, 8.0 Hz, 2H), 7.40 (t, *J* = 7.7 Hz, 1H), 7.30 (t, *J* = 7.6 Hz, 1H), 6.29 (d, *J* = 4.0 Hz, 1H), 6.03 (s, 1H), 5.23 (s, 1H), 4.91 (s, 1H), 4.76 (s, 1H), 4.55 – 4.59 (m, 1H), 4.52 (s, 1H), 4.43 (s, 1H), 2.53 – 2.61 (m, 1H), 2.35 (d, *J* = 10.1 Hz, 1H), 2.04 – 2.24 (m, 4H), 1.73 – 1.86 (m, 2H), 1.68 (q, *J* = 4.0 Hz, 2H), 1.55 – 1.63 (m, 2H), 1.47 (s, 4H), 1.37 – 1.44 (m, 2H), 1.17 (t, *J* = 11.9 Hz, 2H), 1.05 (s, 1H), 1.00 (s, 1H), 0.94 (d, *J* = 11.7 Hz, 3H); ^{13}C NMR (126 MHz, $CDCl_3$) δ 202.58, 201.10, 186.38, 169.38, 155.67, 152.73, 135.63, 128.10, 126.14, 124.53, 122.66, 121.24, 108.52, 104.59, 99.26, 83.31, 70.18, 55.27, 52.89, 49.88, 47.17, 45.89, 43.95, 41.66, 37.23, 35.14, 34.01, 31.88, 31.03, 21.16, 17.55, 14.06. ; IR (NaCl, thin film) ν_{max} (cm^{-1}): 3352, 2931, 1655, 756; HRMS (ESI) m/z: $[M+H]^+$ Calcd for $C_{32}H_{37}NO_5S_2$, 580.2186; found 580.2192.

General procedure for compound 2 and 4 derivitization: Steroid 1 (0.115 g, 0.212 mmol) in 5 mL CH_2Cl_2 was cooled to 0ºC. DMAP (0.065g, 0.531 mmol) and 2-furoyl chloride (0.031g, 0.024 mL, 0.255 mmol) were added and the reaction was warmed to room temperature and allowed to stir for 28 h. The reaction was diluted with 5 mL CH_2Cl_2 and washed with brine (15 mL x 3), dried with $MgSO_4$, filtered, and concentrated *in vacuo*. Purification of the crude product was accomplished using flash chromatography (1% MeOH in CH_2Cl_2) to give a white product.

(8S,9R,10S,11S,13S,14S,16R,17R)-17-(2-(benzo[d]thiazol-2-ylthio)acetyl)-9-fluoro-11-hydroxy-10,13,16-trimethyl-3-oxo-6,7,8,9,10,11,12,13,14,15,16,17-dodecahydro-3H-cyclopenta[a]phenanthren-17-yl furan-2-carboxylate (DX2): white

solid obtained in 70% yield; mp 217.4-224.7ºC; TLC (Silica G w/UV254) R_f = 0.60, 10:1 CH_2Cl_2:MeOH; $[\alpha]_D^{20}$ = +82.78 (c 0.64, CH_2Cl_2); ^{1}H NMR (500 MHz, $CDCl_3$) δ 7.74 – 7.80 (m, 2H), 7.60 (d, *J* = 1.0 Hz, 1H), 7.41 (t, *J* = 7.6 Hz, 1H), 7.31 (t, *J* = 7.6 Hz, 1H), 7.17 – 7.22 (m, 2H), 6.52 (d, *J* = 5.3 Hz, 1H), 6.37 (d, *J* = 10.0 Hz, 1H), 6.16 (s, 1H), 4.44 – 4.60 (m, 3H), 3.52 (s, 1H), 2.63 (t, *J* = 8.3 Hz, 2H), 2.42 (d, *J* = 21.4 Hz, 3H), 1.89 (d, *J* = 12.2 Hz, 3H), 1.66 (dt, *J* = 12.1, 6.3 Hz, 1H), 1.57 (s, 3H), 1.32 – 1.40 (m, 1H), 1.26 (s, 1H), 1.18 (s, 3H), 1.02 (d, *J* = 7.2 Hz, 3H); ^{13}C NMR (126 MHz, $CDCl_3$) δ 186.39, 165.95, 165.67, 158.05, 152.71, 151.68, 147.46, 143.20, 135.61, 130.01, 126.03, 125.25, 124.39, 121.25, 119.47, 112.17, 100.77, 99.37, 72.11, 71.80, 48.62, 47.99, 43.72, 37.27, 36.04, 34.07, 33.91, 33.63, 32.48, 30.91, 27.32, 22.98, 16.84, 16.70; IR (NaCl, thin film) ν_{max} (cm^{-1}): 3419, 2937, 2358, 1662, 757; HRMS (ESI) m/z: $[M+H]^+$ Calcd for $C_{34}H_{34}FNO_6S_2$, 636.1890; found 636.1889.

(8S,9R,10S,11S,13S,14S,16S,17R)-17-(2-(benzo[d]thiazol-2-ylthio)acetyl)-9-fluoro-11-hydroxy-10,13,16-trimethyl-3-oxo-6,7,8,9,10,11,12,13,14,15,16,17-dodecahydro-3H-cyclopenta[a]phenanthren-17-yl furan-2-carboxylate (BM2): white solid obtained in 56% yield; mp 155.4-161.5 ºC; TLC (Silica G w/UV254) R_f = 0.58, 10:1 CH_2Cl_2:MeOH; $[\alpha]_D^{20}$ = +159.0 (c 0.62, CH_2Cl_2); ^{1}H NMR (500 MHz, $CDCl_3$) δ 7.76 (d, *J* = 7.9 Hz, 2H), 7.62 – 7.67 (m, 1H), 7.38 – 7.43 (m, 1H), 7.28 – 7.33 (m, 1H), 7.21 – 7.25 (m, 2H), 6.55 (dd, *J* = 3.5, 1.7 Hz, 1H), 6.39 (d, *J* = 10.1 Hz, 1H), 6.16 (s, 1H), 4.59 (d, *J* = 17.1 Hz, 1H), 4.55 (s, 1H), 4.12 (d, *J* = 17.2 Hz, 1H), 2.77 (d, *J* = 14.3 Hz, 1H), 2.65 (td, *J* = 13.1, 6.1 Hz, 1H), 2.45 – 2.55 (m, 1H), 2.41 (dd, *J* = 13.9, 3.4 Hz, 1H), 2.32 (dt, *J* = 15.3, 7.8 Hz, 1H), 2.18 (dt, *J* = 11.6, 6.0 Hz, 1H), 2.11 (d, *J* = 14.3 Hz, 1H), 1.90 – 2.00 (m, 2H), 1.63 (dd, *J* = 13.0, 4.8 Hz, 1H), 1.58 (s, 3H), 1.41 (d, *J* = 7.5 Hz, 3H), 1.25 (s, 2H), 1.04 (s, 3H; . ^{13}C NMR (126 MHz, $CDCl_3$) δ 186.59, 152.14, 129.84, 126.70, 126.48, 124.99, 122.36, 121.34, 120.42, 91.09, 90.30, 72.24, 68.57, 55.99, 52.09, 48.26, 47.57, 46.78, 43.38, 40.59, 39.19, 38.39, 37.68, 35.13, 33.69, 32.65, 31.50, 30.92, 27.53, 23.85, 23.01, 21.10, 19.98, 17.53; IR (NaCl, thin film) ν_{max} (cm^{-1}): 3382, 2933, 2358, 1717, 757; HRMS (ESI) m/z: $[M+H]^+$ Calcd for $C_{34}H_{34}FNO_6S_2$, 636.1890; found 636.1890.

(8S,9S,10R,11S,13S,14S,17R)-17-(2-(benzo[d]thiazol-2-ylthio)acetyl)-11-hydroxy-10,13-dimethyl-3-oxo-6,7,8,9,10,11,12,13,14,15,16,17-dodecahydro-3H-cyclopenta[a]phenanthren-17-yl furan-2-carboxylate (PN2): white solid obtained in 82% yield; mp 149.3 - 156.9 ºC; TLC (Silica G w/UV254) R_f = 0.56, 10:1 CH_2Cl_2:MeOH; $[\alpha]_D^{20}$ = +115.44 (c 0.56, CH_2Cl_2); ^{1}H NMR (500 MHz, $CDCl_3$) δ 7.75 (dd, *J* = 14.9, 8.1 Hz, 2H), 7.60 (s, 1H), 7.38 (t, *J* = 7.7 Hz, 1H), 7.29 (d, *J* = 13.8 Hz, 2H), 7.22 (d, *J* = 3.5 Hz, 1H), 6.53 (d, *J* = 5.4 Hz, 1H), 6.31 (d, *J* = 10.1 Hz, 1H), 6.04 (s, 1H), 4.57 (d, *J* = 17.1 Hz, 2H), 4.37 (d, *J* = 17.1 Hz, 1H), 2.99 – 3.11 (m, 1H), 2.54 – 2.64 (m, 1H), 2.35 (d, *J* = 13.7 Hz, 2H), 2.18 – 2.25 (m, 1H), 2.09 – 2.18 (m, 1H), 2.06 (s, 1H), 1.95 – 2.02 (m, 1H), 1.79 (td, *J* = 17.9, 8.3 Hz, 2H), 1.67 (s, 1H), 1.50 – 1.56 (m, 1H), 1.48 (s, 3H), 1.13 – 1.20 (m, 2H), 1.10 (s, 3H); ^{13}C NMR (126 MHz, $CDCl_3$) δ 197.51, 186.67, 169.93, 158.28, 156.54, 147.52, 146.19, 143.65, 128.15, 127.88, 126.75, 122.57, 121.58, 119.93, 119.55, 112.33, 96.66, 70.08, 55.41, 55.30, 52.75, 47.33, 44.22, 43.27, 39.20, 34.00, 32.01, 31.92, 31.77, 31.24, 24.34, 20.92, 16.26; IR (NaCl, thin film) ν_{max} (cm^{-1}): 3565, 2935, 2308, 1655, 756; HRMS (ESI) m/z: $[M+H]^+$ Calcd for $C_{33}H_{33}NO_6S_2$, 604.1822; found 604.1823.

(6S,8S,9R,10S,11S,13S,14S,16R,17R)-17-(2-(benzo[d]thiazol-2-ylthio)acetyl)-6,9-difluoro-11-hydroxy-10,13,16-trimethyl-3-oxo-6,7,8,9,10,11,12,13,14,15,16,17-dodecahydro-3H-cyclopenta[a]phenanthren-17-yl furan-2-carboxylate (FM2): white solid obtained in 60.7% yield; mp 231.4-237.0ºC; TLC (Silica G w/UV254) R_f = 0.56, 10:1 CH_2Cl_2:MeOH; $[\alpha]_D^{20}$ = +176.9 (c 0.56, CH_2Cl_2); ^{1}H NMR (500 MHz, $cdcl_3$) δ 7.79 (dd, *J* = 19.7, 8.4 Hz, 2H), 7.61 (d, *J* = 0.9 Hz, 1H), 7.42 (t, *J* = 7.0 Hz, 1H), 7.30 – 7.35 (m, 1H), 7.20 (d, *J* = 3.5 Hz, 1H), 7.12 (d, *J* = 10.3 Hz, 1H), 6.53 (dd, *J* = 3.5, 1.7 Hz, 1H), 6.47 (s, 1H), 6.40 (dd, *J* = 10.1, 1.9 Hz, 1H), 5.41 (ddd, *J* = 48.5, 10.7, 5.7 Hz, 1H), 4.61 (d, *J* = 16.4 Hz, 1H), 4.48 (s, 1H), 3.54 (s, 1H), 2.62 (d, *J* = 16.4 Hz, 1H), 2.47 (d, *J* = 10.5 Hz, 2H), 2.30 – 2.34 (m, 1H), 1.94 (dd, *J* = 22.7, 12.6 Hz, 2H), 1.80 – 1.87 (m, 1H), 1.55 (s, 3H), 1.39 (s, 1H), 1.33 (s, 1H), 1.26 (s, 1H), 1.17 (d, *J* = 11.2 Hz, 3H), 1.03 (d, *J* = 7.1 Hz, 2H), 0.87 – 0.93 (m, 1H); ^{13}C NMR (126 MHz, DMSO) δ 184.90, 166.28, 163.37, 158.03, 152.77, 152.29, 149.11, 143.14, 135.33, 129.65, 126.86, 125.05, 122.35, 121.56, 120.26, 113.18, 101.12, 99.72, 88.00, 86.57, 70.70, 70.42, 48.35, 43.68, 36.08,

35.75, 34.18, 33.31, 32.44, 23.15, 16.97, 16.34.IR (NaCl, thin film) ν_{max} (cm^{-1}): 3382, 2932, 2358, 1716, 757; HRMS (ESI) m/z: $[M+H]^+$ Calcd for $C_{34}H_{33}F_2NO_6S_2$, 654.1790; found 654.1792

General procedure for S-thiobenzoate intermediate: PPh_3 (0.668 g, 2.55 mmol) and diisopropyl-azodicarboxylate (DIAD) (0.5 mL, 2.55 mmol) were stirred in THF (10 mL) at 0ºC for 30 min. A solution of the appropriate steroid (0.5 g, 1.27 mmol) and thiobenzoic acid in THF (5 mL) were then transferred dropwise via cannula and allowed to react for 1 h at 0ºC, followed by an additional hour at room temperature. The reaction was quenched with 30 mL of saturated bicarbonate and the product was extracted with 30 mL ethyl acetate and concentrated *in vacuo*. Purification of the crude product was accomplished using flash chromatography (40% EtOAc in hexanes) to give a white solid.

S-(2-((8S,9S,10R,11S,13S,14S,17R)-11,17-dihydroxy-10,13-dimethyl-3-oxo-2,3,6,7,8,9,10,11,12,13,14,15,16,17-tetradecahydro-1H-cyclopenta[a]phenanthren-17-yl)-2-oxoethyl) benzothioate (HCbz): ^{1}H NMR (500 MHz, $CDCl_3$) δ 7.97 (d, *J* = 8.4 Hz, 2H), 7.60 (t, *J* = 7.5 Hz, 1H), 7.43 – 7.48 (m, 2H), 5.70 (s, 1H), 4.49 (d, *J* = 16.6 Hz, 2H), 3.72 (d, *J* = 16.8 Hz, 1H), 2.97 (s, 1H), 2.87 (s, 1H), 2.45 – 2.55 (m, 2H), 2.37 (dt, *J* = 16.8, 4.2 Hz, 1H), 2.15 – 2.29 (m, 3H), 1.99 – 2.11 (m, 2H), 1.80 – 1.93 (m, 3H), 1.75 (d, *J* = 11.1 Hz, 1H), 1.59 (s, 1H), 1.54 (s, 2H), 1.46 (s, 3H), 1.17 (d, *J* = 12.8 Hz, 1H), 1.08 (d, *J* = 11.1 Hz, 1H), 1.01 (s, 3H); HRMS (ESI) m/z: $[M+H]^+$ Calcd for $C_{28}H_{34}O_5S$, 483.2205; found 483.2203.

S-(2-((8S,9R,10S,11S,13S,14S,16R,17R)-9-fluoro-11,17-dihydroxy-10,13,16-trimethyl-3-oxo-6,7,8,9,10,11,12,13,14,15,16,17-dodecahydro-3H-cyclopenta[a]phenanthren-17-yl)-2-oxoethyl) benzothioate (DXbz): ^{1}H NMR (500 MHz, $CDCl_3$) δ 7.96 (d, *J* = 7.3 Hz, 2H), 7.60 (t, *J* = 7.5 Hz, 1H), 7.40 – 7.51 (m, 2H), 7.20 (d, *J* = 10.1 Hz, 1H), 6.35 (d, *J* = 10.1 Hz, 1H), 6.13 (s, 1H), 4.47 (d, *J* = 16.6 Hz, 1H), 4.42 (d, *J* = 9.5 Hz, 1H), 3.59 (d, *J* = 16.8 Hz, 1H), 3.20 (s, 1H), 3.17 (s, 1H), 2.62 (d, *J* = 13.7 Hz, 2H), 2.29 – 2.44 (m, 3H), 1.82 – 1.88 (m, 1H), 1.71 – 1.80 (m, 1H), 1.65 (d, *J* = 12.2 Hz, 2H), 1.58 (s, 2H), 1.51 (t, *J* = 2.9 Hz, 1H), 1.27 (s, 1H), 1.24 (s, 1H), 1.07

(s, 3H), 0.96 (d, *J* = 7.2 Hz, 3H); HRMS (ESI) m/z: $[M+H]^+$ Calcd for $C_{29}H_{33}FO_5S$, 513.2111; found 513.2108.

S-(2-((8S,9R,10S,11S,13S,14S,16S,17R)-9-fluoro-11,17-dihydroxy-10,13,16-trimethyl-3-oxo-6,7,8,9,10,11,12,13,14,15,16,17-dodecahydro-3H-cyclopenta[a]phenanthren-17-yl)-2-oxoethyl) benzothioate (BMbz): ^{1}H NMR (500 MHz, cdcl$_3$) δ 7.97 (d, *J* = 7.2 Hz, 2H), 7.60 (t, *J* = 7.5 Hz, 1H), 7.43 – 7.49 (m, 2H), 7.23 (d, *J* = 10.0 Hz, 1H), 6.36 (d, *J* = 12.0 Hz, 1H), 6.14 (s, 1H), 4.40 (d, *J* = 11.2 Hz, 1H), 4.12 (d, *J* = 1.0 Hz, 1H), 2.64 (td, *J* = 14.1, 6.5 Hz, 1H), 2.40 (d, *J* = 11.6 Hz, 3H), 2.20 (q, *J* = 7.7 Hz, 1H), 2.06 – 2.14 (m, 2H), 1.87 – 1.93 (m, 2H), 1.58 – 1.68 (m, 3H), 1.26 (t, *J* = 7.1 Hz, 4H), 1.19 (s, 1H), 1.17 (s, 2H), 1.15 (s, 4H); HRMS (ESI) m/z: $[M+H]^+$ Calcd for $C_{29}H_{33}FO_5S$, 513.2111; found 513.2106.

S-(2-((8S,9S,10R,11S,13S,14S,17R)-11,17-dihydroxy-10,13-dimethyl-3-oxo-6,7,8,9,10,11,12,13,14,15,16,17-dodecahydro-3H-cyclopenta[a]phenanthren-17-yl)-2-oxoethyl) benzothioate (PNbz): ^{1}H NMR (500 MHz, cdcl$_3$) δ 7.96 (d, *J* = 7.2 Hz, 2H), 7.60 (t, *J* = 7.5 Hz, 1H), 7.51 – 7.42 (m, 2H), 7.28 (s, 1H), 6.28 (d, *J* = 10.1 Hz, 1H), 6.03 (s, 1H), 4.46 (d, *J* = 16.8 Hz, 1H), 3.74 (d, *J* = 16.8 Hz, 1H), 2.91 (s, 1H), 2.86 (t, *J* = 11.6 Hz, 1H), 2.55 – 2.62 (m, 1H), 2.36 (d, *J* = 10.6 Hz, 1H), 2.24 – 2.10 (m, 3H), 2.04 (s, 1H), 1.84 – 1.91 (m, 1H), 1.78 (dd, *J* = 30.1, 11.8 Hz, 2H), 1.47 (s, 4H), 1.26 (t, *J* = 7.2 Hz, 2H), 1.15 (dd, *J* = 11.2, 3.4 Hz, 2H), 1.02 (s, 3H); Calcd for $C_{28}H_{32}O_5S$, 481.2049; found 481.2042.

S-(2-((6S,8S,9R,10S,11S,13S,14S,16R,17R)-6,9-difluoro-11,17-dihydroxy-10,13,16-trimethyl-3-oxo-6,7,8,9,10,11,12,13,14,15,16,17-dodecahydro-3H-cyclopenta[a]phenanthren-17-yl)-2-oxoethyl) benzothioate (FMbz): ^{1}H NMR (500 MHz, CDCl$_3$) δ 7.95 (d, *J* = 8.6 Hz, 2H), 7.60 (t, *J* = 7.5 Hz, 1H), 7.46 (t, *J* = 7.4 Hz, 2H), 7.13 (d, *J* = 10.1 Hz, 1H), 6.44 (s, 1H), 6.38 (d, *J* = 10.1 Hz, 1H), 5.30 – 5.46 (m, 1H), 4.46 (d, *J* = 16.7 Hz, 1H), 4.42 (ddd, *J* = 9.2, 4.4, 2.3 Hz, 1H), 3.58 (d, *J* = 16.7 Hz, 1H), 3.24 (s, 1H), 2.63 (d, *J* = 14.5 Hz, 1H), 2.37 – 2.52 (m, 2H), 2.26 (d, *J* = 3.9 Hz, 1H), 1.74 – 1.83 (m, 2H), 1.67 (d, *J* = 14.8 Hz, 1H), 1.62 (t, *J* = 2.9 Hz, 1H), 1.59 (s, 2H), 1.30 – 1.33 (m, 1H), 1.27 (s, 1H), 1.24 (s, 1H), 1.06 (s, 3H), 0.97 (d, *J* = 7.2 Hz, 3H); Calcd for $C_{29}H_{32}F_2O_5S$, 531.2017; found 531.2020.

General procedure for compound 3 derivatization: A solution of steroid S-thiobenzoate (0.937 mmol) in MeOH (25 mL) and 1 N NaOH (2.5 mL) was stirred for 30 min at room temperature. Iodomethane (0.319 g, 0.140 mL, 2.25 mmol) was added and the reaction proceeded for 3 h at room temperature. The reaction was quenched with water (50 mL) and the product was extracted with ethyl acetate. Purification of the crude product was accomplished using flash chromatography (40% EtOAc in hexanes) to give a white product.

(8S,9S,10R,11S,13S,14S,17R)-11,17-dihydroxy-10,13-dimethyl-17-(2-(methylthio)acetyl)-1,2,6,7,8,9,10,11,12,13,14,15,16,17-tetradecahydro-3H-cyclopenta[a]phenanthren-3-one (HC3): white solid obtained in 33% yield; mp 226.6 - 231.3 ºC; TLC (Silica G w/UV254) R_f = 0.52, 10:1 CH_2Cl_2:MeOH; $[\alpha]_D^{20}$ = +122.06 (c 0.89, CH_2Cl_2); ^{1}H NMR (500 MHz, $CDCl_3$) δ 5.69 (s, 1H), 4.47 (s, 1H), 3.49 (d, *J* = 13.6 Hz, 1H), 3.28 (d, *J* = 13.6 Hz, 1H), 2.73 (t, *J* = 11.7 Hz, 1H), 2.42 – 2.51 (m, 2H), 2.36 (dt, *J* = 16.8, 4.3 Hz, 1H), 2.25 (d, *J* = 17.4 Hz, 1H), 2.19 (s, 1H), 2.16 (t, *J* = 4.5 Hz, 1H), 2.12 (s, 2H), 2.05 (d, *J* = 14.2 Hz, 3H), 1.86 (td, *J* = 13.4, 4.3 Hz, 2H), 1.80 – 1.72 (m, 1H), 1.64 – 1.53 (m, 3H), 1.49 (d, *J* = 11.8 Hz, 1H), 1.44 (s, 3H), 1.25 (s, 1H), 1.14 (d, *J* = 9.3 Hz, 1H), 1.04 (d, *J* = 11.1 Hz, 1H), 0.99 (d, *J* = 17.5 Hz, 3H); ^{13}C NMR (126 MHz, $CDCl_3$) δ 206.13, 199.39, 171.87, 122.44, 89.57, 68.49, 56.00, 51.59, 48.06, 39.95, 39.74, 39.21, 35.05, 34.81, 33.81, 32.72, 32.07, 31.43, 24.00, 21.05, 17.91, 15.80; IR (NaCl, thin film) ν_{max} (cm^{-1}): 3430, 2933, 2360, 1664, 1298, 760; HRMS (ESI) m/z: $[M+H]^+$ Calcd for $C_{22}H_{32}O_4S$, 393.2094; found 393.2097.

(8S,9R,10S,11S,13S,14S,16R,17R)-9-fluoro-11,17-dihydroxy-10,13,16-trimethyl-17-(2-(methylthio)acetyl)-6,7,8,9,10,11,12,13,14,15,16,17-dodecahydro-3H-cyclopenta[a]phenanthren-3-one (DX3): white solid obtained in 65.1% yield; mp 194.8 - 198.3 ºC; TLC (Silica G w/UV254) R_f = 0.52, 10:1 CH_2Cl_2:MeOH; $[\alpha]_D^{20}$ = +128.40 (c 1, CH_2Cl_2); ^{1}H NMR (500 MHz, $CDCl_3$) δ 7.18 (d, *J* = 10.1 Hz, 1H), 6.34 (d, *J* = 8.2 Hz, 1H), 6.13 (s, 1H), 4.36 (d, *J* = 7.6 Hz, 1H), 3.55 (d, *J* = 12.8 Hz, 1H), 3.07 (s, 1H), 3.03 (d, *J* = 12.7 Hz, 1H), 2.49 – 2.65 (m, 2H), 2.28 – 2.41 (m, 3H), 2.16 (d, *J* = 12.4 Hz, 1H), 2.09 (s, 2H), 1.81 (d, *J* = 11.1 Hz, 1H), 1.75 (d, *J* = 10.8 Hz, 1H), 1.57 (d, *J* = 12.4 Hz, 2H), 1.54 (s, 4H), 1.36 (d, *J* = 16.6 Hz, 1H), 1.23 – 1.27 (m, 1H), 1.06 (d, *J* = 8.1 Hz,

3H), 0.92 (d, J = 7.2 Hz, 3H); ^{13}C NMR (126 MHz, $CDCl_3$) δ 205.40, 186.48, 165.85, 151.76, 129.97, 125.21, 100.75, 91.34, 72.14, 62.54, 48.69, 43.86, 39.06, 37.33, 36.05, 34.21, 32.39, 31.05, 27.32, 22.95, 17.42, 15.56, 14.59; IR (NaCl, thin film) ν_{max} (cm^{-1}): 3454, 2939, 1660, 1239, 891; HRMS (ESI) m/z: $[M+H]^+$ Calcd for $C_{23}H_{31}FO_4S$, 423.2000; found 423.2002.

(8S,9R,10S,11S,13S,14S,16S,17R)-9-fluoro-11,17-dihydroxy-10,13,16-trimethyl-17-(2-(methylthio)acetyl)-6,7,8,9,10,11,12,13,14,15,16,17-dodecahydro-3H-cyclopenta[a]phenanthren-3-one (BM3): white solid obtained in 24.4% yield; mp 186.2 - 191.5ºC; TLC (Silica G w/UV254) R_f = 0.46, 10:1 CH_2Cl_2:MeOH; $[\alpha]_D^{20}$ = + 106.47 (c 0.77, CH_2Cl_2); ^{1}H NMR (500 MHz, $CDCl_3$) δ 7.17 (d, J = 10.1 Hz, 1H), 6.33 (d, J = 9.0 Hz, 1H), 6.12 (s, 1H), 4.38 (d, J = 14.0 Hz, 1H), 3.32 (dd, J = 118.5, 12.7 Hz, 1H), 2.80 (d, J = 13.7 Hz, 1H), 2.63 (t, J = 13.6 Hz, 1H), 2.32 – 2.55 (m, 3H), 2.18 (s, 2H), 1.99 – 2.13 (m, 3H), 1.91 (s, 2H), 1.66 (dd, J = 22.2, 11.1 Hz, 2H), 1.55 (t, J = 12.5 Hz, 5H), 1.42 (dd, J = 33.0, 14.5 Hz, 1H), 1.28 (d, J = 25.6 Hz, 2H), 1.16 (s, 1H), 1.13 (d, J = 6.9 Hz, 3H); ^{13}C NMR (126 MHz, $CDCl_3$) δ 205.36, 186.54, 165.99, 151.95, 129.89, 125.18, 89.63, 72.53, 49.30, 48.97, 48.34, 45.32, 43.56, 41.30, 37.74, 34.99, 33.98, 31.08, 27.59, 22.95, 19.96, 17.64, 15.63; IR (NaCl, thin film) ν_{max} (cm^{-1}): 3384, 2932, 1658, 1051, 703; HRMS (ESI) m/z: $[M+H]^+$ Calcd for $C_{23}H_{31}FO_4S$, 423.2000; found 423.2001.

(8S,9S,10R,11S,13S,14S,17R)-11,17-dihydroxy-10,13-dimethyl-17-(2-(methylthio)acetyl)-6,7,8,9,10,11,12,13,14,15,16,17-dodecahydro-3H-cyclopenta[a]phenanthren-3-one (PN3): white solid obtained in 42% yield; mp 232.9 – 233.0ºC; TLC (Silica G w/UV254) R_f = 0.46, 10:1 CH_2Cl_2:MeOH; $[\alpha]_D^{20}$ = +98.83 (c 0.83, CH_2Cl_2); ^{1}H NMR (500 MHz, $CDCl_3$) δ 7.24 (d, J = 10.1 Hz, 1H), 6.27 (d, J = 10.1 Hz, 1H), 6.02 (s, 1H), 4.49 (s, 1H), 3.39 – 3.53 (m, 1H), 3.27 (d, J = 13.6 Hz, 1H), 2.72 (ddd, J = 14.6, 11.3, 3.1 Hz, 1H), 2.61 – 2.53 (m, 1H), 2.34 (d, J = 11.6 Hz, 1H), 2.18 (d, J = 8.7 Hz, 1H), 2.12 (s, 2H), 1.81 – 1.87 (m, 1H), 1.72 (t, J = 11.2 Hz, 1H), 1.53 – 1.62 (m, 3H), 1.45 (s, 3H), 1.26 (s, 2H), 1.08 – 1.15 (m, 2H), 1.02 (s, 2H), 0.99 (s, 1H), 0.85 (s, 3H); ^{13}C NMR (126 MHz, $CDCl_3$) δ 186.46, 169.70, 155.84, 128.00, 122.53, 89.52, 77.22, 70.37, 55.27, 51.00, 48.26, 44.00, 39.94, 39.70, 34.82, 33.96, 32.01, 31.28, 24.22,

21.13, 17.82, 15.78; HRMS (ESI) m/z: $[M+H]^+$ Calcd for $C_{22}H_{30}O_4S$, 391.1936; found 391.1933.

(6S,8S,9R,10S,11S,13S,14S,16R,17R)-6,9-difluoro-11,17-dihydroxy-10,13,16-trimethyl-17-(2-(methylthio)acetyl)-6,7,8,9,10,11,12,13,14,15,16,17-dodecahydro-3H-cyclopenta[a]phenanthren-3-one (FM3): tan solid obtained in 45.9% yield; mp 142.9-155.2; TLC (Silica G w/UV254) R_f = 0.56, 10:1 CH_2Cl_2:MeOH; $[\alpha]_D^{20}$ = + 138.84 (c 0.41, CH_2Cl_2); ^{1}H NMR (500 MHz, $CDCl_3$) δ 7.10 (d, *J* = 10.1 Hz, 1H), 6.42 (s, 1H), 6.36 (d, *J* = 10.2 Hz, 1H), 5.37 (ddd, *J* = 48.7, 11.7, 6.6 Hz, 1H), 4.38 (s, 1H), 3.54 (d, *J* = 12.7 Hz, 1H), 3.06 – 3.19 (m, 1H), 2.70 – 3.05 (m, 1H), 2.49 – 2.60 (m, 1H), 2.41 (s, 2H), 2.27 (s, 1H), 2.11 (d, *J* = 29.9 Hz, 2H), 1.67 – 1.86 (m, 2H), 1.54 (d, *J* = 15.7 Hz, 4H), 1.31 – 1.44 (m, 2H), 1.27 (d, *J* = 6.3 Hz, 2H), 1.02 – 1.12 (m, 3H), 0.86 – 1.01 (m, 3H); ^{13}C NMR (126 MHz, $CDCl_3$) δ 205.14, 196.90, 185.52, 150.34, 130.32, 121.26, 91.23, 87.31, 85.84, 71.93, 62.47, 48.68, 43.57, 38.97, 37.16, 36.04, 33.81, 32.83, 32.25, 23.07, 17.35, 15.54, 14.54; HRMS (ESI) m/z: $[M+H]^+$ Calcd for $C_{23}H_{30}F_2O_4S$, 441.1906; found 441.1909.

General procedure for compound 4 derivatization: same as compound 2.

(8S,9S,10R,11S,13S,14S,17R)-11-hydroxy-10,13-dimethyl-17-(2-(methylthio)acetyl)-3-oxo-2,3,6,7,8,9,10,11,12,13,14,15,16,17-tetradecahydro-1H-cyclopenta[a]45henanthrene-17-yl furan-2-carboxylate (HC4): white solid obtained in 12.2% yield; mp 152.5-160.8ºC; TLC (Silica G w/UV254) R_f = 0.57, 10:1 CH_2Cl_2:MeOH; $[\alpha]_D^{20}$ = + 81.02 (c 0.54, CH_2Cl_2); ^{1}H NMR (500 MHz, cdcl$_3$) δ 7.62 (t, *J* = 6.4 Hz, 1H), 7.09 – 7.24 (m, 1H), 6.55 (d, *J* = 7.1 Hz, 1H), 5.72 (d, *J* = 7.7 Hz, 1H), 4.54 (s, 1H) 3.37 – 3.54 (m, 1H), 3.31 (s, 1H), 2.99 – 3.16 (m, 1H), 2.76 (s, 1H), 2.47 – 2.56 (m, 2H), 2.31 – 2.43 (m, 2H), 2.23 (d, *J* = 22.3 Hz, 3H), 2.09 (d, *J* = 22.0 Hz, 4H), 1.92 (dd, *J* = 27.1, 10.6 Hz, 3H), 1.79 (d, *J* = 7.8 Hz, 1H), 1.46 (s, 3H), 1.30 (d, *J* = 11.1 Hz, 2H), 1.10 (d, *J* = 11.4 Hz, 1H), 1.05 (s, 2H), 0.92 (d, *J* = 22.1 Hz, 2H); ^{13}C NMR (126 MHz, cdcl$_3$) δ 199.37, 171.69, 157.92, 147.03, 122.49, 119.10, 118.35, 112.12, 96.53, 70.12, 68.25, 55.99, 54.93, 52.94, 47.09, 40.51, 39.22, 35.02, 33.84, 32.62, 32.39, 31.96, 31.49, 30.87, 23.80, 20.98, 17.01; IR (NaCl, thin film) ν_{max} (cm^{-1}): 3482, 2928,

1661, 1300, 761 ; HRMS (ESI) m/z: $[M+H]^+$ Calcd for $C_{27}H_{34}O_6S$, 487.2149; found 487.2156.

(8S,9R,10S,11S,13S,14S,16R,17R)-9-fluoro-11-hydroxy-10,13,16-trimethyl-17-(2-(methylthio)acetyl)-3-oxo-6,7,8,9,10,11,12,13,14,15,16,17-dodecahydro-3H-cyclopenta[a]phenanthren-17-yl furan-2-carboxylate (DX4): white solid obtained in 22.9% yield; mp 158.3-165.3ºC; TLC (Silica G w/UV254) R_f = 0.55, 10:1 CH_2Cl_2:MeOH; $[\alpha]_D^{20}$ = + 36.05 (c 0.46, CH_2Cl_2); ^{1}H NMR (500 MHz, $CDCl_3$) δ 7.60 (d, *J* = 9.9 Hz, 1H), 7.17 (d, *J* = 14.3 Hz, 2H), 6.51 (s, 1H), 6.37 (d, *J* = 10.2 Hz, 1H), 6.16 (s, 1H), 5.71 (d, *J* = 84.1 Hz, 1H), 4.45 (s, 1H), 3.97 – 3.54 (m, 1H), 3.51 – 3.29 (m, 1H), 2.71 – 2.52 (m, 2H), 2.49 – 2.35 (m, 3H), 2.32 – 2.21 (m, 2H), 1.85 (dd, *J* = 22.2, 11.5 Hz, 2H), 1.60 (s, 2H), 1.56 (s, 4H), 1.32 (s, 1H), 1.25 (d, *J* = 6.3 Hz, 3H), 1.18 (s, 1H), 1.10 (t, *J* = 7.8 Hz, 1H), 1.00 (dd, *J* = 24.4, 6.6 Hz, 2H), 0.94 – 0.85 (m, 1H); ^{13}C NMR (126 MHz, $CDCl_3$) δ 186.50, 165.80, 158.05, 151.76, 147.54, 143.52, 130.21, 125.43, 119.32, 112.31, 72.38, 72.06, 60.54, 48.65, 43.95, 37.31, 35.98, 34.30, 34.15, 33.58, 31.11, 27.50, 23.17, 23.12, 21.19, 17.03, 16.56, 14.35; IR (NaCl, thin film) ν_{max} (cm^{-1}): 3392, 2934, 2359, 1660, 1301, 758; HRMS (ESI) m/z: $[M+H]^+$ Calcd for $C_{28}H_{33}FO_6S$, 517.2055; found 517.2058.

(8S,9R,10S,11S,13S,14S,16R,17R)-9-fluoro-11-hydroxy-10,13,16-trimethyl-17-(2-(methylthio)acetyl)-3-oxo-6,7,8,9,10,11,12,13,14,15,16,17-dodecahydro-3H-cyclopenta[a]phenanthren-17-yl furan-2-carboxylate (BM4): white solid obtained in 35.9% yield; mp 203.5-211; TLC (Silica G w/UV254) R_f = 0.54, 10:1 CH_2Cl_2:MeOH; $[\alpha]_D^{20}$ = + 44.98 (c 1.1, CH_2Cl_2); ^{1}H NMR (500 MHz, $CDCl_3$) δ 7.63 (s, 1H), 7.21 (s, 1H), 6.89 (d, *J* = 10.4 Hz, 1H), 6.55 (s, 1H), 6.33 (d, *J* = 10.2 Hz, 1H), 6.14 (s, 1H), 6.03 (d, *J* = 27.2 Hz, 1H), 5.63 (s, 1H), 3.43 (d, *J* = 12.5 Hz, 1H), 3.07 (d, *J* = 12.5 Hz, 1H), 2.61 (d, *J* = 9.5 Hz, 1H), 2.44 (d, *J* = 8.7 Hz, 3H), 2.16 (s, 2H), 2.10 (t, *J* = 6.8 Hz, 1H), 2.07 (s, 1H), 1.94 (d, *J* = 7.0 Hz, 1H), 1.70 – 1.59 (m, 2H), 1.54 (s, 3H), 1.41 (d, *J* = 7.5 Hz, 3H), 1.26 (s, 2H), 1.19 (s, 1H), 1.16 (d, *J* = 6.7 Hz, 1H), 1.12 (d, *J* = 7.0 Hz, 1H), 1.08 (s, 1H), 1.03 (s, 1H); ^{13}C NMR (126 MHz, $CDCl_3$) δ 205.01, 185.97, 164.44, 156.60, 150.15, 147.33, 144.07, 130.52, 125.49, 119.20, 112.22, 89.42, 72.46, 72.12, 49.55, 48.66, 47.37, 43.20, 41.24, 34.93, 33.58, 31.10, 27.52, 23.11, 19.93, 17.31, 15.93, 15.52;

IR (NaCl, thin film) ν_{max} (cm^{-1}): 3384, 2933, 2359, 1700, 1295, 757; HRMS (ESI) m/z: $[M+H]^+$ Calcd for $C_{28}H_{33}FO_6S$, 517.2055; found 517.2061.

(8S,9S,10R,11S,13S,14S,17R)-11-hydroxy-10,13-dimethyl-17-(2-(methylthio)acetyl)-3-oxo-6,7,8,9,10,11,12,13,14,15,16,17-dodecahydro-3H-cyclopenta[a]phenanthren-17-yl furan-2-carboxylate (PN4): white solid obtained in yield 19.9%; mp 159.2-161.3 ; TLC (Silica G w/UV254) R_f = 0.59, 10:1 CH_2Cl_2:MeOH; $[\alpha]_D^{20}$ = 25.7 (c 0.50, CH_2Cl_2); ^{1}H NMR (500 MHz, cdcl$_3$δ 7.61 (d, *J* = 1.0 Hz, 1H), 7.28 (d, *J* = 10.0 Hz, 1H), 7.19 (dd, *J* = 3.5, 0.9 Hz, 1H), 6.53 (dd, *J* = 3.5, 1.7 Hz, 1H), 6.32 (dd, *J* = 10.1, 1.9 Hz, 1H), 6.05 (s, 1H), 4.56 (s, 1H), 3.43 (d, *J* = 15.9 Hz, 1H), 3.28 (d, *J* = 15.9 Hz, 1H), 2.89 – 3.09 (m, 1H), 2.60 (td, *J* = 13.6, 5.5 Hz, 1H), 2.33 – 2.39 (m, 1H), 2.27 (dd, *J* = 14.4, 3.7 Hz, 1H), 2.22 (s, 3H), 2.16 – 2.20 (m, 1H), 2.09 – 2.16 (m, 1H), 1.93 (ddd, *J* = 16.0, 9.3, 6.5 Hz, 1H), 1.85 – 1.89 (m, 1H), 1.79 – 1.84 (m, 1H), 1.74 (dd, *J* = 18.2, 11.0 Hz, 1H), 1.50 – 1.56 (m, 1H), 1.48 (s, 3H), 1.25 (s, 2H), 1.12 – 1.20 (m, 2H), 1.08 (s, 3H)); ^{13}C NMR (126 MHz, $CDCl_3$) δ 200.92, 186.53, 169.79, 157.89, 155.98, 147.11, 144.05, 128.07, 122.61, 119.22, 112.16, 96.55, 70.17, 55.40, 52.41, 47.33, 44.04, 40.43, 39.21, 33.94, 31.94, 31.33, 30.81, 24.02, 21.07, 16.95; IR (NaCl, thin film) ν_{max} (cm^{-1}): 3356, 2922, 1655, 1307, 762; HRMS (ESI) m/z: $[M+H]^+$ Calcd for $C_{27}H_{32}O_6S$, 485.1998; found 485.1982

(6S,8S,9R,10S,11S,13S,14S,16R,17R)-6,9-difluoro-11-hydroxy-10,13,16-trimethyl-17-(2-(methylthio)acetyl)-3-oxo-6,7,8,9,10,11,12,13,14,15,16,17-dodecahydro-3H-cyclopenta[a]phenanthren-17-yl furan-2-carboxylate (FM4): tan solid obtained in 15.9% yield; mp 137.4-155.6; ; TLC (Silica G w/UV254) R_f = 0.59, 10:1 CH_2Cl_2:MeOH; $[\alpha]_D^{20}$ = + 24.91 (c 0.42, CH_2Cl_2); ^{1}H NMR (500 MHz, cdcl$_3$) δ 7.61 (d, *J* = 7.0 Hz, 1H), 7.10 – 7.24 (m, 2H), 6.50 – 6.58 (m, 1H), 6.43 – 6.48 (m, 1H), 6.40 (d, *J* = 10.3 Hz, 1H), 5.31 – 5.76 (m, 2H), 4.43 (s, 1H), 3.31 (s, 1H), 2.50 – 2.69 (m, 3H), 2.23 – 2.33 (m, 3H), 2.19 (s, 1H), 1.85 (dd, *J* = 23.0, 13.8 Hz, 3H), 1.54 (s, 2H), 1.41 (d, *J* = 13.1 Hz, 3H), 1.24 (d, *J* = 10.8 Hz, 2H), 1.17 (s, 1H), 1.09 (s, 1H), 0.95 – 1.02 (m, 3H); ^{13}C NMR (126 MHz, $CDCl_3$) δ 185.41, 157.85, 150.21, 148.80, 147.45, 130.92, 130.42, 124.71, 119.64, 119.27, 112.21, 87.18, 85.72, 71.68, 71.13, 48.50, 48.04, 43.52, 36.95, 35.82, 34.33, 33.69, 33.31, 30.34, 29.71, 23.06, 16.84, 16.48; IR (NaCl, thin film)

ν_{max} (cm^{-1}): 3326, 2980, 2359, 1663, 1297, 753; HRMS (ESI) m/z: $[M+H]^+$ Calcd for $C_{28}H_{32}F_2O_6S$, 535.1960; found 535.1963.

APPENDIX

1.10.1 – ^{1}H NMR AND ^{13}C NMR SPECTRA

Figure 0.10 – ^{1}H NMR of **DX1**

Figure 0.11 – ^{13}C NMR of **DX1**

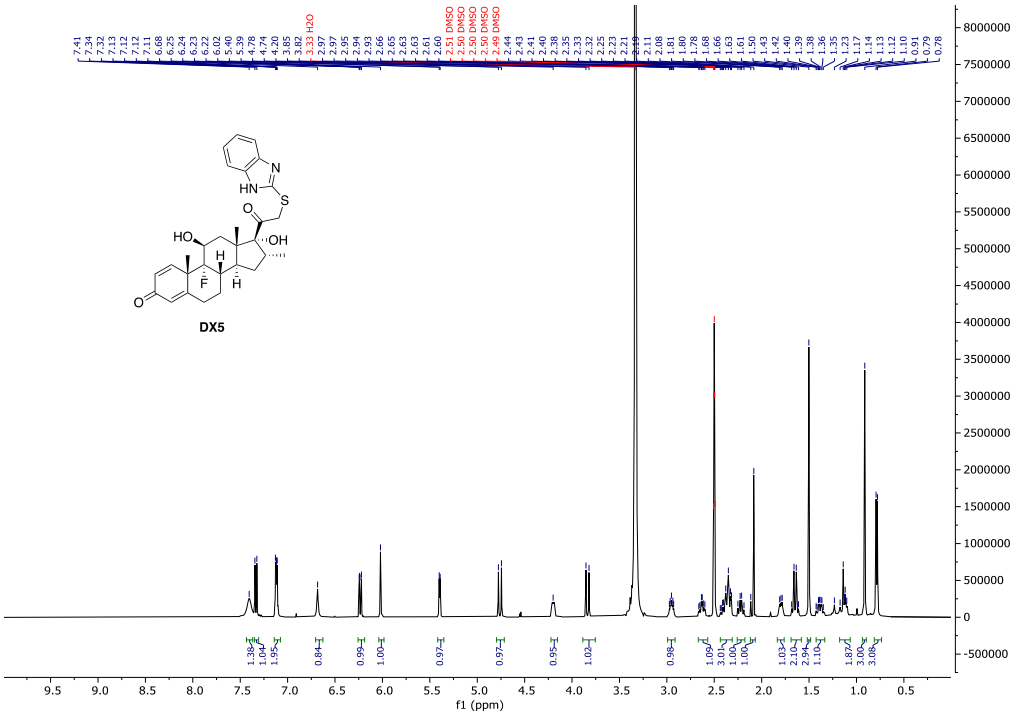

Figure 0.12 – ^{1}H NMR of **DX5**

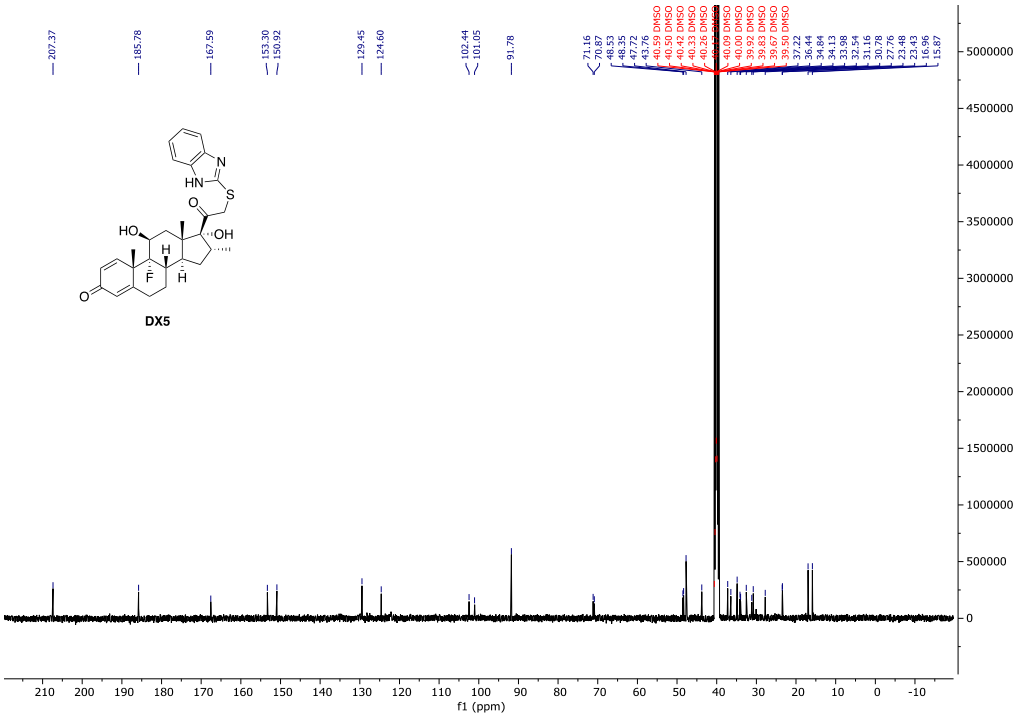

Figure 0.13 – ^{13}C NMR of **DX5**

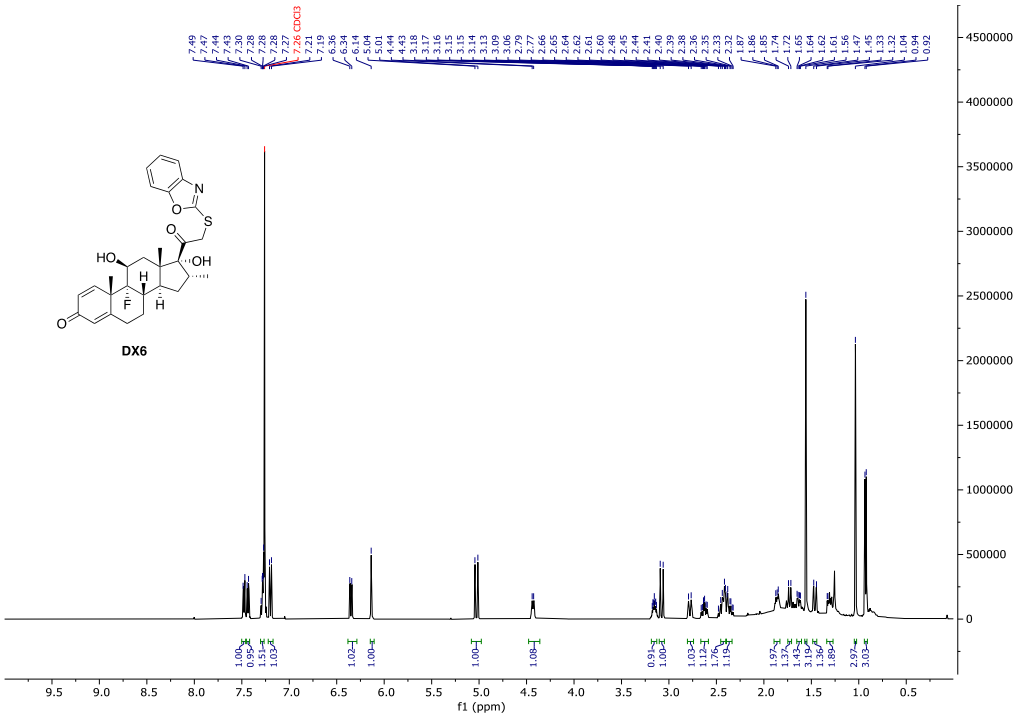

Figure 0.14 – ^{1}H NMR of **DX6**

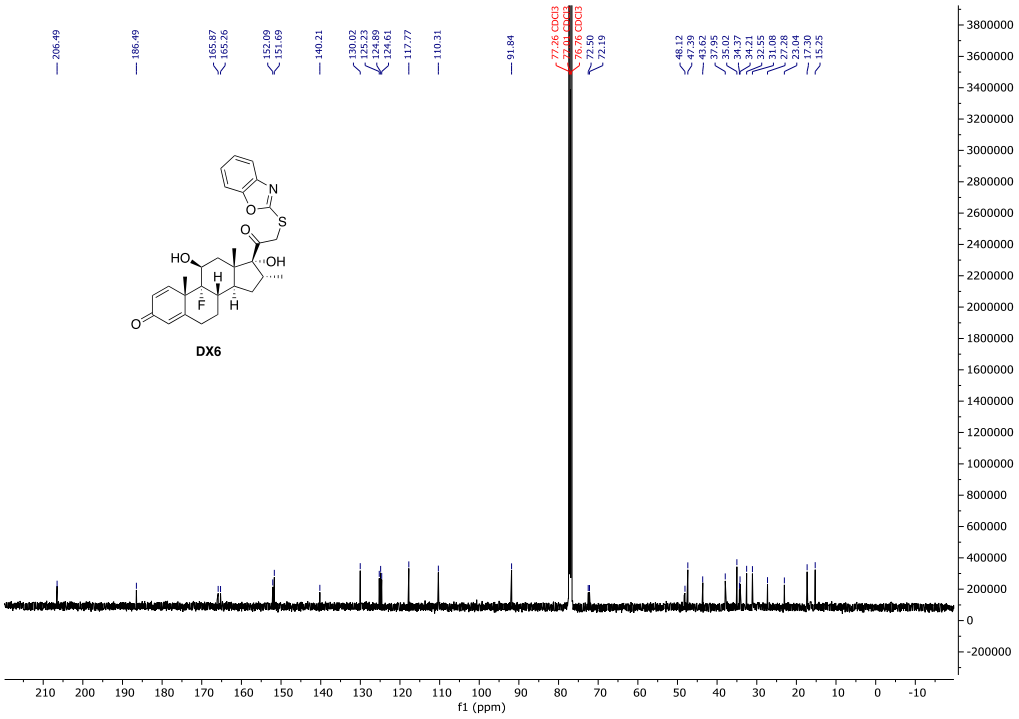

Figure 0.15 – ^{13}C NMR of **DX6**

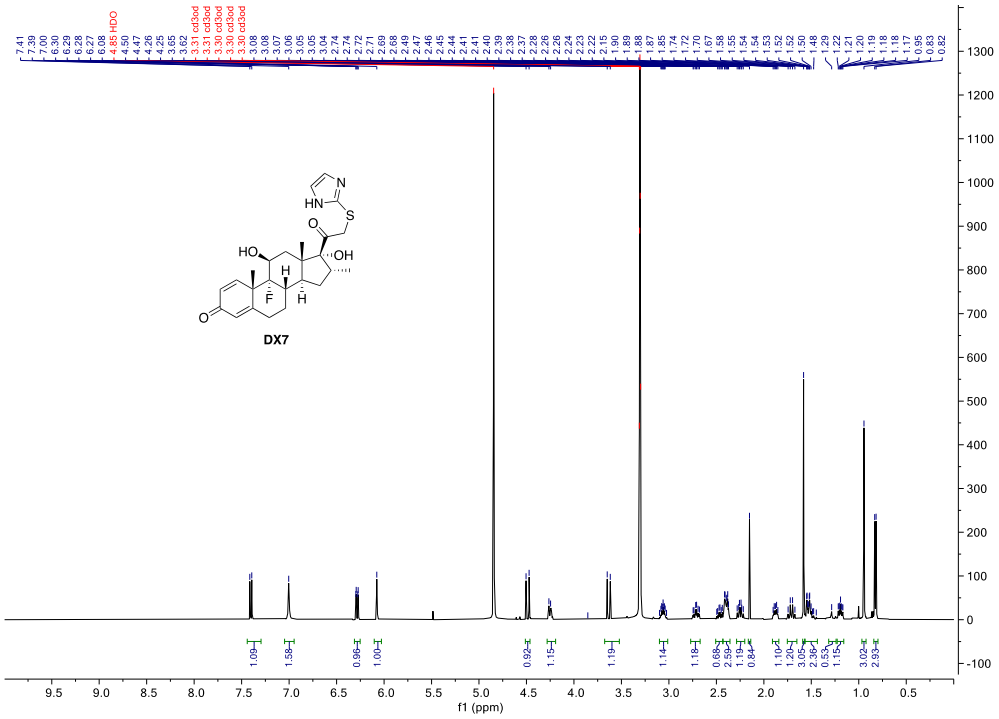

Figure 0.16 – ^{1}H NMR of **DX7**

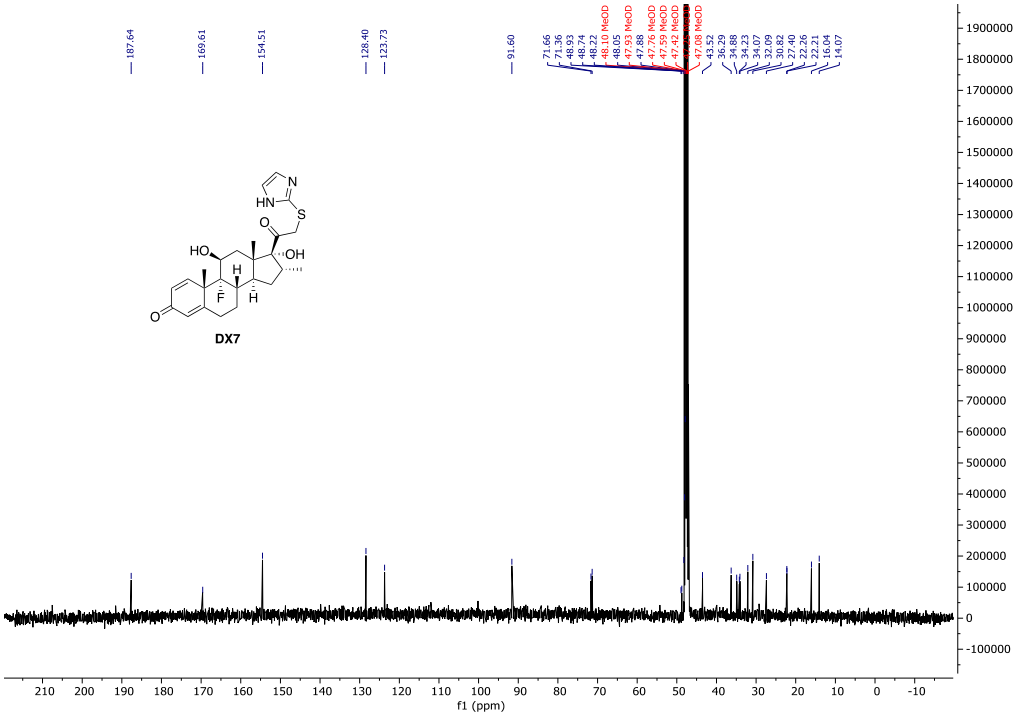

Figure 0.17 – ^{13}C NMR of **DX7**

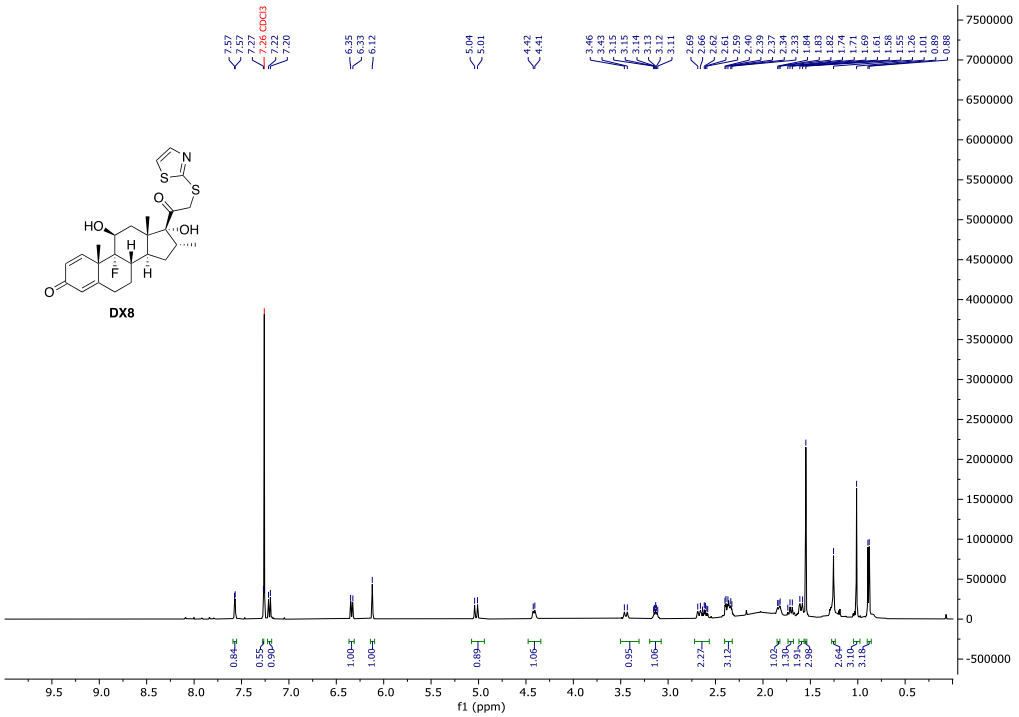

Figure 0.18 – ^{1}H NMR of **DX8**

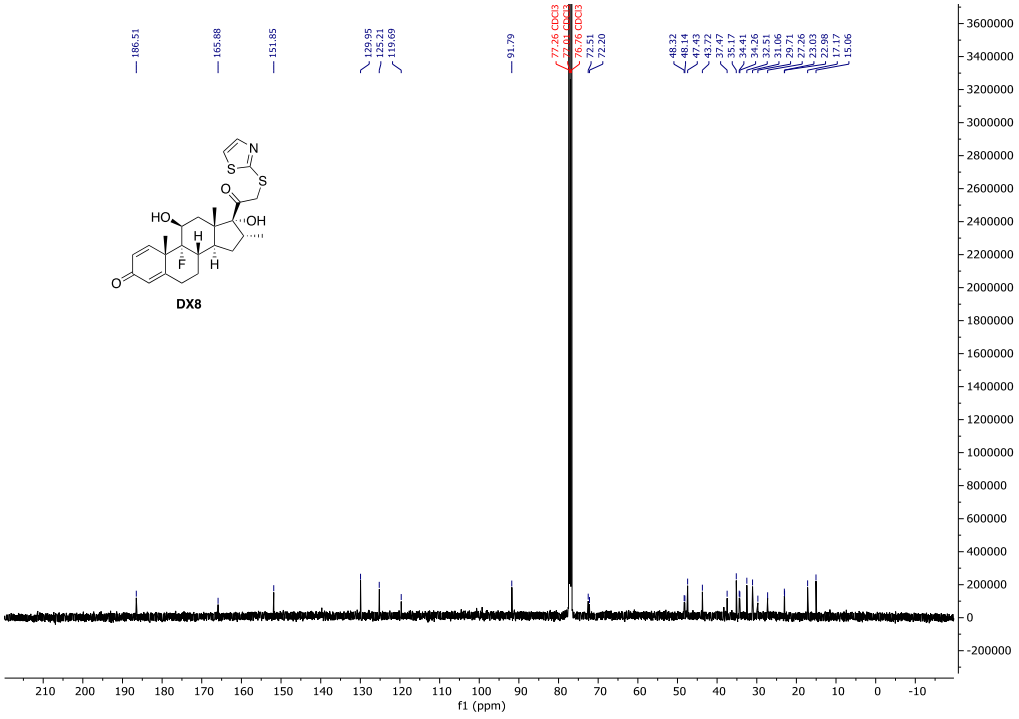

Figure 0.19 – ^{13}C NMR of **DX8**

Figure 0.20 – ^{1}H NMR of **BM1**

Figure 0.21 – ^{13}C NMR of **BM1**

Figure 0.22 – ^{1}H NMR of **PN1**

Figure 0.23 – ^{13}C NMR of **PN1**

Figure 0.24 – ^{1}H NMR of **FM1**

Figure 0.25 – ^{13}C NMR of **FM1**

Figure 0.26 – ^{1}H NMR of **DN1**

Figure 0.27 – ^{13}C NMR of **DN1**

Figure 0.28 – ^{1}H NMR of **BD1**

Figure 0.29 – ^{13}C NMR of **BD1**

Figure 0.30 – ^{1}H NMR of **DX2**

Figure 0.31 – ^{13}C NMR of **DX2**

Figure 0.32 – ^{1}H NMR of **BM2**

Figure 0.33 – ^{13}C NMR of **BM2**

Figure 0.34 – ^{1}H NMR of **PN2**

Figure 0.35 – ^{13}C NMR of **PN2**

Figure 0.36 – ^{1}H NMR of **FM2**

Figure 0.37 – ^{13}C NMR of **FM2**

Figure 0.38 – ^{1}H NMR of **HC3**

Figure 0.39 – ^{13}C NMR of **HC3**

Figure 0.40 – ^{1}H NMR of **DX3**

Figure 0.41 – ^{13}C NMR of **DX3**

Figure 0.42 – ^{1}H NMR of **BM3**

Figure 0.43 – ^{13}C NMR of **BM3**

Figure 0.44 – ^{1}H NMR of **PN3**

Figure 0.45 – ^{13}C NMR of **PN3**

Figure 0.46 – ^{1}H NMR of **FM3**

Figure 0.47 – ^{13}C NMR of **FM3**

Figure 0.48 – ^{1}H NMR of **HC4**

Figure 0.49 – ^{13}C NMR of **HC4**

Figure 0.50 – ^{1}H NMR of **DX4**

Figure 0.51 – ^{13}C NMR of **DX4**

Figure 0.52 – ^{1}H NMR of **BM4**

Figure 0.53 – ^{13}C NMR of **BM4**

Figure 0.54 – ^{1}H NMR of **PN4**

Figure 0.55 – ^{1}H NMR of **PN4**

Figure 0.56 – ^{1}H NMR of **FM4**

Figure 0.57 – ^{13}C NMR of **FM4**

1.10.2 – CCL2 PROMOTER ACTIVITY

Table 0.3 – CCL2 Assay Raw Data

	CCL2 (%max IL-1β response)					
	Concentration of Compound (M)					
Compd	1X10^-10	1X10^-9	1X10^-8	1X10^-7	1X10^-6	1X10^-5
DX	55.4±18.6	45.7±12.2	27.7±5.42	14.8±7.80	12.5±5.80	11.4±0.33
HC3	91.0±24.8	64.3±6.32	85.7±31.6	79.8±22.1	62.9±24.6	73.0±33.1
HC4	46.2±17.8	29.4±14.5	36.6±25.6	29.1±24.7	21.4±12.3	22.6±15.9
DX1	66.6±9.61	68.7±11.8	66.5±14.1	37.7±2.06	18.9±1.51	20.2±6.05
DX2	47.6±5.19	44.2±14.7	22.8±4.35	17.1±3.01	9.63±4.06	10.3±1.69
DX3	34.0±5.53	31.6±9.95	26.7±7.58	25.4±0.94	24.9±4.02	26.3±2.99
DX4	19.3±4.10	16.9±0.26	17.1±2.70	16.2±2.96	15.4±2.46	15.3±1.26
DX5	63.6±22.7	65.3±13.8	61.2±6.29	69.7±13.4	36.8±1.16	32.9±10.1
DX6	64.9±16.8	65.8±18.8	60.5±22.3	49.6±23.9	35.0±19.8	35.4±15.0
DX7	78.4±18.9	70.6±12.5	70.7±19.7	52.0±12.3	34.2±14.1	33.3±13.4
DX8	76.0±22.8	70.6±14.5	66.4±15.8	64.2±9.83	56.2±17.3	46.1±6.61
BM	57.6±10.9	38.5±6.82	31.6±8.18	17.0±4.17	11.3±4.13	14.2±8.11
BM1	72.1±10.2	75.2±13.4	68.2±14.6	39.4±4.25	27.9±5.53	14.3±2.49
BM2	54.0±12.5	51.6±12.9	38.8±11.6	28.3±7.27	20.2±7.95	16.7±7.79
BM3	68.8±7.84	45.7±14.4	35.3±10.3	26.0±2.7	19.5±3.68	16.5±3.31
BM4	79.6±11.2	68.8±4.14	64.1±17.4	42.8±29.8	31.3±29.7	18.4±11.5
PN	87.3±12.3	62.0±15.2	41.8±16.7	20.4±7.90	14.9±4.76	15.8±6.53
PN1	90.3±28.6	89.3±4.98	88.0±7.36	73.2±12.0	60.1±14.2	25.0±8.70
PN2	41.5±5.04	36.9±7.79	18.0±3.13	13.9±3.48	12.2±3.48	9.10±1.18
PN3	98.9±26.9	93.8±24.8	87.7±20.9	72.4±20.7	56.9±12.4	50.4±25.9
PN4	26.0±4.80	25.1±9.12	25.1±6.19	21.4±4.01	19.6±5.70	19.2±5.70
FM	31.7±4.90	23.5±10.6	15.3±7.26	11.9±5.78	9.58±2.32	12.2±5.56
FM1	48.1±11.8	51.1±13.2	39.8±17.6	26.6±7.31	19.9±7.66	14.0±4.75
FM2	31.3±18.9	26.4±2.45	22.0±4.23	16.8±4.26	14.0±4.19	11.7±4.72
FM3	37.6±9.95	26.3±4.77	22.1±3.93	18.6±3.93	18.6±5.60	17.8±4.96
FM4	29.4±8.93	30.9±17.0	27.4±16.7	32.7±22.3	29.3±13.2	24.1±13.4
DN	70.8±13.1	50.1±5.42	31.0±5.73	20.9±0.36	17.2±8.11	16.8±6.86
DN1	95.2±25.8	72.3±11.0	66.5±5.57	44.0±5.76	34.2±8.95	34.4±6.81
BD	20.0±6.86	19.9±4.39	18.9±3.24	17.1±2.01	17.4±3.76	16.6±1.60
BD1	99.3±19.4	86.9±15.1	94.4±6.42	77.9±19.8	53.3±8.33	42.4±3.73

Table 0.4 – Low Dose CCL2 Assay Raw Data

	CCL2 (%max IL-1β response)					
	Concentration of Compound (M)					
Compd	1X10^-18	1X10^-15	1X10^-12	1X10^-9	1X10^-6	1X10^-5
DX	70.5±21.8	51.8±13.4	53.8±25.8	31.3±15.8	16.1±4.16	18.0±4.58
DX4	17.8±3.91	17.4±5.33	17.1±4.05	16.7±2.93	17.6±3.83	18.8±4.03
PN	65.9±15.3	65.3±15.6	69.5±16.8	51.2±17.1	20.3±5.93	26.1±4.53
PN4	31.8±13.6	32.1±11.7	30.2±15.4	25.6±5.59	21.9±4.58	23.9±5.64

Figure 0.58 – CCL2 Data Analysis

Figure 1.57 – Cont.

Figure 1.57 – Cont.

Figure 1.57 – Cont.

Figure 1.57 – Cont.

Figure 1.57 – Cont.

1.10.3 – 3xGRE PROMOTER ACTIVITY

Table 0.5 – 3xGRE Assay Raw Data

	3xGRE (Fold over control – DMSO)					
	Concentration of Compound (M)					
Compd	1X10^-10	1X10^-9	1X10^-8	1X10^-7	1X10^-6	1X10^-5
DX	1.04±0.24	1.56±1.22	1.89±1.58	3.55±0.97	7.75±2.84	7.86±3.36
HC3	5.65±2.15	5.30±2.32	5.13±2.22	4.85±1.39	4.72±2.64	5.06±2.44
HC4	3.94±0.41	3.99±0.28	3.86±0.08	4.08±0.34	3.76±0.29	3.25±0.81
DX1	0.65±0.12	0.73±0.15	0.73±0.23	0.73±0.13	0.96±0.42	0.99±0.31
DX2	0.81±0.06	0.85±0.20	1.84±1.35	2.39±2.04	3.78±2.88	4.89±3.13
DX3	7.42±4.16	6.21±3.02	6.19±3.44	6.20±2.76	5.77±3.29	6.65±3.79
DX4	8.88±4.10	8.07±4.50	8.55±4.55	8.51±4.25	7.34±3.63	7.78±4.02
DX5	1.06±0.19	0.926±0.19	0.84±0.08	0.95±0.12	1.98±0.53	3.20±0.68
BM	6.52±2.20	8.98±2.28	10.3±2.94	10.3±2.91	9.38±2.21	9.42±3.87
BM1	0.80±0.14	0.85±0.13	0.93±0.17	1.68±0.25	1.95±0.90	2.20±0.82
BM2	1.62±0.85	1.89±0.81	2.52±0.74	4.75±1.68	4.58±1.37	4.71±1.05
BM3	3.54±1.70	4.10±1.89	4.07±1.96	4.32±1.85	4.54±1.39	4.76±1.49
BM4	0.93±0.12	0.94±0.18	1.24±0.06	4.34±1.49	4.71±1.68	4.87±1.87
PN	3.50±1.72	6.58±2.91	8.03±2.14	10.0±3.22	7.80±1.55	7.58±1.11
PN1	0.95±0.25	0.85±0.21	0.95±0.13	1.08±0.13	1.85±0.40	2.40±0.96
PN2	2.16±1.34	3.07±0.75	6.76±0.90	7.54±1.55	6.06±1.82	6.24±0.75
PN3	1.06±0.42	1.29±0.49	1.10±0.17	1.85±0.34	2.97±0.70	3.4±0.86
PN4	4.95±1.41	4.59±1.40	4.71±1.15	5.44±1.61	5.29±1.63	5.19±1.38
FM	9.20±4.51	8.48±2.30	8.73±3.36	10.1±4.90	8.73±5.30	10.2±8.71
FM1	2.38±0.31	3.18±0.97	4.40±1.78	4.53±1.79	4.75±1.71	4.68±1.37
FM2	4.60±1.31	6.06±2.39	6.88±1.34	11.7±5.18	9.71±1.42	11.7±7.07
FM3	4.86±0.55	4.72±1.09	5.52±1.03	5.45±1.29	5.63±1.74	4.91±1.13
FM4	4.47±1.73	4.57±0.83	4.92±0.71	4.82±0.69	4.83±1.06	4.46±0.77
DN	5.00±3.55	9.57±3.09	8.33±0.47	8.90±0.85	8.47±0.55	9.33±0.86
DN1	0.88±0.19	0.98±0.25	0.98±0.30	1.68±0.49	2.35±0.69	2.50±0.94
BD	6.30±0.85	6.97±0.85	6.33±0.79	6.71±0.51	6.36±0.33	6.01±0.72
BD1	0.90±0.14	0.95±0.11	0.89±0.12	0.98±0.16	1.50±0.19	1.99±0.20

Table 0.6 – Low Dose 3xGRE Assay Raw Data

	3xGRE (Fold over control – DMSO)					
	Concentration of Compound (M)					
Compd	1X10^-18	1X10^-15	1X10^-12	1X10^-9	1X10^-6	1X10^-5
DX	0.85±0.13	2.94±3.43	3.72±3.83	7.85±1.18	8.75±1.29	9.71±2.06
DX4	6.70±1.16	6.75±1.70	6.67±1.49	6.95±1.48	6.94±1.64	8.82±1.74
PN	2.24±1.97	1.602±1.934	1.17±0.33	4.46±1.49	5.01±2.16	6.21±1.59
PN4	3.85±2.10	4.42±1.29	4.91±0.87	4.99±1.61	4.95±1.61	5.70±1.08

Figure 0.59 – 3xGRE Data Analysis

Figure 1.59 – Cont.

Figure 1.59 – Cont.

Figure 1.59 – Cont.

Figure 1.59 – Cont.

Figure 1.59 – Cont.

Figure 1.59 – Cont.

1.10.4 – ADENYLATE KINASE RELEASE

Table 0.7 – ADK Assay Raw Data

ADK (Fold Over Control) – 100 nM	
DX	1.60±0.16
HC	1.47±0.10
HC1	1.10±0.22
HC2	1.24±0.18
HC3	1.19±0.07
HC4	1.31±0.13
DX1	1.26±0.18
DX2	1.40±0.23
DX3	1.38±0.11
DX4	1.38±0.11
BM	1.63±0.19
BM1	1.23±0.07
BM2	1.18±0.20
BM3	1.05±0.16
BM4	0.99±0.02
PN	1.72±0.53
PN1	1.35±0.24
PN2	1.69±0.29
PN3	1.44±0.41
PN4	1.52±0.42
FM	1.53±0.26
FM1	1.33±0.16
FM2	1.24±0.17
FM3	1.42±0.08
FM4	1.44±0.07
DN	1.73±0.19
DN1	1.34±0.15
BD	1.52±0.16
BD1	1.28±0.09

Figure 0.60 – ADK Release Data Analysis

1.10.5 – MTS REDUCTION

Table 0.8 – MTS Assay Raw Data

	MTS Reduction (% of Control) – 100 nM
DX	63.4±12.2
HC	77.1±7.04
HC1	83.9±3.52
HC2	85.6±5.87
HC3	83.9±2.42
HC4	74.2±4.70
DX1	93.4±6.27
DX2	80.7±12.5
DX3	80.6±5.65
DX4	80.7±10.2
BM	66.5±6.04
BM1	79.6±11.0
BM2	79.7±10.8
BM3	69.1±8.39
BM4	72.4±13.0
PN	74.6±15.4
PN1	91.7±15.9
PN2	77.1±13.5
PN3	80.5±10.1
PN4	76.6±7.28
FM	84.9±22.2
FM1	88.8±13.7
FM2	89.1±12.3
FM3	76.1±8.62
FM4	82.4±8.60
DN	70.8±3.34
DN1	79.4±8.45
BD	81.5±13.7
BD1	89.6±10.8

Figure 0.61 – MTS Reduction Data Analysis

1.10.6 – Ccl2 and Ccl20 GENE EXPRESSION

Table 0.9 – Ccl2 and Ccl20 Gene Expression Raw Data

	Ccl2 Relative mRNA Abundance (% IL-1β Response)	*Ccl20* Relative mRNA Abundance (%IL-1 β Response)
DX	18.9±8.09	23.8±12.1
HC	69.4±11.9	63.2±7.69
HC1	52.2±18.1	59.5±27.1
HC2	39.2±16.0	39.7±11.9
HC3	86.0±20.6	90.9±18.0
HC4	26.8±3.62	34.3±4.50
DX1	53.9±13.8	70.7±28.3
DX2	29.0±14.4	36.2±17.0
DX3	29.9±14.8	48.7±14.3
DX4	21.0±11.6	35.7±9.35
BM	25.0±9.23	26.4±9.85
BM1	53.3±24.8	57.4±34.8
BM2	32.7±7.77	37.3±28.2
BM3	37.1±11.3	47.6±22.7
BM4	40.4±15.6	52.6±5.59
PN	24.6±7.86	32.0±11.0
PN1	54.7±11.9	45.9±20.5
PN2	13.3±7.18	19.5±13.0
PN3	54.4±24.8	64.6±37.0
PN4	21.4±2.41	43.4±31.9
FM	19.8±7.12	22.9±9.79
FM1	33.4±11.4	32.9±24.7
FM2	34.6±8.02	35.7±5.79
FM3	38.1±25.4	38.2±19.0
FM4	21.9±12.4	28.5±16.0
DN	16.1±5.75	24.1±13.5
DN1	40.6±12.1	49.0±13.2
BD	12.1±4.07	20.7±5.43
BD1	73.8±12.7	79.8±33.8

Figure 0.62 – *Ccl2* and *Ccl20* Gene Expression Data Analysis

Figure 1.62 – Cont.

1.10.7 – Sgk1 and Rgs2 GENE EXPRESSION

Table 0.10 – *Sgk1* and *Rgs2* Gene Expression Raw Data

	Sgk1 Relative mRNA Abundance (Fold over Control) – 100 nM	*Rgs2* Relative mRNA Abundance (Fold over Control) – 100 nM
DX	9.28±4.90	104±56.4
HC	2.69±0.22	4.90±0.97
HC1	0.97±0.19	1.33±1.04
HC2	2.18±0.56	4.61±3.45
HC3	1.17±0.39	2.68±1.59
HC4	3.05±1.65	31.3±8.68
DX1	1.35±0.52	9.82±9.06
DX2	2.86±2.62	37.3±37.2
DX3	1.54±0.34	33.6±12.1
DX4	4.77±1.13	71.4±14.0
BM	6.39±2.87	64.8±15.3
BM1	0.76±0.36	4.92±2.79
BM2	0.81±0.49	8.57±2.34
BM3	1.10±0.49	26.0±11.4
BM4	1.11±0.36	7.80±1.38
PN	4.36±3.19	102±43.3
PN1	1.09±0.74	2.28±0.99
PN2	1.86±1.04	50.9±16.4
PN3	1.01±0.46	4.68±2.36
PN4	4.34±1.67	52.2±17.1
FM	7.78±3.44	127±58.2
FM1	1.31±0.43	54.8±22.1
FM2	1.38±0.49	39.6±15.9
FM3	5.76±2.98	58.5±4.45
FM4	4.62±1.29	83.5±35.6
DN	6.65±1.48	82.2±18.3
DN1	0.57±0.29	3.58±2.13
BD	6.51±1.89	84.9±18.7
BD1	0.86±0.23	2.19±0.97

Table 0.11 – Low Dose *Sgk1* Gene Expression Raw Data

	Sgk1 Assay Raw Data					
	Concentration of Compound (M)					
Compd	1X10^-18	1X10^-15	1X10^-12	1X10^-9	1X10^-6	1X10^-5
DX	1.20±0.68	0.71±0.21	1.72±1.02	4.15±1.06	6.32±0.77	1.20±0.68
DX4	3.67±0.60	4.96±0.76	4.36±1.79	4.99±1.77	4.54±2.06	3.67±0.60
PN	1.17±0.36	0.77±0.06	1.75±1.23	3.81±1.60	7.51±1.87	1.17±0.36
PN4	3.43±0.29	4.87±0.82	4.30±1.44	4.75±1.26	4.37±0.49	3.43±0.29

Table 0.12 – Low Dose *Rgs2* Gene Expression Raw Data

	Rgs2 Assay Raw Data				
	Concentration of Compound (M)				
Compd	1X10^-18	1X10^-15	1X10^-12	1X10^-9	1X10^-6
DX	16.7±7.92	33.1±15.4	56.2±22.6	62.5±39.2	95.8±23.5
DX4	110±44.8	105±18.0	88.9±8.09	94.4±26.2	88.3±16.2
PN	1.02±0.45	4.70±3.70	60.7±64.7	144±53.1	153±62.8
PN4	76.2±28.6	114±37.0	106±23.6	115±59.9	170±64.6

Figure 0.63 – *Sgk1* and *Rgs2* Gene Expression Data Analysis

Figure 1.63 – Cont.

Figure 1.63 – Cont.

Figure 1.63 – Cont.

Figure 1.63 – Cont.

1.10.8 – LIGPLOT ANALYSIS OF CLUSTERED FRAME OF MOLECULAR DYNAMIC SIMULATION IN 7PRV

Figure 0.64 – LigPlot Analysis of Selected Ligands

Figure 1.64 – Cont.

Figure 1.64 – Cont.

1.10.9 – RMSD AND RMSFPLOTS THROUGHOUT THE MD TRAJECTORY OF 100NS

Figure 0.65 – Alpha carbon protein backbone root mean square deviation values for 100 ns simulations.

Figure 0.66 – Ligand root mean square deviation values for 100 ns simulations.

Figure 0.67 – Residue root mean square fluctuation values.

CHAPTER 2: ARYL PYRAZOLE-MODIFIED HYDROCORTISONE AS A HIGHLY POTENT AND SELECTIVE AGONIST FOR THE GLUCOCORTICOID RECEPTOR

A version of this chapter is expected to be part of a future publication by:

Seaton, W.B., Lato, A.M., Burke, S.J., Collier, J.J., Campagna, S.R.

Contributions:

Conceptualization, W.B.S., A.M.L, J.J.C. and S.R.C.; methodology, W.B.S., A.M.L, S.J.B., J.J.C. and S.R.C.; validation, W.B.S., S.J.B. and S.R.C.; formal analysis, W.B.S., S.J.B., J.J.C. and S.R.C.; investigation, W.B.S., A.M.L, S.J.B.; resources, J.J.C. and S.R.C.; writing, W.B.S.; visualization, W.B.S.; supervision, J.J.C. and S.R.C.; funding acquisition, J.J.C. and S.R.C.

2.1 - ABSTRACT

Glucocorticoids (GCs) are used to treat a variety of inflammatory and immunological disorders by activating the glucocorticoid receptor (GR), a nuclear receptor (NR) which regulates the transcription of thousands of genes. However, most GCs exhibit off target effects due to their substandard selectivity. The ligand binding pocket (LBP) of the GR is highly flexible and, as such, can be exploited to regulate transcriptional output. In this study, a systematic derivatization of hydrocortisone was performed to probe the unoccupied cavities within the LBP of the GR. The synthesis of C21 mercaptobenzothiazole (**1a**) and mercaptobenzoxazole analogues (**1c**) produced modulated GCs with reduced transactivation and maintained anti-inflammatory activity. Furthermore, aryl pyrazole addition to the A ring of hydrocortisone resulted in two compounds (**6** and **7**) with potency in the attomolar region and high specificity for the GR over the remaining 47 nuclear receptors. Interestingly, functionalizing hydrocortisone with both moieties did not result in a single GC with all the aforementioned activity. Previous work corroborated that potency is linked with LBP expansion, while computational experiments presented here suggest that decreased free binding energy with N564 may explain the high selectivity of these compounds.

2.2 - INTRODUCTION

Cortisol is a steroidal hormone naturally secreted by the adrenal glands in response to physiological and psychological stresses.[25] Therapeutically, cortisol is known as hydrocortisone (HC) and is one of many glucocorticoids (GCs) used to treat a variety of diseases including eczema, Crohn's disease, septic shock, and asthma.[23, 25] Despite being the primary choice when treating inflammatory diseases, GC use is often accompanied by a variety of undesired side effects including diabetes, skin and muscle atrophy, hyperglycemia and hypertension.[63, 64]

GC's possess a high affinity towards a specific nuclear receptor (NR) known as the glucocorticoid receptor (GR) and function through two transcriptional mechanisms.[63] First, following translocation to the nucleus, the GC-GR complex can suppress the transcription of pro-inflammatory cytokines by binding to and inhibiting various transcription factors, such as those involved in the NF-κB pathway, in a process known as

transrepression (TR).[65] In contrast, unwanted side effects like diabetes can result from induced anabolic activity, such as gluconeogenesis, through transcription of specific genome sequences known as glucocorticoid responsive elements (GREs) upon GC-GR complex recruitment.[64] This process is known as transactivation (TA) and there has been a significant effort to produce a selective GC agonist capable of discerning between these two modes of transcription.[66-68]

Many approaches have been taken to synthesize these selective GR modulators (SGRMs) but to date none have been approved for clinical use.[12, 69, 70] For example, substitution of the C-21 hydroxyl group of hydrocortisone or dexamethasone with a mercaptobenzothiazole (MBT) moiety resulted in reduced TA and subsequent impact on islet β-cell function while maintaining anti-inflammatory properties.[67, 71] Additionally, modification of the A-ring with an aryl pyrazole moiety, or C-17 derivatization to furoate ester has led to increased cytotoxicity in leukemia cells and increased potency in experiments measuring cytokine inhibition, respectively.[23, 72] These studies were made possible in part by efforts from Suino-Powell and coworkers who crystalized deacylcortivazol (DAC) in the ligand binding pocket (LBP) of the GR and displayed the protein's flexibility which allows it accommodate such modifications as the aryl pyrazole moiety.

Herein, the flexibility of the GR LBP is further investigated by modifying HC with a combination of aryl pyrazole moieties at the A-ring, mercapto- moieties at the C-21 site, and furoate ester at the C-17 position. Additionally, these compounds were designed with the aim of being both highly selective and highly potent, meeting a previously suggested "dosage window" which demonstrates TR but is too low for TA.[23] These compounds were subjected to *in vitro* assays evaluating both TR and TA, while simultaneously exploring their ability to fit within available space in the LBP through molecular dynamic (MD) simulations. Biological assays reveal that aryl pyrazole addition alone increases the potency and selectivity of hydrocortisone while producing an increase in free binding energy with key amino acid residues near the A ring.

2.3 – SYNTHETIC METHODS

Compounds were synthesized according to previously published routes with some modifications.[67, 73, 74] A general synthetic procedure is outlined in **Figure 2.1**. Briefly, a divergent synthesis was performed on commercially available hydrocortisone. To begin, compounds **1a-e** were synthesized through mesylation and subsequent substitution of C21 with the appropriate mercapto- reagent. Following this, **2a-e** were obtained by reacting each compound with 2-furoyl chloride. Compounds **6**, **7**, **8a-e**, and **9** also began with hydrocortisone which was subjected to a protection reaction in which a change of reagent from formaldehyde to trioxane was employed to minimize impurities. Formylation of ketal **3** was preformed using sodium hydride and ethyl formate in toluene to yield enol **4**. Addition of p-fluorophenylhydrazine hydrochloride or phenylhydrazine hydrochloride produced aryl pyrazole **5** which subsequently underwent a deprotection in 50% formic acid to yield compounds **6** and **7**, respectively. Changes in the workup procedure produced higher yields and simplified purification. Compound **6** was subjected to mesylation and substitution as described above to produce **8a-e**. Final furoylation of C17 OH of **8a** produced **9**.

2.4 – BIOLOGICAL ASSAYS

The ability of the compounds to reduce the proinflammatory activity of IL-1β was examined using a reporter gene assay consisting of a multimerized NF-κB luciferase reporter construct that contains five copies of an NF-κB element upstream of a luciferase gene (5X-NF- κB-Luc).[67] 832/13 cells, a rat insulinoma cell line, were cultured as described previously and determined to be free of mycoplasma contamination.[39] The 832/13 cells were grown in 24-well plates and transfected with the 5X-NF-κB-Luc reporter plasmid. Twenty-four hours after transfection, the cells were exposed to each synthetic compound for one hour, followed by culture for four hours with 1 ng/mL IL-1β. Transactivation activity was determined by analyzing the ability of the synthetic compounds to drive transcriptional activity from plasmid construct containing three copies of a glucocorticoid response element (3xGRE).[67] The 832/13 cells were grown in 24-well plates and transfected with the 3xGRE luciferase reporter plasmid. Twenty-four

Figure 0.68 – Divergent Synthetic Route. Reagents and conditions: (i) methanesulfonyl chloride, DIPEA, CH_2Cl_2, 0 °C to rt, 15 h, (ii) HS-R^1, K_2CO_3, acetone, reflux, (iii) furoyl chloride, DMAP, CH_2Cl_2, 0 °C to rt, (iv) trioxane, conc. HCl, $CHCl_3$, 4 h, (v) ethyl formate, NaH, toluene, rt, 16 h, (vi) NaOAc, AcOH, rt, 24 h, (vii) 50% formic acid, reflux, 40 min

hours post-transfection, the cells were exposed to each synthetic compound for four hours. At the end of each respective treatment period, the cells were harvested using passive lysis buffer (Promega, Madison, WI) and luciferase activity measured in a Glomax luminometer (Promega, Madison, WI). Luciferase activity was normalized to total protein to account for differences in cell numbers between experiments.

GR target gene expression of *Sgk1* and *Rgs2* were investigated using 832/13 cells treated with each compound for 6 h. TRI Reagent (Sigma, St. Louis, Mo, USA) was used to lyse the cells and RNA-extracted, cDNA-synthesized, and mRNA expression levels were determined as previously described.[42] Hydrocortisone was purchased from Sigma Aldrich (St. Louis, MO, USA) and primer sequences of *Rgs2* and *Sgk1* are available upon request.

2.5 – COMPUTATIONAL EXPERIMENTS

2.5.1 – MOLECULAR DOCKING

To analyze ligand-receptor interactions hydrocortisone, DAC, 6, 7, and 9 were modeled in the GR LBD. The ligands were initially prepared by minimizing their energy in Chem3D (PerkinElmer), followed by docking utilizing AutoDock Vina (The Scripps Research Institute).[44] Two different GR LBD files from the Protein Data Bank (PDB) were chosen for this process by comparing the structures of both the crystallized and synthesized ligands. PDB file 3BQD is crystallized with DAC and was therefore chosen for compounds 6, 7, and 9 which all possess an aryl pyrazole moiety. PDB file 5NFP contains budesonide which lacks the aryl pyrazole moiety but is structurally similar to hydrocortisone. For this reason, 5NFP was used to dock hydrocortisone. All excess water molecules and starting compounds were removed from the GR LBD prior to docking.

2.5.2 – MOLECULAR DYNAMICS AND MMPBSA ANALYSIS

It was understood that docking studies alone would most likely not predict true ligand-protein interactions due to the flexible nature of the GR and the size differences between the crystallized ligands in 3BQD/5NFP and the synthesized compounds. Furthermore, crystallization of the GR has previously proven difficult. As a result, in order to more accurately and swiftly model these ligands in the GR LBD, molecular

dynamic (MD) simulations were performed on all ligand-protein complexes to allow each ligand to find a more realistic position within the LBP.

All compounds were simulated in the appropriate GR LBD with any cofactors removed for 100 ns using GROMACS software version 2021.5-gcc.[46] CHARMM36 force fields were used for both ligands and proteins.[47] Each system was solvated in a cubic box with TIP3P water model.[48] The protein was centered at least 1 nm away from the edge of the box and Na^+ or Cl^- ions were added to maintain a neutral system. The system's energy was minimized by subjecting it to 50,000 steps and stopped when a maximum force of 10 kJ/mol was achieved. Next, NVT and NPT equilibration were run for 50,000 steps each with the temperature kept constant at 300 K and the pressure at 1 bar. 100 ns MD simulations were conducted, and the resulting trajectories were clustered based on the protein active site. This active site was identified as all protein residues within 10 Å of the starting position of each ligand in VMD.[46, 49, 50] Gromos clustering was used based on the RMSD of the C-alpha atoms within the active site and the most central member of the most populated cluster was chosen for 3D analysis and used to determine the volume of the LBP using CASTp with a 1.4 Å radius probe.[52]

The ligand-protein binding free energies were calculated using the Molecular Mechanics Poisson-Boltzmann Surface Area (MMPBSA) approach from the trajectory files produced following MD simulation.[75] The average ligand-protein binding free energies, and the free energy decomposition which determines the contribution of each residue within 4 Å of the ligand's initial position, were calculated using the gmx_MMPBSA tool. All binding free energy calculations assumed the ligand-protein complex in an aqueous solvent ($\boldsymbol{\Delta G_{bind,aq}}$) and was determined as follows:

$$\Delta G_{bind,aq} = \Delta H - T\Delta S$$

Previous work has assumed that the enthalpy calculations are sufficient for calculating binding free energy and, therefore, the entropic term was dismissed.[76] Herein, the enthalpy term is defined as the sum of the gas phase molecular mechanical energy change (ΔE_{MM}) and the solvation free energy change ($\Delta G_{bind,solv}$)

$$\Delta H = \Delta E_{MM} + \Delta G_{bind,solv}$$

Finally, ΔE_{MM} can be broken down into the sum of the covalent ($\Delta E_{covalent}$), electrostatic ($\Delta E_{electrostatic}$), and van der Walls (ΔE_{vdW}) energy change and $\Delta G_{bind,solv}$ is the sum of the change of energy in the polar (ΔG_{polar}) and nonpolar ($\Delta G_{non-polar}$) solvation terms.

$$\Delta E_{MM} = \Delta E_{covalent} + \Delta E_{electrostatic} + \Delta E_{vdW},$$

$$\Delta G_{bind,solv} = \Delta G_{polar} + \Delta G_{non-polar}$$

2.6 – RESULTS

2.6.1 – BIOLOGICAL EVALUATION

Substitution of the C21 hydroxyl group of **HC** with a variety of mercapto-moieties resulted in compounds **1a**-**1e** (**Figure 2.2A**). **1a**'s biological activity was previously reported in detail and was shown to maintain TR potential while exhibiting a decrease in TA.[67] Here, **1c** was also shown to slightly outperform HC with a 3% higher anti-inflammatory response in the CCl2 assay. Additionally, **1c** only elicited 26% of the activity of that of **HC** in the 3xGRE assay at 100 nM while **1b**, **1d**, and **1e** all lost potency across both assays (**Figure 2.2B**). Furthermore, C17 furoyl addition to yield **2a** was previously reported to reintroduce TA potential.[67] Interestingly, this trend was preserved for mercaptobenzoxazole (**2c**) and mercaptothiazole (**2e**) substituted compounds with an increase in maximal 3xGRE activity by 1.3- and 3.2-fold, respectively. By contrast, imidazole containing compounds **2b** and **2d** exhibited no change in 3xGRE luciferase activity or CCl2 suppression with **1b** and **2b** displaying identical pIC50's of 6.4 (**Table 2.1**).

The aryl pyrazole modification increased anti-inflammatory activity in all cases. Compounds **6** and **7** only differ from the **HC** scaffold through the addition of an aryl pyrazole moiety. Interestingly, they showed the greatest increase in anti-inflammatory response, with 80-90% response at 0.1 nM concentrations while HC elicits no anti-inflammatory response at this concentration and only achieves a maximal 73.4% response at a concentration of 100 nM (**Figure 2.2B**). Additionally, **6** and **7** displayed a 4.6- and 5.5-fold over control in the 3xGRE assay at 0.1 nM, respectively.

Figure 0.69 – Derivatization of hydrocortisone induces GR modulation. (A) Structure Hydrocortisone (HC) and the synthesized derivatives used in this study. (B) GR-ligand activity in CCL2-Luc (TR) and 3xGRE-Luc (TA) assays as a percent response against hydrocortisone at 100 nM.

Table 0.13 – General Biological Analysis of CCL2 (TR) and 3xGRE (TA) Promoter Activity

	CCL2			3xGRE		
Compd	pIC_{50}	E_{max}	[b]%HC	pEC_{50}	E_{max}	[b]%HC
HC	6.5	73.5	100.0	7.3	6.5	100
[a]**1a**	6.9	77.0	104.8	5.3	1.8	27.7
1b	6.4	60.0	81.6	NDR	1.3	20.0
1c	5.7	76.3	103.4	7.3	1.7	26.2
1d	6.1	22.2	30.2	5.8	1.4	21.5
1e	5.8	46.8	63.7	5.7	1.4	21.5
2a	6.2	72.8	99.0	7.4	8.2	126.2
2b	6.4	47.7	64.9	NDR	1.3	20.0
2c	7.0	75.0	102.0	7.6	3.0	46.2
2d	6.2	37.1	50.5	NDR	1.2	18.5
2e	6.3	75.5	102.7	6.5	4.6	70.8
6	AAC	82.4	112.1	AAC	6.4	98.5
7	AAC	88.3	120.1	AAC	5.9	90.8
8a	7.2	80.2	109.1	6.3	4.1	63.1
8b	7.7	79.2	107.8	7.2	5.0	76.9
8c	7.9	82.1	111.7	7.9	2.6	40.0
8d	7.7	81.3	110.6	7.3	3.5	53.9
8e	8.6	84.9	115.5	8.0	4.6	70.8
9	7.1	78.2	106.4	6.4	4.7	72.3

[a]Selected values taken from previously published work.[36]

[b]Values represented as percentage of maximal response of hydrocortisone

AAC = Active at all concentrations

NDR = No dose-dependent response

With comparable activity, the fluorophenyl- modified structure **7** was chosen for further derivatization with mercapto- moieties since yields were greater than for **6**.

The improved potency resulting from the addition of the fluoroarylpyrazole moiety, in combination with the reduced TA observed with mercapto- modified structures, made **8a**-**8e** promising SGRMs. **8a**-**8e** outperformed **HC** in the CCl2 assay showing an 8-16% higher maximal response. **8c** displayed the highest increase in potency with a pIC_{50} of 7.9 compared to HC's pIC_{50} of 6.5. Furthermore, **8c** elicited lower TA potential than HC with an Emax of 2.6- and 6.5-fold over control, respectively. Finally, **8a** was modified with a furoyl moiety to produce **9** and examine the impact of all 3 substituents. Despite nearly doubling the molecular weight of HC from 362.5 g/mol to 723.9 g/mol, **9** did not exhibit a dramatic change in activity with only a 6.4% increase in TR activity and 17.7% decrease in TA activity when compared with HC.

Intrigued by the increase in potency of **6** and **7**, we further diluted both compounds and HC to 10^{-18} M (1 aM) and tested their response in both CCL2 and 3xGRE luciferase assays. Additionally, these three compounds were tested for their capacity to induce the transcription of GR target genes *Sgk1* and *Rgs2*. HC induced little reduction in CCL2 promoter activity at 1 aM with 19% anti-inflammatory activity (**Figure 2.3A**). However, at the same concentration, **6** and **7** retained high TR capabilities, exhibiting an 87% and 81% reduction, respectively. Likewise, at 1 aM **6** and **7** prompted a 5.2- and 4.5- fold increase in the 3xGRE assay, respectively (**Figure 2.3B**). Shockingly, the relative mRNA abundance of Sgk1 is 19- and 21-fold greater than the control at 1 aM (**Figure 2.3C**). At the same concentration, **6** and **7** also strongly induced the expression of Rgs2 mRNA abundance by 310- and 380-fold, respectively (**Figure 2.3D**). HC, 6, and 7 TR and TA activity was plotted over a concentration range of 1 aM to 1 mM and while HC displayed a gradual increase in activity, **6** and **7** maintained consistent luciferase activity and gene expression across all concentrations tested without a dose-dependent response.

Figure 0.70 – Dose-response curves of the transcriptional activities of HC, **6**, and **7**. (A) CCL2-promoter-luciferase-reporter assay. (B) 3xGRE-promoter luciferase reporter activity assay. (C) Sgk1 gene expression. (D) Rgs2 gene expression.

Synthetic GCs frequently induce unwanted side effects by acting on other NRs. For example, hydrocortisone and prednisolone have been shown to activate the mineralocorticoid receptor (MR) leading to higher blood pressure, while dexamethasone can activate the pregnane X receptor (PXR) which is associated with a loss of GC circadian rhythm, impaired stress responses, and hypertrophy of the adrenal cortex.[77-79] Therefore, highly potent GCs **6** and **7** were screened for ability to act as agonists for all 48 NRs. At 5 mM **6** and **7** induced approximately a 15.1- and 15.4- fold increase in GR activity against a DMSO control with no significant activation of any other NR (**Figure 2.4**).

2.6.2 – COMPUTATIONAL ANALYSIS

Further exploration into how these ligands interact with the LBP of the GR was carried out through a series of computational experiments. Compounds **6**, **7**, and **9** were analyzed and compared with HC and DAC to investigate the interactions that may be responsible for their unique activity. HC had the lowest average binding free energy over the 100 ns MD simulations at -36.87 kcal/mol (**Table 2.2**). **6**, **7**, and DAC all had comparable binding free energies at -45.40, -44.21 and -49.99 kcal/mol, respectively. Notably, **9**, despite inducing less GR activity, but displayed the highest binding free energy at -56.21 kcal/mol.

Interactions within the binding pocket were further probed through a decomposition analysis in which the specific energy contribution of each amino acid within 4 Å of the starting position of each ligand was determined. **9** had the most contacts in the LBP, interacting with 30 amino acids while HC only interacted with 21 (**Table 2.2**). Interestingly, M604 contributed the greatest to the binding energy of all ligands except for hydrocortisone which displays a stronger interaction with N564 (**Figure 2.5B**). Q570's energetic contribution to HC is only -0.76 kcal/mol, while all other aryl pyrazole containing compounds exhibit an interaction between -2.25 and -2.41 kcal/mol.

Figure 0.71 – Nuclear receptor agonist screening.

Table 0.14 – Binding Free Energy Contribution of Selected Residues

	Total Contacts	Total Average DH (kcal/mol)	DH N:564 (kcal/mol)	DH Q:570 (kcal/mol)	DH M:604 (kcal/mol)	DH R:611 (kcal/mol)	DH Q:642 (kcal/mol)
HC	21	-36.87	-2.181	-0.7578	-1.787	-0.04893	-1.437
DAC	24	-49.99	-1.571	-2.247	-2.759	-0.5006	-1.507
6	25	-45.40	-1.586	-2.407	-2.590	-0.4206	-1.689
7	23	-44.21	-1.485	-2.349	-2.818	-0.4846	-1.731
9	30	-56.21	-1.845	-2.343	-2.948	-0.4584	-1.416

Furthermore, R611, whose positioning has previously been implicated in LBP channel expansion, has a 10-fold weaker interaction with HC than any aryl pyrazole containing compound.[71] All of the ligand free energy decomposition values were subsequently clustered using Euclidean distance methods. This clustering analysis revealed that the interactions observed by DAC, **6**, and **7** are more similar than HC or **9** (**Figure 2.5A**). HC, DAC, **6**, and **7** were subclustered together, with **6** and **7** being the most alike. There were no interactions unique to **6** and **7** that were not found with DAC. Indeed, only MET646 exhibited a significant energetic difference, being 46% weaker in **6** and **7** than with DAC.

2.7 – DISCUSSION

GCs are critical medications for patients suffering from autoimmune disorders, allergies, asthma, and cancer.[29] The flexible nature of the GR allows it to accommodate both steroidal and non-steroidal compounds that are dramatically different from of its native ligand, cortisol.[80] However, it is still not fully understood why these ligands induce such a wide array of activity. The problem is made more complex when considering the ubiquitous nature of the GR, its capacity to elicit both TR and TA, and the number of off-target NRs that are activated by GCs. Thus, there is a need to produce a highly selective GC with sustained anti-inflammatory activity.

Systematic derivatization of hydrocortisone revealed that GR activity is readily modulated. For example, initial substitution of the C21 hydroxyl group with MBO in **1c** reduced TA activity by 73.8% at 10 μM while maintaining comparable TR potential at the same concentration. Subsequent furoyl esterification of the C17 tertiary alcohol produced **2c** and nearly doubled its 3xGRE luciferase activity. This trend was both expected and consistent with other previously published, similarly derivatized GCs.[67, 71] However, aryl pyrazole addition to hydrocortisone yielded DAC-like compounds **6** and **7** which, shockingly, resulted in both *Sgk1* and *Rgs2* gene expression at 1aM concentrations. Furthermore, these compounds accomplished the desired GR selectivity with no significant activation of any other NRs, making them potentially powerful alternatives to existing treatment options.

Figure 0.72 – Active site residue interactions between selected ligands and the GR. (A) Decomposition binding free energy values represented as a heatmap showing per-residue energy contribution for all amino acids within 4 Å of all ligands. Scale: Euclidean distance clustering method grouped ligands based on decomp raw values (kcal/mol). Black color indicates no interaction between ligand and residue. 3D representation of notable interactions between (**B**) hydrocortisone (green) and (**C**) compound **7** (magenta). Polar and non-polar interactions between the ligand and amino acids presented as orange dashed lines.

Given these initial results, we hypothesized that a GC modified with MBT, furoyl ester, and an aryl pyrazole moiety would exhibit reduced TA, be highly potent, and display high selectivity for the GR. Interestingly, compound **9**, despite being twice the molecular weight of hydrocortisone, incited similar activity to its parent molecule, showing comparable dose-response curves and pIC_{50} values of 7.1 and 6.5, respectively, in the CCL2-luc assay. These results imply that the GR must be regulated through a unique mechanism. To better understand these results, series of molecular dynamic simulations and free-energy calculations were performed to give the first view of how individual amino acid energy contributions may influence GR activity.

The average free-binding energy of hydrocortisone was lower than all other tested molecules by at least 8 kcal/mol. However, **9** had the highest average free-binding energy at -56.21 kcal/mol, thus indicating that total binding energy alone is not a good predictor of GR activity or response. A decomposition analysis provided the average energetic contribution of all amino acids within 4 Å of hydrocortisone, DAC, **6**, **7**, and **9**. Notably, hydrocortisone displays a lower average free-binding energy with all residues except for N564. This residue is known to interact with the C11 hydroxyl group of steroids and is a crucial residue in helix 3 (H3), a component of the activation function 2 (AF-2) site responsible for binding coregulators.[60] Previous studies have also shown that dehydration of the C11 hydroxyl group has resulted in maintained NF-κB inhibition and reduced TA properties.[81] As a result, we conclude that improved GR selectivity results from decreasing free-binding energy interactions with N564.

2.8 – CONCLUSION

To our knowledge, this study is the first to examine the energetic contribution of individual amino acids within the active site of the GR and compare them with a multitude of GCs which display a vast range of activity. The addition of an aryl pyrazole moiety alone to a steroidal scaffold dramatically improves its potency and selectivity. This selectivity results from decreased enthalpic contribution from N564. Furthermore, compounds **6** and **7** display high selectivity for the GR over the other 47 NRs, as well as potency in the aM region. As such, they may prove useful as anti-inflammatory candidates with reduced side-effects.

2.9 – METHODS

2.9.1 – MATERIALS

All reactions were performed under inert atmosphere. Reagents were purchased from Fisher Scientific, VWR, or Sigma Aldrich and used without further purification. Dry ethereal solvents were obtained by distillation from a potassium-benzophenone ketyl still, all other dry solvents were obtained via distillation over CaH_2. Thin-layer chromatography (TLC) was carried out using Sorbent Technologies silica G w/UV254 TLC plates. All purified compounds of interest were visualized as single spots using short-wave UV light; more permanent staining of TLC spots was achieved using vanillin. ^{1}H and ^{13}C NMR spectra were recorded on a Varian Inova 500 MHz instrument (Palo Alto, CA) in solutions of $CDCl_3$ or CD_3OD. High resolution mass spectrometry (HRMS) was performed using an Exactive™ Plus Orbitrap mass spectrometer with an ESI source operating in positive ionization mode. Optical rotation was measured using a Perkin-Elmer 241 polarimeter (Waltham, MA) equipped with a sodium source lamp. IR spectra were collected using a Thermo Scientific Nicolet™ iS5 FTIR spectrometer (Waltham, MA). All synthetic methods, annotated characterization data, including NMR spectra of final compounds, and bioassay data can be found in the appendix.

1.9.2 – SYNTHETIC PROCEDURES AND CHARACTERIZATION

General synthesis for compound 1a-e: Synthesis for compounds **1a-e** was performed following a previously published method.[10] Briefly, hydrocortisone (5 mmol) was dissolved in 100 mL dichloromethane (DCM) and cooled to 0˚C. Diisopropylethylamine (DIPEA) (4.8 mmol) was added via syringe followed by addition of mesylchloride (MsCl) (7.5 mmol). The reaction warmed to room temperature and was allowed to stir overnight (~16 hours). The reaction was concentrated *in vacuo*, before being redissolved in DCM (50 mL) and washed with saturated bicarbonate. The aqueous fraction was re-extracted with DCM (20 mL), combined organic fractions were washed twice with brine, dried with $MgSO_4$, filters, and concentrated *in vacuo* to yield a tan solid. Mesylated hydrocortisone (0.5 mmol) was dissolved in acetone to which potassium carbonate (5 mmol) and the appropriate merapto- reagent (1 mmol) was added. The

reaction was refluxed for 1 hour, filtered through a short pad of silica, and concentrated *in vacuo*.

(10*R*,11*S*,13*S*,17*R*)-17-(2-(benzo[*d*]thiazol-2-ylthio)acetyl)-11,17-dihydroxy-10,13-dimethyl-1,2,6,7,8,9,10,11,12,13,14,15,16,17-tetradecahydro-3*H*-cyclopenta[*a*]phenanthren-3-one (1a): Using commercially available mercaptobenzothiazole, compound **1a** was obtain as a white solid in 74% yield; TLC (Silica G w/UV254) R_f = 0.32, 50:50 Hex:EtOAc; ^{1}H NMR (500 MHz, Chloroform-*d*) δ 7.77 (dd, 2H), 7.43 (t, 1H), 7.34 (t, 1H), 6.01 (s, 1H), 5.73 (d, 1H), 5.04 (s, 1H), 4.53 (s, 1H), 3.52 (s, 1H), 3.27 (d, 1H), 2.90 – 2.82 (m, 1H), 2.54 – 2.36 (m, 3H), 2.29 (d, 1H), 2.21 (dd, 1H), 2.14 – 1.84 (m, 5H), 1.68 – 1.57 (m, 3H), 1.48 (s, 3H), 1.28 – 1.10 (m, 3H), 0.99 (s, 3H); HRMS (ESI) m/z: $[M+H]^+$ Calcd for $C_{28}H_{33}NO_4S_2$: 512.19238; found: 512.1927.

(10*R*,11*S*,13*S*,17*R*)-17-(2-((1*H*-benzo[*d*]imidazol-2-yl)thio)acetyl)-11,17-dihydroxy-10,13-dimethyl-1,2,6,7,8,9,10,11,12,13,14,15,16,17-tetradecahydro-3*H*-cyclopenta[*a*]phenanthren-3-one (1b): Using commercially available mercaptobenzimidizole, compound **1b** was obtain as a pale yellow solid in 72% yield; mp 210.1-212.9˚C; TLC (Silica G w/UV254) R_f = 0.12, 50:50 Hex:EtOAc; $[\alpha]_D^{20}$ = +101.4 (c 1.0, MeOH); ^{1}H NMR (500 MHz, Chloroform-*d*) δ 7.59 (d, 1H), 7.39 (s, 2H), 7.18 – 7.08 (m, 2H), 5.70 (s, 1H), 5.08 – 4.90 (m, 1H), 4.46 (s, 1H), 3.11 (d, 1H), 2.80 (ddd, 1H), 2.53 – 2.44 (m, 2H), 2.38 (t, 2H), 2.25 (d, 1H), 2.16 (d, 1H), 2.07 – 2.00 (m, 2H), 1.99 – 1.92 (m, 1H), 1.91 – 1.81 (m, 2H), 1.59 (t, 2H), 1.44 (s, 4H), 1.29 – 1.06 (m, 4H), 0.94 (s, 3H); ^{13}C NMR (500 MHz, Chloroform-*d*) δ 17.81, 21.10, 23.87, 31.51, 32.13, 32.63, 33.82, 34.42, 34.74, 35.04, 39.19, 40.75, 46.62, 52.15, 55.95, 68.61, 76.78, 77.00, 77.21, 90.95, 122.32, 122.66, 122.92, 149.81, 172.46, 199.73, 208.95; FT-IR ν_{max} (cm^{-1}): 3298 (OH), 2924 (w), 2360, 2338, 1705, 1615, 1513, 1222, 1128, 837; HRMS (ESI) m/z: $[M+H]^+$ Calcd for $C_{28}H_{34}N_2O_4S$: 495.2312; found: 495.2313.

(10*R*,11*S*,13*S*,17*R*)-17-(2-(benzo[*d*]oxazol-2-ylthio)acetyl)-11,17-dihydroxy-10,13-dimethyl-1,2,6,7,8,9,10,11,12,13,14,15,16,17-tetradecahydro-3*H*-cyclopenta[*a*]phenanthren-3-one (1c): Using commercially available mercaptobenzoxazole, compound **1c** was obtain as a tan solid in 18% yield; mp 217.7-

220.1˚C; TLC (Silica G w/UV254) R_f = 0.24, 50:50 Hex:EtOAc; $[\alpha]_D^{20}$ = +9.9 (c 1.0, MeOH); ^{1}H NMR (500 MHz, Chloroform-*d*) δ 7.51 (d, 1H), 7.44 (d, 1H), 7.29 (d, 2H), 5.74 (s, 1H), 5.70 (s, 1H), 4.94 (d, 1H), 4.51 (s, 1H), 3.27 (s, 1H), 2.83 (t, 1H), 2.53 – 2.46 (m, 2H), 2.39 – 2.35 (m, 2H), 2.29 – 2.24 (m, 1H), 2.22 – 2.18 (m, 1H), 2.09 – 2.03 (m, 2H), 1.95 – 1.86 (m, 3H), 1.65 – 1.57 (m, 2H), 1.46 (s, 4H), 1.19 (d, 1H), 1.11 (d, 1H), 1.05 (s, 1H), 0.97 (s, 3H); ^{13}C NMR (500 MHz, Chloroform-*d*) δ 17.72, 19.71, 21.11, 23.80, 29.69, 31.49, 31.95, 32.07, 32.65, 33.81, 34.66, 35.13, 35.42, 39.16, 40.65, 46.82, 52.11, 56.02, 68.59, 76.74, 76.99, 77.24, 90.84, 110.26, 117.75, 122.44, 124.51, 124.71, 140.55, 152.05, 165.24, 171.82, 199.34, 206.59; FT-IR ν_{max} (cm^{-1}): 3246 (OH), 2927 (w), 2336, 2323, 1707, 1623, 1513, 1220, 1109, 837; HRMS (ESI) m/z: $[M+H]^+$ Calcd for $C_{28}H_{33}NO_5S$: 496.21522; found: 496.2144.

(10*R*,11*S*,13*S*,17*R*)-17-(2-((1*H*-imidazol-2-yl)thio)acetyl)-11,17-dihydroxy-10,13-dimethyl-1,2,6,7,8,9,10,11,12,13,14,15,16,17-tetradecahydro-3*H*-cyclopenta[*a*]phenanthren-3-one (1d): Using commercially available mercapimidizole, compound **1d** was obtain as a white solid in 22% yield; mp 204.2-205.8˚C; TLC (Silica G w/UV254) R_f = 0.06, 50:50 Hex:EtOAc; $[\alpha]_D^{20}$ = +70.9 (c 1.0, MeOH);^{1}H NMR (500 MHz, Methanol-d_4) (exchangeable protons not observed) δ 7.04 (s, 2H), 5.65 (s, 1H), 4.38 (d, 2H), 3.91 (d, 1H), 2.75 – 2.69 (m, 1H), 2.59 – 2.45 (m, 2H), 2.33 – 2.18 (m, 3H), 2.08 – 2.00 (m, 3H), 1.91 – 1.83 (m, 1H), 1.76 (t, 2H), 1.65 (dd, 1H), 1.46 (s, 4H), 1.37 (d, 1H), 1.29 (d, 1H), 1.15 – 1.07 (m, 1H), 0.99 (dd, 1H), 0.82 (s, 3H); ^{13}C NMR (500 MHz, Methanol-d_4) δ 16.39, 19.98, 23.16, 29.23, 31.44, 31.86, 32.85, 32.92, 32.94, 33.18, 34.43, 39.28, 39.47, 41.49, 47.22, 47.40, 47.57, 51.97, 56.16, 67.28, 89.87, 115.58, 121.08, 139.34, 175.14, 201.05, 206.88, 206.93; FT-IR ν_{max} (cm^{-1}): 3520, 3137 (OH), 2974, 2941, 2873, 2648, 1357, 2331, 1694, 1615, 1575, 1381, 1229, 1084, 737; HRMS (ESI) m/z: $[M+H]^+$ Calcd for C24H32N2O4S: 445.21555; found: 445.2158.

(10*R*,11*S*,13*S*,17*R*)-11,17-dihydroxy-10,13-dimethyl-17-(2-(thiazol-2-ylthio)acetyl)-1,2,6,7,8,9,10,11,12,13,14,15,16,17-tetradecahydro-3*H*-cyclopenta[*a*]phenanthren-3-one (1e): Using commercially available mercaptothiazole, compound **1e** was obtain as a tan solid in 60% yield; mp 178.8-180˚C; TLC (Silica G w/UV254) R_f = 0.18, 50:50 Hex:EtOAc; $[\alpha]_D^{20}$ = +57.1 (c 1.0, MeOH); ^{1}H NMR (500

MHz, Chloroform-*d*) δ 7.50 (d, 1H), 7.20 (d, 1H), 5.80 (s, 1H), 5.69 (s, 1H), 4.86 (d, 1H), 4.49 (s, 1H), 3.24 (d, 1H), 2.84 – 2.75 (m, 1H), 2.50 – 2.44 (m, 2H), 2.39 – 2.30 (m, 2H), 2.27 – 2.17 (m, 2H), 2.05 (d, 2H), 1.90 – 1.82 (m, 3H), 1.61 – 1.49 (m, 2H), 1.44 (s, 4H), 1.21 – 1.07 (m, 3H), 0.94 (s, 3H); ^{13}C NMR (500 MHz, Chloroform-*d*) δ 17.74, 21.08, 23.75, 31.47, 32.07, 32.66, 33.80, 34.43, 35.09, 36.59, 39.16, 40.60, 46.73, 52.07, 56.01, 68.57, 76.74, 77.00, 77.25, 90.87, 119.31, 122.40, 141.11, 165.19, 171.97, 199.41, 207.16; FT-IR ν_{max} (cm^{-1}): 3517, 3138 (OH), 2912, 2872, 2650, 2360, 2341, 1692, 1634, 1483, 1230, 1059, 737; HRMS (ESI) m/z: $[M+H]^+$ Calcd for $C_{24}H_{31}NO_4S_2$: 462.17673; found: 462.1766.

General synthesis for compounds 2b-e and 9: Synthesis for compounds **2b-2e** was performed following a previously published method. Appropriate steroid steroid (0.406mmol) and DMAP (1.02mmol) were dissolved in CH_2Cl_2 and cooled to 0ºC. 2-furoyl chloride (0.488mmol) was added and the reaction was stirred and warmed to room temperature. After 28 h, the reaction was diluted with 10 mL CH_2Cl_2 and washed with brin (20 mL x 3). The organic layer was dried using $MgSO_4$, filtered, and concentrated *in vacuo*. The product was purified using flash chromatography (0.5% MeOH in CH_2Cl_2) to give a solid product.

(10*R*,11*S*,13*S*,17*R*)-17-(2-((1*H*-benzo[*d*]imidazol-2-yl)thio)acetyl)-11-hydroxy-10,13-dimethyl-3-oxo-2,3,6,7,8,9,10,11,12,13,14,15,16,17-tetradecahydro-1*H*-cyclopenta[*a*]phenanthren-17-yl furan-2-carboxylate (2b): white solid obtained in 6% yield; mp 180.6-187.8ºC; TLC (Silica G w/UV254) R_f = 0.34, 10:1 CH_2Cl_2:MeOH; $[\alpha]_D^{20}$ = +2.8 (c 0.5, MeOH); ^{1}H NMR (500 MHz, Methanol-*d*$_4$) δ 7.83 (s, 1H), 7.63 (d, *J* = 3.7 Hz, 1H), 7.37 (dd, *J* = 6.0, 3.3 Hz, 2H), 7.16 (dd, *J* = 6.1, 3.2 Hz, 2H), 6.65 (d, *J* = 2.0 Hz, 1H), 5.58 (s, 1H), 4.27 – 4.02 (m, 2H), 2.50 (td, *J* = 13.8, 5.3 Hz, 1H), 2.44 – 2.31 (m, 2H), 2.25 – 2.17 (m, 2H), 2.15 – 2.11 (m, 1H), 2.11 – 2.07 (m, 1H), 2.03 (d, *J* = 8.5 Hz, 1H), 1.96 (d, *J* = 7.0 Hz, 1H), 1.93 (d, *J* = 11.3 Hz, 1H), 1.81 – 1.71 (m, 2H), 1.59 (dd, *J* = 11.7, 6.1 Hz, 1H), 1.53 – 1.45 (m, 2H), 1.42 (d, *J* = 12.2 Hz, 1H), 1.38 (s, 2H), 1.19 (s, 4H), 1.14 (s, 2H), 0.96 (dd, *J* = 10.9, 3.7 Hz, 1H), 0.80 (t, *J* = 6.7 Hz, 1H); ^{13}C NMR (126 MHz, Methanol-*d*$_4$) δ 201.01, 199.45, 174.78, 148.73, 143.51, 123.12, 121.23, 120.44, 113.35, 112.98, 101.20, 96.92, 85.92, 66.84, 55.90, 53.81, 50.58, 48.22,

48.11, 48.05, 47.94, 47.88, 47.77, 47.60, 47.43, 47.25, 47.09, 39.33, 38.56, 34.38, 33.19, 32.81, 32.56, 31.80, 31.61, 29.16, 25.00, 24.24, 19.96, 14.80; FT-IR ν_{max} (cm^{-1}): 3384 (OH), 2927, 1653, 758 ; HRMS (ESI) m/z: $[M+H]^+$ Calcd for $C_{33}H_{36}N_2O_6S$, 589.2372; found 589.2368.

(10*R*,11*S*,13*S*,17*R*)-17-(2-(benzo[*d*]oxazol-2-ylthio)acetyl)-11-hydroxy-10,13-dimethyl-3-oxo-2,3,6,7,8,9,10,11,12,13,14,15,16,17-tetradecahydro-1*H*-cyclopenta[*a*]phenanthren-17-yl furan-2-carboxylate (2c): white solid obtained in 7% yield; mp 176.9-177.9ºC; TLC (Silica G w/UV254) R_f = 0.43, 10:1 CH_2Cl_2:MeOH; $[\alpha]_D^{20}$ = +102.4 (c 0.5, CH_2Cl_2); ^{1}H NMR (500 MHz, Chloroform-*d*) δ 7.63 (s, 1H), 7.58 – 7.51 (m, 1H), 7.47 – 7.39 (m, 1H), 7.30 – 7.26 (m, 2H), 7.24 (d, *J* = 3.5 Hz, 1H), 6.56 (dd, *J* = 3.5, 1.7 Hz, 1H), 5.72 (s, 1H), 4.62 – 4.52 (m, 2H), 4.37 (d, *J* = 17.1 Hz, 1H), 3.13 – 3.03 (m, 1H), 2.52 (td, *J* = 15.3, 4.9 Hz, 2H), 2.44 – 2.33 (m, 2H), 2.30 – 2.22 (m, 2H), 2.14 (dd, *J* = 10.9, 3.8 Hz, 1H), 2.11 – 2.06 (m, 2H), 2.03 (s, 1H), 1.95 (ddd, *J* = 18.1, 11.5, 5.4 Hz, 2H), 1.87 – 1.80 (m, 2H), 1.52 (dd, *J* = 11.2, 6.7 Hz, 1H), 1.48 (s, 3H), 1.25 (s, 1H), 1.14 (dd, *J* = 11.3, 3.2 Hz, 1H), 1.08 (s, 3H); ^{13}C NMR (126 MHz, Chloroform-*d*) δ 199.45, 198.58, 171.71, 164.36, 158.16, 151.99, 147.22, 144.01, 141.35, 124.45, 124.18, 122.54, 119.56, 118.17, 112.23, 110.11, 96.24, 77.27, 77.02, 76.76, 68.28, 56.03, 52.91, 47.41, 41.44, 40.42, 39.27, 35.04, 33.85, 32.65, 31.98, 31.53, 31.23, 23.92, 21.01, 16.74; FT-IR ν_{max} (cm^{-1}): 3428 (OH), 2931, 1654, 744; HRMS (ESI) m/z: $[M+H]^+$ Calcd for $C_{33}H_{35}NO_7S$, 590.2213; found 590.2206.

(10*R*,11*S*,13*S*,17*R*)-17-(2-((1*H*-imidazol-2-yl)thio)acetyl)-11-hydroxy-10,13-dimethyl-3-oxo-2,3,6,7,8,9,10,11,12,13,14,15,16,17-tetradecahydro-1*H*-cyclopenta[*a*]phenanthren-17-yl furan-2-carboxylate (2d): tan solid obtained in 10% yield; mp 180.4-187.8ºC; TLC (Silica G w/UV254) R_f = 0.28, 10:1 CH_2Cl_2:MeOH; $[\alpha]_D^{20}$ = -29.2 (c 0.5, CH_2Cl_2); ^{1}H NMR (500 MHz, Chloroform-*d*) δ 7.88 (d, *J* = 3.5 Hz, 1H), 7.75 (s, 1H), 7.08 (s, 2H), 6.67 (dd, *J* = 3.6, 1.6 Hz, 1H), 5.67 (s, 1H), 4.36 (d, *J* = 3.0 Hz, 1H), 2.51 – 2.45 (m, 1H), 2.44 – 2.35 (m, 2H), 2.31 (d, *J* = 4.2 Hz, 1H), 2.29 – 2.22 (m, 2H), 2.14 (d, *J* = 10.2 Hz, 2H), 2.03 – 1.98 (m, 2H), 1.81 (td, *J* = 13.7, 4.7 Hz, 2H), 1.73 (dd, *J* = 10.8, 6.7 Hz, 1H), 1.60 (dt, *J* = 11.8, 5.9 Hz, 1H), 1.54 – 1.47 (m, 2H), 1.46 (s, 1H), 1.43 (s, 3H), 1.26 (d, *J* = 14.0 Hz, 2H), 1.22 (s, 3H), 1.00 (dd, *J* = 11.2, 3.2

Hz, 1H), 0.89 – 0.86 (m, 1H); ^{13}C NMR (126 MHz, Chloroform-*d*) δ 199.55, 171.88, 170.97, 147.95, 143.09, 123.63, 122.44, 121.62, 113.33, 100.95, 77.27, 77.02, 76.76, 74.47, 69.15, 67.76, 62.30, 61.99, 55.74, 53.76, 50.59, 39.26, 34.86, 34.13, 32.68, 31.65, 29.50, 25.27, 24.77, 20.93, 15.93, 14.05; FT-IR ν_{max} (cm^{-1}): 3338 (OH), 2928, 1664, 758; HRMS (ESI) m/z: $[M+H]^+$ Calcd for $C_{29}H_{34}N_2O_6S$, 539.2216; found 539.2204.

(10*R*,11*S*,13*S*,17*R*)-11-hydroxy-10,13-dimethyl-3-oxo-17-(2-(thiazol-2-ylthio)acetyl)-2,3,6,7,8,9,10,11,12,13,14,15,16,17-tetradecahydro-1*H*-cyclopenta[*a*]phenanthren-17-yl furan-2-carboxylate (2e): white solid obtained in 46% yield; mp 1169.1-169.6ºC; TLC (Silica G w/UV254) R_f = 0.34, 10:1 CH_2Cl_2:MeOH; $[\alpha]_D^{20}$ = +88.9 (c 0.505, CH_2Cl_2); ^{1}H NMR (500 MHz, Chloroform-*d*) δ 7.62 (dd, *J* = 2.1, 1.3 Hz, 2H), 7.24 (d, *J* = 3.4 Hz, 1H), 7.22 (dd, *J* = 3.5, 0.8 Hz, 1H), 6.54 (dd, *J* = 3.5, 1.7 Hz, 1H), 5.70 (s, 1H), 4.58 – 4.51 (m, 2H), 4.25 (d, *J* = 17.0 Hz, 1H), 3.08 – 2.99 (m, 1H), 2.54 – 2.45 (m, 2H), 2.42 – 2.35 (m, 1H), 2.31 – 2.20 (m, 3H), 2.12 (td, *J* = 10.7, 3.7 Hz, 1H), 2.08 – 2.04 (m, 1H), 2.04 – 1.98 (m, 1H), 1.97 – 1.88 (m, 2H), 1.85 – 1.74 (m, 2H), 1.49 (d, *J* = 6.8 Hz, 1H), 1.46 (s, 3H), 1.25 (s, 1H), 1.16 (td, *J* = 13.5, 4.3 Hz, 1H), 1.10 (dd, *J* = 11.3, 3.3 Hz, 1H), 1.00 (s, 3H); ^{13}C NMR (126 MHz, Chloroform-*d*) δ 199.53, 198.41, 171.78, 158.19, 156.60, 147.32, 143.87, 139.37, 122.51, 120.31, 119.64, 112.25, 96.61, 77.27, 77.01, 76.76, 68.14, 55.98, 53.14, 47.15, 43.13, 39.94, 39.32, 34.92, 33.89, 32.70, 32.01, 31.77, 31.19, 24.04, 20.82, 16.55; FT-IR ν_{max} (cm^{-1}): 3367 (OH), 2926, 1653, 758.42; HRMS (ESI) m/z: $[M+H]^+$ Calcd for C29H33NO6S2, 556.1828; found 556.1821.

(10*R*,11*S*,13*S*)-11-hydroxy-10,13-dimethyl-1,6,7,8,9,10,11,12,13,14,15,16-dodecahydrodispiro[cyclopenta[*a*]phenanthrene-17,4'-[1,3]dioxolane-5',4''-[1,3]dioxolan]-3(2*H*)-one (3): Hydrocortisone (2.5 g, 4 mmol) and trioxane (3.1 g, 34.5 mmol) were added to round bottom flask and dissolved in 50 mL of chloroform. Concentrated HCl (5 mL) was added, and the reaction stirred vigorously at room temperature for 4 hours. The reaction was diluted with chloroform (100 mL) and washed with water, saturated sodium bicarbonate, and brine. The organic layer was dried with $MgSO_4$, filter, and concentrated *in vacuo* to yield a white powder. The crude product was purified using flash chromatography (75% diethyl ether/hexanes) and obtained as a white

powder in 86% yield. TLC (Silica G w/UV254) R_f = 0.55, 100% diethyl ether; ^{1}H NMR (500 MHz, Chloroform-*d*) δ 5.67 (d, 1H), 5.22 (s, 1H), 5.06 – 5.00 (m, 3H), 4.42 (p, 1H), 3.99 (q, 2H), 2.52 – 2.42 (m, 2H), 2.35 (dt, 1H), 2.26 – 2.16 (m, 2H), 2.11 – 1.96 (m, 4H), 1.90 – 1.82 (m, 2H), 1.77 – 1.71 (m, 2H), 1.67 – 1.62 (m, 1H), 1.44 (s, 4H), 1.12 (s, 3H), 1.03 – 0.99 (m, 1H); HRMS (ESI) m/z: $[M+H]^+$ Calcd for $C_{23}H_{32}O_6$: 405.2272; found: 405.2277.

(10*R*,11*S*,13*S*)-11-hydroxy-2-(hydroxymethylene)-10,13-dimethyl-1,6,7,8,9,10,11,12,13,14,15,16-dodecahydrodispiro[cyclopenta[*a*]phenanthrene-17,4'-[1,3]dioxolane-5',4''-[1,3]dioxolan]-3(2*H*)-one (4): Compound **3** (2.05 g, 5 mmol) and NaH (60% dispersed in mineral oil) (2.1 g, 52.5 mmol) were added to a round bottom flask and dissolved in dry toluene (40 mL). The reaction was allowed to stir for one hour before adding freshly distilled ethyl formate (4.1 mL, 40 mmol) via syringe. After stirring 24 hours, the reaction was slowly acidified with 4N HCl (50 mL) and extracted with DCM until no more color transfer was observed (20 mL X 5). The organic fractions were combined and concentrated *in vacuo*. The remaining residue was redissolved in DCM (20 mL) and extracted with 1N NaOH until no color transfer was observed (20 mL X 6). The combined aqueous fractions were acidified with conc. HCl and subsequently re-extracted with DCM (30 mL X 5). The organic fractions were washed with brine, dried with $MgSO_4$, filtered, and concentrated *in vacuo* to obtain a yellow solid in 89% yield. The product was pushed to the next step without purification. ^{1}H NMR (500 MHz, Chloroform-*d*) δ 7.37 (s, 1H), 5.73 (d, 1H), 5.22 (d, 1H), 5.04 – 5.01 (m, 3H), 3.99 (d, 2H), 2.52 – 2.42 (m, 3H), 2.34 – 2.24 (m, 2H), 2.00 – 1.96 (m, 3H), 1.87 – 1.84 (m, 1H), 1.77 – 1.73 (m, 3H), 1.67 – 1.65 (m, 1H), 1.46 – 1.38 (m, 3H), 1.33 (d, 3H), 1.26 (d, 1H), 1.12 (s, 4H); HRMS (ESI) m/z: $[M+H]^+$ Calcd for $C_{24}H_{32}O_7$: 433.2221; found: 433.2229.

(10a*R*,11*S*,12a*S*)-7-(4-fluorophenyl)-10a,12a-dimethyl 3,3a,3b,4,5,7,10,10a,10b,11,12,12a-dodecahydro-2*H*-dispiro[cyclopenta[5,6]naphtho[1,2-*f*]indazole-1,4'-[1,3]dioxolane-5',4''-[1,3]dioxolan]-11-ol (5): 4-fluorophenyl hydrazine hydrochloride (0.28 g, 1.7 mmol) and sodium acetate (0.14 g, 1.7 mmol) were stirred in 10 mL H_2O and 5 mL glacial acetic acid. Once dissolved, this mixture was added to compound **4** (0.50 g, 1.1 mmol) in a

solution of glacial acetic acid (20 mL) and stirred for 24 hours. The reaction was diluted with 1N HCl **(**100 mL) and extracted with DCM (3 x 50 mL). The organic extracts were combined and washed with saturated sodium bicarbonate (50 mL), brine (50 mL), dried with $MgSO_4$, filtered, and concentrated *in vacuo* to obtain compound 4 as a brown solid. The crude compound was purified using flash chromatography (30% ethyl acetate/hexanes) from which the purified product was obtained as an orange solid in 63% yield. ^{1}H NMR (500 MHz, Chloroform-*d*) δ 7.45 (ddd, 3H), 7.17 – 7.11 (m, 2H), 6.05 (d, 1H), 5.25 – 5.12 (m, 2H), 5.08 – 5.00 (m, 2H), 4.43 (dq, 1H), 4.07 – 3.86 (m, 2H), 2.99 (dd, 1H), 2.67 (d, 1H), 2.54 – 2.44 (m, 1H), 2.27 (ddt, 1H), 2.13 – 2.05 (m, 1H), 2.02 – 1.89 (m, 3H), 1.88 – 1.81 (m, 1H), 1.80 – 1.65 (m, 3H), 1.50 – 1.34 (m, 2H), 1.32 (d, 3H), 1.24 – 1.16 (m, 1H), 1.12 (d, 4H); HRMS (ESI) m/z: $[M+H]^+$ Calcd for $C_{30}H_{35}FN_2O_5$: 523.2603; found: 523.2612.

1-((1*R*,10a*R*,11*S*,12a*S*)-7-(4-fluorophenyl)-1,11-dihydroxy-10a,12a-dimethyl-1,2,3,3a,3b,4,5,7,10,10a,10b,11,12,12a-tetradecahydrocyclopenta[5,6]naphtho[1,2-*f*]indazol-1-yl)-2-hydroxyethan-1-one (6): Compound **5** (0.83 g, 1.6 mmol) was dissolved in 50% formic acid (50 mL) and gently refluxed for 40 minutes. The reaction was diluted with water (10 mL) and extracted with DCM (3 x 25 mL). The combined organic fractions were washed with saturated sodium bicarbonate (20 mL), brine (20 mL), dried with $MgSO_4$, filtered, and concentrated *in vacuo* to obtain a yellow solid. The crude compound was purified using flash chromatography (3% MeOH/DCM) from which the purified product was obtained as a tan solid in 47% yield. ^{1}H NMR (500 MHz, Chloroform-*d*) δ 7.45 (dd, 2H), 7.40 (s, 1H), 7.15 (t, 2H), 6.06 (s, 1H), 4.66 (dd, 1H), 4.53 (s, 1H), 4.32 (dd, 1H), 3.08 (t, 1H), 2.99 (d, 1H), 2.75 – 2.70 (m, 1H), 2.68 (d, 1H), 2.48 (d, 1H), 2.28 (d, 1H), 2.04 – 1.93 (m, 3H), 1.91 – 1.86 (m, 1H), 1.78 – 1.71 (m, 1H), 1.58 (d, 2H), 1.31 (s, 3H), 1.24 (d, 2H), 1.13 – 1.05 (m, 2H), 0.97 (s, 3H); HRMS (ESI) m/z: $[M+H]^+$ Calcd for $C_{28}H_{33}FN_2O_4$: 481.24971; found: 481.2499.

1-((1*R*,10a*R*,11*S*,12a*S*)-1,11-dihydroxy-10a,12a-dimethyl-7-phenyl-1,2,3,3a,3b,4,5,7,10,10a,10b,11,12,12a-tetradecahydrocyclopenta[5,6]naphtho[1,2-*f*]indazol-1-yl)-2-hydroxyethan-1-one (7): Phenyl hydrazine hydrochloride (0.28 mL, 2.7 mmol) and sodium acetate (0.23 g, 2.7 mmol) were stirred in 10 mL H_2O and 5 mL

glacial acetic acid. Once dissolved, this mixture was added to compound **4** (0.8 g, 1.8 mmol) in a solution of glacial acetic acid (20 mL) and stirred for 24 hours. The reaction was diluted with 1N HCl (100 mL) and extracted with DCM (3 x 50 mL). The organic extracts were combined and washed with saturated sodium bicarbonate (50 mL), brine (50 mL), dried with $MgSO_4$, filtered, and concentrated *in vacuo* to obtain the crude product as a brown solid. The crude compound was purified using flash chromatography (30% ethyl acetate/hexanes) from which the purified product was obtained as an orange solid in 57% yield.

The purified product was dissolved in 50% formic acid (50 mL) and gently refluxed for 40 minutes. The reaction was diluted with water (10 mL) and extracted with DCM (3 x 25 mL). The combined organic fractions were washed with saturated sodium bicarbonate (20 mL), brine (20 mL), dried with $MgSO_4$, filtered, and concentrated *in vacuo* to obtain a yellow solid. The crude compound was purified using flash chromatography (3% MeOH/DCM) from which the purified product was obtained as a tan solid in 31% yield. ^{1}H NMR (500 MHz, Chloroform-*d*) δ 7.52 – 7.29 (m, 6H), 6.14 (d, 1H), 4.66 (d, 1H), 4.54 (s, 1H), 4.32 (d, 1H), 3.15 – 2.90 (m, 2H), 2.78 – 2.66 (m, 2H), 2.49 (t, 1H), 2.28 (d, 1H), 2.04 – 1.83 (m, 4H), 1.79 – 1.71 (m, 1H), 1.58 (d, 1H), 1.42 (s, 1H), 1.31 (d, 3H), 1.26 (t, 3H), 1.16 – 1.05 (m, 2H), 0.94 (d, 3H); HRMS (ESI) m/z: $[M+H]^+$ Calcd for $C_{28}H_{34}N_2O_4$: 463.2591; found: 463.2607.

General synthesis for compound 8a-e: Synthesis for compounds **7a-e** was performed following a previously published method.[74] Briefly, compound **5** (2 mmol) was dissolved in 100 mL dichloromethane (DCM) and cooled to 0˚C. Diisopropylethylamine (DIPEA) (1.9 mmol) was added via syringe followed by addition of mesylchloride (MsCl) (3 mmol). The reaction warmed to room temperature and was allowed to stir overnight (~16 hours). The reaction was concentrated *in vacuo*, before being redissolved in DCM (50 mL) and washed with saturated bicarbonate. The aqueous fraction was re-extracted with DCM (20 mL), combined organic fractions were washed twice with brine, dried with $MgSO_4$, filters, and concentrated *in vacuo* to yield a tan solid. Mesylated aryl pyrazole hydrocortisone (0.5 mmol) was dissolved in acetone to which potassium carbonate (5 mmol) and the appropriate merapto- reagent (1 mmol) was

added. The reaction was refluxed for 1 hour, filtered through a short pad of silica, and concentrated *in vacuo*.

2-(benzo[*d*]thiazol-2-ylthio)-1-((1*R*,10a*R*,11*S*,12a*S*)-7-(4-fluorophenyl)-1,11-dihydroxy-10a,12a-dimethyl-1,2,3,3a,3b,4,5,7,10,10a,10b,11,12,12a-tetradecahydrocyclopenta[5,6]naphtho[1,2-*f*]indazol-1-yl)ethan-1-one (8a): Using commercially available mercaptobenzothiazole, compound **7a** was obtain as a white solid in 35% yield. TLC (Silica G w/UV254) R_f = 0.41, 50:50 Hex:EtOAc; ^{1}H NMR (500 MHz, Chloroform-*d*) δ 7.75 (dd, 2H), 7.49 – 7.43 (m, 2H), 7.40 (d, 2H), 7.33 – 7.28 (m, 1H), 7.16 (t, 2H), 6.07 (s, 1H), 5.96 (s, 1H), 5.01 (d, 1H), 4.56 (s, 1H), 3.26 (d, 1H), 3.00 (d, 1H), 2.85 (t, 1H), 2.70 (d, 1H), 2.50 (t, 1H), 2.40 (d, 1H), 2.30 (d, 1H), 2.04 – 1.90 (m, 4H), 1.68 (d, 1H), 1.61 – 1.57 (m, 1H), 1.48 – 1.40 (m, 1H), 1.33 (s, 4H), 1.17 (d, 2H), 0.98 (s, 3H); HRMS (ESI) m/z: $[M+H]^+$ Calcd for $C_{35}H_{36}FN_3O_3S_2$: 630.22549; found: 630.2253.

2-((1*H*-benzo[*d*]imidazol-2-yl)thio)-1-((1*R*,10a*R*,11*S*,12a*S*)-7-(4-fluorophenyl)-1,11-dihydroxy-10a,12a-dimethyl-1,2,3,3a,3b,4,5,7,10,10a,10b,11,12,12a-tetradecahydrocyclopenta[5,6]naphtho[1,2-*f*]indazol-1-yl)ethan-1-one (8b): Using commercially available mercaptobenzimidizole, compound **7b** was obtain as an off white solid in 16% yield; mp 225.8-226.9˚C; TLC (Silica G w/UV254) R_f = 0.13, 50:50 Hex:EtOAc; $[\alpha]_D^{20}$ = +80.4 (c 1.0, MeOH); ^{1}H NMR (500 MHz, Chloroform-*d*) δ 9.11 (s, 1H), 7.48 – 7.45 (m, 2H), 7.42 (s, 1H), 7.20 – 7.12 (m, 4H), 6.07 (d, 1H), 5.02 (d, 1H), 4.56 (s, 1H), 3.04 (dd, 2H), 2.81 (t, 1H), 2.70 (d, 1H), 2.48 (dd, 2H), 2.30 (d, 1H), 2.05 – 1.89 (m, 4H), 1.66 – 1.52 (m, 3H), 1.43 (d, 1H), 1.33 (s, 5H), 1.27 – 1.07 (m, 3H), 0.96 (s, 3H); ^{13}C NMR (500 MHz, Chloroform-*d*) δ 17.97, 22.40, 24.00, 31.84, 32.13, 32.15, 34.07, 34.16, 34.76, 40.87, 41.40, 46.65, 52.46, 56.65, 60.39, 68.73, 76.74, 76.99, 77.25, 91.05, 107.55, 113.79, 115.92, 116.10, 123.52, 125.39, 125.46, 135.87, 136.95, 137.89, 149.83, 151.82, 160.47, 162.43, 208.76; FT-IR ν_{max} (cm^{-1}): 3190 (OH), 2932 (w), 2356, 2325, 1705, 1615, 1513, 1439, 1223, 1109, 837; HRMS (ESI) m/z: $[M+H]^+$ Calcd for $C_{35}H_{37}FN_4O_3S$: 613.26432; found: 613.2646.

2-(benzo[*d*]oxazol-2-ylthio)-1-((1*R*,10a*R*,11*S*,12a*S*)-7-(4-fluorophenyl)-1,11-dihydroxy-10a,12a-dimethyl-1,2,3,3a,3b,4,5,7,10,10a,10b,11,12,12a-

tetradecahydrocyclopenta[5,6]naphtho[1,2-*f*]indazol-1-yl)ethan-1-one (8c): Using commercially available mercaptobenzoxazole, compound **7c** was obtain as an off white solid in 44% yield; mp 186.9-188.2˚C; TLC (Silica G w/UV254) R_f = 0.42, 50:50 Hex:EtOAc; $[\alpha]_D^{20}$ = +123.0 (c 1.0, MeOH); ^{1}H NMR (500 MHz, Chloroform-*d*) δ 7.51 (d, 1H), 7.46 (s, 3H), 7.41 (s, 1H), 7.27 (s, 2H), 7.16 (d, 2H), 6.07 (s, 1H), 5.80 (s, 1H), 4.96 (d, 1H), 4.56 (s, 1H), 3.29 (d, 1H), 3.00 (d, 1H), 2.87 – 2.81 (m, 1H), 2.70 (d, 1H), 2.51 (d, 1H), 2.38 (d, 1H), 2.31 (s, 1H), 2.05 – 1.96 (m, 3H), 1.93 (d, 1H), 1.68 (d, 1H), 1.57 (t, 1H), 1.49 – 1.41 (m, 1H), 1.32 (s, 4H), 1.18 (s, 1H), 1.12 (s, 1H), 0.98 (s, 3H); ^{13}C NMR (500 MHz, Chloroform-*d*) δ 17.85, 22.40, 23.92, 31.80, 32.11, 32.18, 34.07, 34.63, 35.48, 40.69, 41.41, 46.88, 52.42, 56.69, 68.63, 76.78, 76.99, 77.20, 89.82, 90.95, 107.62, 110.26, 113.76, 115.92, 116.07, 117.75, 124.49, 124.70, 125.36, 125.42, 130.83, 136.85, 137.90, 140.57, 151.59, 152.05, 165.29, 206.58; FT-IR ν_{max} (cm^{-1}): 3309 (OH), 2919, 2360, 2322, 1705, 1615, 1513, 1452, 1218, 1130, 836; HRMS (ESI) m/z: $[M+H]^+$ Calcd for $C_{35}H_{36}FN_3O_4S$: 614.24833; found: 614.2481.

2-((1*H*-imidazol-2-yl)thio)-1-((1*R*,10a*R*,11*S*,12a*S*)-7-(4-fluorophenyl)-1,11-dihydroxy-10a,12a-dimethyl-1,2,3,3a,3b,4,5,7,10,10a,10b,11,12,12a-tetradecahydrocyclopenta[5,6]naphtho[1,2-*f*]indazol-1-yl)ethan-1-one (8d): Using commercially available mercapimidizole, compound **7d** was obtain as a white solid in 56% yield; mp 188.4-190.1˚C; TLC (Silica G w/UV254) R_f = 0.04, 50:50 Hex:EtOAc; $[\alpha]_D^{20}$ = +96.6 (c 1.0, MeOH); ^{1}H NMR (500 MHz, Chloroform-*d*) δ 9.00 (s, 1H), 7.46 (dd, 2H), 7.41 (s, 1H), 7.17 – 7.13 (m, 2H), 6.95 (s, 2H), 6.06 (d, 1H), 4.77 (d, 1H), 4.53 (s, 1H), 3.06 (d, 1H), 2.99 (d, 1H), 2.79 (t, 1H), 2.69 (d, 1H), 2.53 – 2.45 (m, 1H), 2.38 (d, 1H), 2.28 (d, 1H), 2.00 – 1.86 (m, 4H), 1.59 (d, 1H), 1.57 – 1.50 (m, 2H), 1.44 – 1.37 (m, 1H), 1.31 (s, 3H), 1.17 – 1.09 (m, 2H), 0.92 (s, 3H); ^{13}C NMR (500 MHz, Chloroform-*d*) δ 17.91, 22.37, 23.87, 32.15, 34.36, 35.05, 40.79, 41.39, 46.69, 52.37, 56.68, 68.67, 76.74, 76.99, 77.25, 90.74, 107.55, 113.79, 116.08, 125.36, 125.43, 136.89, 137.89, 140.73, 151.73, 208.99; FT-IR ν_{max} (cm^{-1}): 3307 (OH), 2922, 2360, 2323, 1705, 1615, 1513, 1220, 1109, 836; HRMS (ESI) m/z: $[M+H]^+$ Calcd for $C_{31}H_{34}FN_3O_3S_2$: 563.24867; found: 563.2489.

1-((1*R*,10a*R*,11*S*,12a*S*)-7-(4-fluorophenyl)-1,11-dihydroxy-10a,12a-dimethyl-1,2,3,3a,3b,4,5,7,10,10a,10b,11,12,12a-tetradecahydrocyclopenta[5,6]naphtho[1,2-*f*]indazol-1-yl)-2-(thiazol-2-ylthio)ethan-1-one (8e): Using commercially available mercaptothiazole, compound **7e** was obtain as a white solid in 29% yield; mp 138.7-140.5˚C; TLC (Silica G w/UV254) R_f = 0.25, 50:50 Hex:EtOAc; $[\alpha]_D^{20}$ = +113.0 (c 1.0, MeOH); ^{1}H NMR (500 MHz, Chloroform-*d*) δ 7.50 (d, 1H), 7.46 (dd, 2H), 7.41 (s, 1H), 7.20 (d, 1H), 7.15 (t, 2H), 6.06 (s, 1H), 5.89 (s, 1H), 4.88 (d, 1H), 4.53 (s, 1H), 3.23 (d, 1H), 2.99 (d, 1H), 2.85 – 2.78 (m, 1H), 2.69 (d, 1H), 2.54 – 2.46 (m, 1H), 2.35 (d, 1H), 2.28 (d, 1H), 2.02 – 1.87 (m, 4H), 1.64 (d, 1H), 1.51 (d, 1H), 1.47 – 1.39 (m, 1H), 1.32 (s, 3H), 1.30 – 1.20 (m, 2H), 1.19 – 1.12 (m, 1H), 1.10 (d, 1H), 0.95 (s, 3H); ^{13}C NMR (500 MHz, Chloroform-*d*) δ 17.90, 22.38, 23.86, 32.18, 34.06, 34.40, 36.52, 40.69, 41.40, 46.78, 52.37, 56.69, 68.63, 76.74, 76.99, 77.24, 90.99, 107.60, 113.77, 116.07, 119.28, 125.34, 125.41, 136.84, 137.90, 141.08, 151.60, 160.44, 165.28, 207.16; FT-IR ν_{max} (cm^{-1}): 3318 (OH), 2920, 2358, 2339, 1705, 1615, 1513, 1222, 1109, 836; HRMS (ESI) m/z: $[M+H]^+$ Calcd for $C_{31}H_{35}FN_4O_3S$: 580.20984; found: 580.2097.

(1*R*,10a*R*,11*S*,12a*S*)-1-(2-(benzo[*d*]thiazol-2-ylthio)acetyl)-7-(4-fluorophenyl)-11-hydroxy-10a,12a-dimethyl-1,2,3,3a,3b,4,5,7,10,10a,10b,11,12,12a-tetradecahydrocyclopenta[5,6]naphtho[1,2-*f*]indazol-1-yl furan-2-carboxylate (9): white solid obtained in 60% yield; mp 125.0-131.1˚C; TLC (Silica G w/UV254) R_f = 0.51, 10:1 CH_2Cl_2:MeOH; $[\alpha]_D^{20}$ = +108.6 (c 0.521, CH_2Cl_2); ^{1}H NMR (500 MHz, Chloroform-*d*) δ 7.80 (d, *J* = 7.5 Hz, 1H), 7.74 (d, *J* = 8.1 Hz, 1H), 7.62 (s, 1H), 7.49 – 7.43 (m, 3H), 7.41 – 7.37 (m, 1H), 7.29 (t, *J* = 7.0 Hz, 1H), 7.24 (d, *J* = 3.5 Hz, 1H), 7.19 – 7.14 (m, 2H), 6.54 (dd, *J* = 3.5, 1.8 Hz, 1H), 6.09 (s, 1H), 4.65 (s, 1H), 4.62 (d, *J* = 17.1 Hz, 1H), 4.37 (d, *J* = 17.1 Hz, 1H), 3.10 (d, *J* = 11.1 Hz, 1H), 3.05 (d, *J* = 15.3 Hz, 1H), 2.79 (d, *J* = 14.5 Hz, 1H), 2.52 (t, *J* = 13.4 Hz, 1H), 2.39 (dd, *J* = 14.1, 3.9 Hz, 1H), 2.35 – 2.26 (m, 1H), 2.14 (dd, *J* = 13.9, 2.8 Hz, 1H), 2.08 (dd, *J* = 10.8, 3.6 Hz, 1H), 2.00 (dd, *J* = 15.6, 6.5 Hz, 2H), 1.91 – 1.79 (m, 2H), 1.38 (d, *J* = 3.3 Hz, 1H), 1.36 (s, 3H), 1.26 (s, 3H), 1.10 (s, 3H); ^{13}C NMR (126 MHz, Chloroform-*d*) δ 198.64, 165.65, 162.51, 160.55, 158.15, 152.76, 151.63, 147.11, 144.17, 137.83, 136.88, 135.67, 126.05, 125.47, 125.41, 124.39, 121.30, 121.16, 119.34, 116.17, 115.99, 113.79, 112.16, 107.63, 96.67, 77.27,

77.01, 76.76, 68.37, 56.76, 53.23, 47.47, 41.51, 40.53, 34.01, 32.22, 32.12, 31.74, 31.19, 29.70, 24.01, 22.52, 16.89; FT-IR ν_{max} (cm^{-1}): 3499 (OH), 2921, 1707, 1514, 1308, 1228, 1016, 756, 427; HRMS (ESI) m/z: $[M+H]^+$ Calcd for $C_{40}H_{38}FN_3O_5S_2$: 724.2315; found: 724.2310.

APPENDIX

2.10.1 – ^{1}H NMR AND ^{13}C NMR SPECTRA

Figure 0.73 – ^{1}H NMR of **1a**

Figure 0.74 – ^{1}H NMR of **1b**

Figure 0.75 – ^{13}C NMR of **1b**

Figure 0.76 – ^{1}H NMR of **1c**

Figure 0.77 – ^{13}C NMR of **1c**

Figure 0.78 – ^{1}H NMR of **1d**

Figure 0.79 – ^{13}C NMR of **1d**

Figure 0.80 – ^{1}H NMR of **1d**

Figure 0.81 – ^{13}C NMR of **1e**

Figure 0.82 – ^{1}H NMR of **2b**

Figure 0.83 – ^{13}C NMR of **2b**

Figure 0.84 – ^{1}H NMR of **2c**

Figure 0.85 – ^{13}C NMR of **2c**

Figure 0.86 – ^{1}H NMR of **2d**

Figure 0.87 – ^{13}C NMR of **2d**

Figure 0.88 – ^{1}H NMR of **2e**

Figure 0.89 – ^{13}C NMR of **2e**

Figure 0.90 – ^{1}H NMR of **6**

Figure 0.91 – ^{1}H NMR of **7**

Figure 0.92 – ^{1}H NMR of **8a**

Figure 0.93 – ^{1}H NMR of **8b**

Figure 0.94 – ^{13}C NMR of **8b**

Figure 0.95 – ^{1}H NMR of **8c**

Figure 0.96 – ^{13}C NMR of **8c**

Figure 0.97 – ^{1}H NMR of **8d**

Figure 0.98 – ^{13}C NMR of **8d**

Figure 0.99 – ^{1}H NMR of **8e**

Figure 0.100 – ^{13}C NMR of **8e**

Figure 0.101 – ^{1}H NMR of **9**

Figure 0.102 – ^{13}C NMR of **9**

2.10.2 – CCL2 PROMOTER ACTIVITY

Table 0.15 – CCL2 Assay Raw Data

	CCL2 (%max IL-1β response)					
	Concentration of Compound (M)					
Cmpd	1X10^-10	1X10^-9	1X10^-8	1X10^-7	1X10^-6	1X10^-5
HC	96.3±31.0	85.5±28.5	78.9±27.0	72.1±24.1	42.4±18.7	26.6±9.25
1b	83.4±13.6	80.3±18.9	95.8±3.57	73.0±16.4	55.5±0.45	40.0±31.4
1c	93.8±20.4	101±26.9	97.3±22.1	81.8±6.76	66.9±3.95	23.7±13.3
1d	82.6±5.04	94.7±31.1	105±28.1	106±51.3	80.0±38.5	77.8±22.7
1e	100±14.5	114±34.6	126±34.8	107±19.0	86.6±16.6	53.2±30.6
2b	96.5±4.48	98.4±10.7	85.3±5.62	85.1±12.7	63.3±7.59	52.3±11.3
2c	85.4±14.2	75.3±16.6	71.2±13.2	53.8±20.0	37.9±19.1	25.0±9.90
2d	89.9±14.7	94.0±30.3	93.2±24.6	85.0±17.0	71.2±22.4	62.9±16.4
2e	43.6±7.14	43.8±6.87	49.7±10.8	38.9±11.8	32.4±9.83	24.5±8.32
6	12.8±1.66	9.78±0.45	11.9±2.22	12.0±2.22	10.2±0.54	13.1±2.35
7	16.7±3.71	20.1±5.09	17.4±1.36	18.6±9.11	15.3±0.65	17.0±3.71
8a	99.9±16.8	95.9±9.00	92.8±14.4	51.7±8.42	19.8±9.44	20.7±6.19
8b	125±9.25	109±27.3	85.2±16.6	40.5±18.5	17.8±10.3	20.8±9.21
8c	92.2±27.4	74.4±19.4	58.7±15.1	23.8±10.1	21.0±5.38	17.9±4.67
8d	43.4±11.5	50.4±20.7	35.6±13.1	26.6±10.0	18.7±3.86	18.9±4.04
8e	66.2±10.9	48.6±12.6	32.6±11.0	24.4±9.32	15.1±5.19	17.3±4.56
9	90.6±4.02	82.5±15.1	73.7±7.45	52.1±4.82	26.5±1.17	21.8±6.28

Table 0.16 – Low Dose CCL2 Assay Raw Data

	CCL2 (%max IL-1β response)					
	Concentration of Compound (M)					
Cmpd	1X10^-18	1X10^-15	1X10^-12	1X10^-9	1X10^-6	1X10^-5
HC	81.4±33.3	63.7±16.8	56.8±17.2	51.5±21.7	13.9±14.9	NA
6	12.6±3.11	11.9±3.19	13.1±4.25	11.7±3.63	12.2±3.04	15.8±7.84
7	18.9±1.92	19.7±3.58	19.8±3.79	20.6±6.03	17.6±1.47	25.9±8.61

Figure 0.103 – CCL2 Data Analysis

Figure 2.36 – Cont.

Figure 2.36 – Cont.

2.10.3 – 3xGRE PROMOTER ACTIVITY

Table 0.17 – 3xGRE Assay Raw Data

3xGRE (Fold over control – DMSO)						
	Concentration of Compound (M)					
Cmpd	1X10^-10	1X10^-9	1X10^-8	1X10^-7	1X10^-6	1X10^-5
HC	1.56±1.30	1.93±2.08	2.33±2.09	4.77±2.16	5.37±2.60	6.53±3.48
1b	1.29±0.617	1.05±0.542	1.15±0.395	1.02±0.322	1.33±0.492	1.28±0.256
1c	0.925±0.070	0.830±0.267	0.893±0.224	1.38±0.232	1.65±0.575	1.58±0.584
1d	0.885±0.205	0.840±0.0140	0.940±0.226	0.950±0.113	1.12±0.311	1.41±0.330
1e	0.853±0.167	0.747±0.266	0.837±0.095	0.887±0.095	1.04±0.0600	1.39±0.391
2b	0.878±0.164	0.957±0.144	1.06±0.241	1.28±0.619	1.06±0.239	1.34±0.405
2c	1.01±0.234	0.955±0.379	1.10±0.152	3.06±1.99	2.87±0.936	2.98±1.98
2d	1.14±0.534	0.938±0.196	1.03±0.226	1.11±0.188	1.21±0.531	1.03±0.158
2e	2.14±1.01	2.31±1.20	2.89±1.54	2.89±0.811	4.22±0.790	4.64±0.392
6	4.80±1.58	5.22±0.523	7.02±0.120	5.06±0.113	6.37±0.481	5.44±0.368
7	5.47±0.779	5.18±1.06	5.04±1.26	5.86±1.58	5.31±1.48	5.65±1.46
8a	0.933±0.181	0.950±0.113	1.293±0.718	2.05±0.361	2.84±0.786	4.05±1.68
8b	2.10±1.27	2.10±1.40	2.37±1.45	3.88±2.13	4.34±2.15	4.95±2.32
8c	1.06±0.477	1.17±0.491	1.71±0.681	2.41±1.34	2.50±0.898	2.60±0.530
8d	1.95±0.549	1.69±0.163	2.11±0.330	2.93±0.948	3.28±0.760	3.53±1.56
8e	0.940±0.241	1.14±0.135	2.61±0.510	4.17±1.33	4.27±1.20	4.57±1.04
9	0.888±0.171	0.930±0.239	0.899±0.280	1.73±0.864	3.82±0.680	4.94±0.859

Table 0.18 – Low Dose 3xGRE Assay Raw Data

3xGRE (Fold over control – DMSO)						
	Concentration of Compound (M)					
Cmpd	1X10^-18	1X10^-15	1X10^-12	1X10^-9	1X10^-6	1X10^-5
HC	1.11±0.595	2.77±2.19	2.06±1.49	5.72±1.26	5.90±0.722	7.35±1.48
6	5.01±0.992	5.20±1.22	5.05±0.928	4.75±0.716	4.90±1.30	5.86±0.562
7	4.97±0.716	4.52±0.433	4.89±0.740	4.78±0.946	4.91±1.31	6.36±1.50

Figure 0.104 – 3xGRE Data Analysis

Figure 2.37 – Cont.

Figure 2.37 – Cont.

2.10.4 – Sgk1 and Rgs2 GENE EXPRESSION

Table 0.19 – *Sgk1* Gene Expression Raw Data

	Sgk1 Relative mRNA Abundance (Fold over Control)				
	Concentration of Compound (M)				
Cmpd	1X10^-18	1X10^-15	1X10^-12	1X10^-9	1X10^-6
HC	0.808±0.544	0.763±0.489	0.728±0.354	0.720±0.483	6.55±4.54
6	19.1±8.18	19.2±13.4	15.2±8.82	20.8±10.1	21.8±12.3
7	21.4±9.82	15.9±7.02	19.3±6.03	17.6±3.44	22.2±9.01

Table 0.20 – *Rgs2* Gene Expression Raw Data

	Rgs2 Relative mRNA Abundance (Fold over Control)				
	Concentration of Compound (M)				
Cmpd	1X10^-18	1X10^-15	1X10^-12	1X10^-9	1X10^-6
HC	1.30±0.29	21.1±29.3	1.28±0.79	9.25±8.66	504.8±117.7
6	310.1±238.4	290.7±212.7	250.9±154.5	216.3±124.6	203.1±119.1
7	379.5±243.1	369.7±259.8	416.4±336.4	379.1±232.5	424.6±246.1

Figure 0.105 – *Sgk1* gene expression data analysis

Figure 0.106 – Rgs2 gene expression data analysis

2.10.5 – RMSD AND RMSF PLOTS THROUGHOUT THE MD TRAJECTORY OF 100 NS

Figure 0.107 – Alpha carbon protein backbone root mean square deviation values.

Figure 0.108 – Ligand root mean square deviation values.

Figure 0.109 – Root mean square fluctuation values.

2.10.6 – TOTAL ENERGY DECOMPOSITION

Table 0.21 – Average Per Residue Total Energy Decomposition in kcal/mol

Residue	**HC**	**DAC**	**6**	**7**	**9**
W:557	0	0	0	0	-0.63176
I:559	0	0	0	0	-0.22186
M:560	-1.31467	-1.43309	-1.12604	-1.01291	-2.34705
L:563	-1.38398	-1.21235	-1.16466	-1.10456	-1.1655
N:564	-2.18137	-1.57139	-1.5962	-1.48486	-1.84546
L:566	-0.9632	-1.13766	-1.16296	-1.12875	-1.09273
G:567	-1.0996	-1.40955	-1.5565	-1.44508	-1.49067
Q:570	-0.75779	-2.24692	-2.40676	-2.35883	-2.3434
W:600	-0.05765	0.112665	0.188409	0.136655	0.164804
M:601	-1.34946	-1.09464	-1.03429	-1.0365	-0.9687
L:603	0	-0.18782	-0.20104	0	0
M:604	-1.78696	-2.75887	-2.58956	-2.81797	-2.94763
A:605	-0.52019	-0.54078	-0.45529	-0.46399	-0.57517
A:607	0	-1.00776	-1.02541	-0.96653	-1.06123
L:608	-0.83278	-2.10641	-1.9249	-1.79601	-1.84003
R:611	-0.04893	-0.5006	-0.42064	-0.48455	-0.45841
C:622	0	-0.37376	-0.36324	-0.34992	-0.44311
F:623	-1.16948	-1.31991	-1.32444	-1.36932	-1.58594
M:639	0	0	0	0	-2.15808
Q:642	-1.4374	-1.57071	-1.68885	-1.73088	-1.41561
C:643	0	0	0	0	-0.33477
M:646	-1.05448	-1.47573	-0.81944	-0.81495	-1.5893
L:732	-1.27056	-1.49352	-1.16937	-1.14114	-1.13926
Y:735	-1.23256	-1.4423	-1.35649	-1.16293	-2.06045
C:736	-1.39432	-1.60596	-1.48169	-1.53553	-1.65902
Q:738	0	0	0	0	0.010864
T:739	-1.20286	-0.98164	-1.21959	-1.00921	-0.94755
M:745	0	0	0	0	-0.52354
I:747	0	-0.32322	-0.2725	-0.29957	-1.68849
F:749	-0.29463	-0.43026	-0.41632	-0.45313	-0.74767
L:753	-0.04201	0	0.041414	0	0.042335

CHAPTER 3: DISCOVERY OF MULTIPLE ALLOSTERICALLY INDUCED INTERDOMAIN INTERACTIONS WITHIN THE GLUCOCORTICOID RECEPTOR DIMER COMPLEX

A version of this chapter is expected to be part of a future publication by:
Seaton, W.B. and Campagna, S.R.

Contributions:
Conceptualization, W.B.S. and S.R.C.; methodology, W.B.S. and S.R.C.; validation, W.B.S. and S.R.C.; formal analysis, W.B.S. and S.R.C.; investigation, W.B.S.; resources, S.R.C.; writing, W.B.S.; visualization, W.B.S.; supervision, S.R.C.; funding acquisition, S.R.C.

3.1 - ABSTRACT

The glucocorticoid receptor (GR) is a ligand dependent nuclear receptor that influences the transcription of numerous genes throughout the body. Structurally, the GR is comprised of a disordered *N*-terminal domain (NTD) and a DNA-binding domain (DBD) that is connected to a ligand-binding domain (LBD) by a linear chain of amino acids known as the hinge region (HR). Glucocorticoids (GCs), such as dexamethasone, function as anti-inflammatory drugs and bind to the GR as agonists, inducing both transrepression and transactivation in a monomer and dimer state, respectively. Other GCs, such as mifepristone, act as antagonists and inhibit GR activity to treat diseases such as Cushing's syndrome. Agonistic and antagonistic GCs exist as both steroidal and non-steroidal structures and have been studied extensively to produce compounds with minimal side effects. Despite this, little is known about what protein conformational changes occur upon ligand binding and how those changes influence factors such as dimerization. This gap of knowledge stems from the fact that the whole GR is difficult to crystalize as it is poorly soluble, inherently unstable, and the HR lacks sufficient electron density for proper resolution. Herein, a method was developed to better understand how the binding of GCs in the LBD impacts the overall structure of the GR. To this end, we have utilized AI program AlphaFold to generate a GR consisting of a DBD, HR, and LBD. Following validation of the structure's identity, a dimer was constructed and placed on a known glucocorticoid binding sequence (GBS). A series of molecular dynamic (MD) simulations were subsequently performed with a group of docked agonistic and antagonistic ligands. Consistently, agonists induced cooperative interactions between the two domains that never occur in the presence of antagonists. These results provide novel insight into how functionally distinct GCs allosterically influence GR dimer stability.

3.2 – INTRODUCTION

The glucocorticoid receptor (GR) is a ligand-dependent, nuclear receptor (NR) that regulates immune function, inflammation, and glucose homeostasis.[9] GR agonists, such as prednisolone, are frequently employed to manage allograft rejection in solid organ transplants. Notably, 43% of liver transplant patients require immunosuppressants for over six months.[82] Less frequently prescribed GR antagonists, like mifepristone, are

used to treat diseases such as Cushing's syndrome, which results from excess cortisol production in the adrenal glands.[9]

Structurally, the GR is comprised of four domains: a disordered amino-terminal domain (NTD), a DNA binding domain (DBD), a linear sequence of amino acids known as the hinge region (HR), and a highly conserved ligand-binding domain (LBD).[14] GR agonists and antagonists bind to the same ligand binding pocket within the LBD. Upon agonist binding, the GR is translocated to the nucleus, forms homodimers, and binds a variety of GR-binding sequences (GBS) to exert its effects.[83] These effects are further dictated by the specific ligand used and subsequent co-regulators recruited by the GR.[84] By contrast, GR antagonists competitively bind to the GR, preventing dimerization and reducing the activity of endogenously produced cortisol.[24, 25] Taken together, these factors highlight the high plasticity of ligand dependent GR-regulated gene networks.

The GR has proven difficult to crystallize as a full structure due to the presence of highly disordered regions with low electron density.[14, 85] Despite this, several crystal structures of both the DBD and LBD currently exist and have been subjected to both biological and computational experiments to better understand their behavior. For example, molecular dynamic (MD) simulations of both the wild type and well characterized Ala458Thr substitution mutant GR DBD revealed that the zinc finger D-loop region plays a key role in both dimerization and GR transcriptional output.[18] Furthermore, additional *in silico* experiments of an individual LBD have shown that the dynamic helix 12 (H12) population is determined by the presence of an agonistic or antagonistic ligand.[86] More recently, the first quaternary structure of the GR was elucidated (PDB ID: 7prv) with the agonist fluticasone furoate inducing the formation of an asymmetric dimer with unique interdomain interactions.[14] Despite this accomplishment, the crystal structure presented did not contain electron density for the HR and little is still known regarding how GR ligands allosteric drive dimerization.

Here, a structure of the GR containing the DBD, HR, and LBD was obtained from AI system AlphaFold and used to construct an unbiased dimer on a natural GBS bound to a diverse group of ligands. Subsequent MD simulations were performed to see how ligands allosterically influence the dimer complex. Additionally, this system was

compared with the existing quaternary structure of the GR to see how different GBSs impact protein conformation. Finally, MMPBSA calculations revealed free binding energy trends between the ligand-protein complexes.

3.3 – METHODS

3.3.1 – CONSTRUCTION OF GLUCOCORTICOID DIMER

The AlphaFold database was utilized to find a structure of the GR that contained the DNA binding domain, hinge region, and the ligand binding domain.[87] Efforts were made to ensure that all folded components of the protein had an acceptable pLDDT score (70>pLDDT) (**Figure 3.1**). Additionally, the desired protein would match the human amino acid sequence of the GR. The final chosen structure (UniProt: B7Z7I2) met these criteria with a sequence containing 380 amino acids which equates to residues 398 – 777 (**Figure 3.2A**). Residues 398-421 were removed since the goal of this study was to understand how ligand binding influenced dimerization while dismissing residues that comprise the highly disordered NTD. Further validation of the final structure was performed by aligning real crystal structures of the DBD (PDB ID: 3g6p) and LBD (PDB ID:5nfp) with the GR from AlphaFold, producing RMSD values of 0.442 and 0.435, respectively (**Figure 3.2B-D**).

Once the structure of the GR was confirmed, we sought to incorporate it onto a segment of DNA that is known to be transcribed in response to GR agonists. FKBP5 is a well-established GR-binding sequence (GBS) whose crystal structure is available on the protein data bank with the bound GR-DBD dimer (PDB ID: 3g6p).[88] Two copies of the GR structure obtained from AlphaFold were thus incorporated in place of the existing GR-DBD dimer with PyMOL to form a complete GR dimer bound to *FKBP5*.[89] The four zinc atoms from 3g6p were left in place to form zinc fingers which coordinate to cysteine residues across the DBD. The complete structure was saved as a pdb file for the proceeding experiments.

Figure 0.110 – AlphaFold structure prediction of the glucocorticoid receptor.

Figure 0.111– Construction and validation of the quaternary structure of the GR. A) Amino acid sequence of human GR used during experiments. Blue, DBD; magenta, HR; red, LBD. B) Modified structure of the GR obtained from AlphaFold (magenta) and verified through alignment with LBD 5nfp (red) and DBD 3g6p (blue). C) Final constructed quaternary GR on FKBP5. D) Cartoon representation of dimer GR.

Since this project began, a quaternary crystal structure of the GR with another GBS, *sgk1*, has been published.[14] To compare the system created within AlphaFold and this folded structure, we replaced *FKBP5* with *sgk1* for an analysis of the native ligand, fluticasone furoate.

3.3.2 – MOLECULAR DOCKING AND DYNAMIC SIMULATIONS

Molecular docking was performed on the GR complex using AutoDock Vina (The Scripps Research Institute).[44] Ligands were drawn in ChemDraw 21.0.0 and their energies were minimized in Chem3D. Following this, the ligand binding pocket was identified for each half of the dimer and ligands were inserted sequentially. The optimal orientation of each ligand was chosen based on binding energy and position of the native ligand, deacylcortivazol (DAC). All ligands were docked on the GR bound to *FKBP5* except FF, which was docked to both the GR bound to *FKBP5* and *SGK*.

Molecular dynamic (MD) simulations of the resulting GR with and without docked ligands, as well as with 7prv, were performed using GROMACS software version 2021.5-gcc for 100 ns at 303.15 K and a pH of 7.[46] The solution builder input generator of CHARMM-GUI was employed, along with CHARMM36m and the online server CGenFF, to prepare the protein and ligand force field parameters and topologies, respectively.[90-93] HR residues for 7prv lacked electron density sufficient for resolution. Therefore, the missing residues for chain A (489-527) and chain B (489-526) were modeled using with GalaxyFill. Cysteine residues 421, 424, 438, 441, 457, 463, 473, and 476 were deprotonated on each chain to ensure coordination to the four total zinc atoms that make up the zinc finger regions of the DBD. The system was placed in a cubic box with all atoms at least 10 Å from the box edge and solvated with TIP3P model water molecules.[94] Sodium and chlorine were added to neutralize the system. The energy of the system was minimized once a maximum force of 10 kJ/mol was achieved after 5000 steps. An NVT ensemble was used to equilibrate the system for 250 ps and an NPT ensemble was used in the production simulation for 100 ns. Root-mean-square deviation (RMSD) and root-mean-square fluctuation (RMSF) were plotted to analyze the stability of the system (**Appendix Figure 3.10** and **Figure 3.11**). To ensure this time frame was sufficient for the system to converge, an additional 100 ns simulation was performed for

a single agonist, dexamethasone, and antagonist, mifepristone. The resulting trajectories were concatenated to produce a 200 ns simulation. RMSD graphs of both the protein backbone and all ligands revealed that the systems converged at approximately 40 ns.

3.3.3 – BINDING FREE ENERGY CALCULATIONS AND HYDROGEN BOND ANALYSIS

Molecular Mechanics Poisson-Boltzmann Surface Area (MMPBSA) approach was used to determine the binding free energy from the produced MD trajectories.[75] Specifically, the gmx_MMPBSA tool was used to calculate ligand-protein binding free energies, as well as free energy decomposition to give the contribution of each residue within the active site defined as 4 Å from the ligand. The binding free energy of the bound ligand-receptor complex in an aqueous solvent ($\Delta G_{bind,aq}$) was calculated by

$$\Delta G_{bind,aq} = \Delta H - T\Delta S$$

The entropic term was dismissed since enthalpy calculations are assumed to be sufficient for calculating the binding free energy of the ligand.[76] The enthalpy term can be further broken down into the gas phase molecular mechanical energy change (ΔE_{MM}) plus the solvation free energy change ($\Delta G_{bind,solv}$)

$$\Delta H = \Delta E_{MM} + \Delta G_{bind,solv}$$

This ΔE_{MM} is the sum of the covalent ($\Delta E_{covalent}$), electrostatic ($\Delta E_{electrostatic}$), and van der Walls (ΔE_{vdW}) energy change, while $\Delta G_{bind,solv}$ is the sum of the change of energy in the polar (ΔG_{polar}) and nonpolar ($\Delta G_{non-polar}$) solvation components.

$$\Delta E_{MM} = \Delta E_{covalent} + \Delta E_{electrostatic} + \Delta E_{vdW},$$

$$\Delta G_{bind,solv} = \Delta G_{polar} + \Delta G_{non-polar}$$

Interactions between chains A and B of the protein were analyzed using the hydrogen bond analysis plugin within VMD.[50] The donor-acceptor distance was set to 3.5 Å with an angle cutoff of 20 degrees. Detailed information for all hydrogen bonds were produced as a percent occupancy throughout the 100 ns simulation. The 200 ns concatenated trajectories for dexamethasone and mifepristone were also subjected to a hydrogen bond analysis to further demonstrate that no new interactions were formed past 100 ns.

3.4 – RESULTS

3.4.1 – EVALUATION OF THE QUATERNARY GR AND THE APOT STATE MD SIMULATIONS

The initial GR structure obtained from AlphaFold (UniProt: B7Z7I2) consists of the DBD, HR, and LBD. Prior to simulation, these three domains share no contacts, thus making it a suitable scaffold to evaluate how protein conformation is influenced in the presence or absence of ligands with a variety of biological activity. Upon construction of the quaternary structure, a series of hydrogen bond interactions were formed between the DBDs of chain A and chain B. Specifically, residues 456, 458, 464, 469, and 472 all participate in these initial monomer-monomer interactions (**Figure 3.3A**). These residues make up components of both the D-loop and helix 2 (H2) of the DBD and have been previously implicated as critical to glucocorticoid activity.[18, 95] Furthermore, this model exhibits contacts between the GBS, *FKBP5*, and helix 1 (H1) of the DBD in both chains A and chain B which is consistent with existing literature (**Figure 3.3A**).[84] By contrast, both of the HRs and LBDs begin at a distance great enough to not participate in any intradomain nor interdomain interactions (**Figure 3.3B**). Finally, it is important to note that helix 12 (H12) of the LBD is highly flexible and can occupy a variety of conformations implicated in modulating agonistic and antagonistic activity.[96, 97] When comparing H12 of the constructed GR with an antagonist state (PDB ID: 3h52), and an agonist state (PDB ID: 1m2z), it is clear that our structure begins in an agonistic conformation (**Figure 3.3C**).

Despite the GR being ligand-activated, it seemed appropriate to benchmark future studies against this apo system. Therefore, the ligand-free complex (GR_{apo}) was subjected to a 100 ns MD simulation. A Root Mean Square Deviation (RMSD) plot of the system showed convergence at approximately 20 ns and maintained a value below 4 Å (**Figure 3.4A**). The deprotonated cysteine residues 421, 424, 438, 441, 457, 463, 473, and 476 on both chains effectively coordinated with zinc atoms to form four stable zinc fingers throughout the simulation. Additionally, a Root Mean Square Fluctuation (RMSF) analysis, which is a representation of each residue's fluctuation on average over time, revealed that the DBD dimer successfully maintained contacts between H1 and the GBS,

Figure 0.112 – Starting position of the constructed quaternary structure of the GR. A) DBDA and DBDB interactions on FKBP5. B) LBDA and LBDB components of the GR with sufficient distance to avoid intermolecular contact. C) Aligned LBDA of constructed GR (green) with LBDA of agonist state 1m2z (orange) and LBDA of antagonist state 3h52 (grey).

Figure 0.113 – 100 ns simulation of GR_{apo}. A) Root mean square deviation (RMSD) of GR_{apo} over 100 ns with respect to backbone atoms. B) RMSF values of GR_{apo}, chain A (CA) in blue and chain B (CB) in orange. C) Final position of GR_{apo} after 100 ns with CA in blue/green and CB in red/orange.

and interdomain contacts within the D-loop with each chain having similar fluctuations between 1 Å and 2 Å (**Figure 3.4B**). Interestingly, the two LBDs move in opposite directions with chain B folding onto the DBD and chain A moving away from the whole complex and forming no new interactions (**Figure 3.4C**). This behavior is highlighted by the noticeable difference in fluctuation between both chain's residues comprising the HR and LBD.

3.4.2 – EVALUATION OF MD SIMULATIONS WITH AGONISTIC LIGANDS BOUND TO THE GR

A series of clinically available GR agonists with a wide range of potency were docked using AutoDock Vina (The Scripps Research Institute) in each LBD to understand how they may impact GR conformation.[44] Dexamethasone (GR_{DX}), hydrocortisone (GR_{HC}), prednisolone (GR_{PN}), budesonide (GR_{BD}), and fluticasone furoate (GR_{FF_FKBP5}) were all subjected to 100 ns MD simulations with GBS *FKBP5*. RMSD values of the backbone atoms for each system were analyzed to determine the stability of the MD trajectories (**Figure 3.5A**). After approximately 30 ns the systems converged. However, to further examine whether this time was sufficient, an additional 100 ns simulation was performed on the system bound with DX, GR_{DX}, and the two trajectories were concatenated. The results confirmed that 100 ns was sufficient for convergence as the system was stabilized at approximately 3 Å with little to no fluctuation from 100 ns to 200 ns (**Appendix Figure 3.16**). Additionally, the stability of the systems were confirmed through RMSD plots of all ligands over time with convergence for all ligands observed at approximately 60 ns (**Appendix Figure 3.12**).

Visual inspection of the systems revealed that GR_{DX}, GR_{HC}, and GR_{PN} all display stabilizing, interdomain interactions, not including DBD contacts, in response to ligand binding (**Figure 3.5 B-D**). For example, GR_{DX} exhibits three sites of interaction between residues from chain A and chain B that, once formed, do not break, even through 200 ns. These include contacts between chain A's and chain B's LBDs, as well as between two different sites of the DBD from chain A and the LBD of chain B. Similarly, GR_{HC}

Figure 0.114 – Agonists induce interdomain interactions on GBS FKBP5. A) RMSD of 5 agonist systems with respect to backbone atoms. Final conformations of B) GR_{DX}, C) GR_{HC}, D) GR_{PN}, E) GR_{BD}, F) GR_{FF_FKBP5}.

displays one site of interdomain contacts between the two LBDs that stabilizes the system. However, these are unique to GR_{HC} and not found throughout any other ligand-complex simulation. GR_{PN} also displays only one site of interdomain contacts, but these are found between residues of each LBD before the first helix (H1). By contrast, the BD complex, GR_{BD}, and FF complex, GR_{FF_FKBP5}, exhibit no interdomain contacts. Instead, LBDB of both GR_{BD} and GR_{FF_FKBP5} remains above DBDB, while both LBDs on chain A move away from chain B and form contacts with the sugar phosphate backbone of *FKBP5* (**Figure 3.5E-F**).

In addition, a recent study by Postel *et al*. has unveiled the first high-resolution, multi-domain structure of the GR (PDB ID: 7prv) in complex with FF on GBS serum and glucocorticoid-regulated kinase-1 (*SGK1*).[14] This provided an excellent opportunity to investigate how our GR complex, when docked with FF and in complex with *SGK1* (GR_{FF_SGK1}), compared with its equivalent *in vitro* complex. MD simulations revealed 7prv was highly stabilized with protein backbone RMSD values between 0.5 and 1 Å. Interestingly, GR_{FF_SGK1} had some meaningful similarities with 7prv and differences with GR_{FF_FKBP5}. First, unlike GR_{FF_FKBP5}, GR_{FF_SGK1} displays interdomain interactions between helices 9 (H9) and 10 (H10) of LBDB and DBDA. The LBDs move closer together to such a degree that the overall RMSD between GR_{FF_SGK1} and 7prv is only 22.011 (**Figure 3.6A-B**). This is remarkably similar when considering the multitude of possible conformations the GR complex is capable of producing. When isolating the LBDs (residues 527-777), the two systems display a RMSD of 19.854 (**Figure 3.6C**), while the isolated DBDs (residues 422-488) RMSD was only 1.569 (**Figure 3.6D**). Despite this, the interdomain interactions are not the same, with 7prv displaying far more interactions, particularly between its two LBDs.

3.4.3 – Evaluation of MD Simulations with Antagonistic Ligands Bound to the GR

GR antagonists, such as mifepristone, are important in the treatment of diseases caused by excess cortisol activity such as Cushing's syndrome.[98] These antagonists act by blocking cortisol and, unlike agonistic ligands, would not induce transcription of genes like *FKBP5*. Therefore, it is important to understand how antagonistic ligands may influence GR conformation. Two GR antagonists, mifepristone (GR_{MPS}) and

Figure 0.115 – Final conformations of A) GR_{FF_SGK1} and B) 7prv. C) Aligned final conformation of the isolated C) LBDs and D) DBDs from GR_{FF_SGK1} and 7prv.

CORT125281 (GR_{CT}), a novel and selective non-steroidal GR antagonist, were docked within the GR complex on *FKBP5* and subjected to 100 ns MD simulations.[9]

RMSD plots of the protein backbone show that both systems converged at approximately 60 ns where they maintained a RMSD at approximately 3 Å (**Appendix Figure 3.11**). Intriguingly, both GR_{MPS} and GR_{CT} produced no interdomain interactions with one chain moving away from the rest of the structure (**Figure 3.7A-B**). Mifepristone was simulated for an additional 100 ns and the trajectories were concatenated to give a 200 ns simulation to see if this dissociation persisted. Indeed, even with doubling the time of the simulation we observed no interactions beyond the initial stabilized interactions between the two DBDs. The LBD from one chain never came close enough to any part of the opposite chain to form an anchored structure as was seen when the GR was bound with agonistic ligands.

3.4.4 – PROTEIN-LIGAND INTERACTIONS AND TRENDS

The MMPBSA method was employed to calculate the binding free energy of each ligand and better understand how they allosterically impact GR conformation.[75] The average binding free energy for agonist GR complexes on *FKBP5* increased with hydrocortisone (-33.19 kcal/mol) < prednisolone (-34.24 kcal/mol) < dexamethasone (-36.32 kcal/mol) < budesonide (-37.77 kcal/mol) < fluticasone furoate (-40.1 kcal/mol) (Figure 3.8A). These free energies positively correlate with the relative potency of each GC found in literature.[99, 100] Furthermore, the average binding free energy of fluticasone furoate in complex with *SGK1* was -40.97 kcal/mol, while within 7prv it was -44.39 kcal/mol. Despite this difference, both GR_{FF_SGK1} and 7prv had the highest free binding energy among all agonists. The binding free energies of antagonists mifepristone and CORT125281 was -43.43 kcal/mol and -44.49 kcal/mol, respectively. This once again coorelates with existing literature as mifepristone is known to have a higher binding affinity for the GR than dexamethasone.[101] Additionally, the ability of mifepristone and CORT125281 to inhibit corticosteroid induced transcription of *FKBP5* has been previously measured with mifepristone being slighly stronger at 1 mM.[102]

Figure 0.116 – Final conformations following 100 ns MD simulation of A) GR_{MPS} and B) GR_{CT}.

Figure 0.117 – MMPBSA analysis results. A) Average binding free energy of ligand-protein complex for both chain A and chain B. B) Pairwise heat map using Euclidean distance matrix to calculate similarities between ligands. C) Decomposition binding free energy values showing per-residue energy contribution for all amino acids. Scale: all values in kcal/mol, white color indicates no interaction between ligand and residue. Clustering analysis: Euclidean distance clustering method grouping ligands based on decomp raw values.

The binding free energy was decomposed for each ligand-residue interaction across all complexes. This provided insight into the total energy contributed by each individual residue within the active site which was defined as 4 Å from the ligand. Asn564 consistently contributed the highest binding energy with all agonists, exhibiting values between -2.13 kcal/mol to -2.99 kcal/mol (**Appendix Table 3.2**). This interaction is known to take place with the C_{11} hydroxyl group and is therefore significantly decreased in mifepristone and CORT125281 with average binding energies of -0.089 kcal/mol and -0.202 kcal/mol, respectively.[60] Furthermore, Euclidean distance methods were used to cluster all ligands based on their decomposition free energy values. First, a pairwise comparison shows clear differences between agonists and antagonists (**Figure 3.8B**). Clustering analysis further divided the agonistic compounds into two distinct groups with dexamethasone, hydrocortisone, prednisolone, and budesonide in one group and all fluticasone furoate simulations in another (**Figure 3.8C**). The main structural difference between these groups is the presence or absence of the C_{17} hydroxyl moiety. The presence of this hydroxyl moiety is known to form strong hydrogen bonding with Gln642.[60] Less discussed residues, such as Met639 and Cys643, display few interactions with agonists in the first cluster but do interact with all agonists in the second cluster. Finally, while all ligands interacted with Met604, both antagonists displayed the strongest interactions with this residue. In particular, CORT125281 nearly doubled its average binding energy with Met604 with a value of -3.55 kcal/mol compared with dexamethasone with a value of -1.74 kcal/mol. This is important to consider as allosteric communication that leads to reduced interdomain interactions may originate with strong antagonistic binding to specific residues like Met604. However, further experimentation would be needed to validate this hypothesis.

The GR ligand binding pocket (LBP) is highly flexible and responds to both small and large ligands to produce pleiotropic effects.[103, 104] This plasticity has recently been shown to positively correlate with potency as well.[71] To follow up on these results, we utilized the online tool Computed Atlas of Surface Topography of proteins (CASTp) to determine the binding pocket volume for both LBDs of all complexes (**Table 3.1**).[52] All

Table 0.22 – Average Protein-ligand Binding Free-energy and Pocket Volume

Complex Name	Ligand	GBS	Ligand Type	DH (kcal/mol) Chain A	DH (kcal/mol) Chain B	Chain A Pocket Volume (SA) Å^3	Chain B Pocket Volume (SA) Å^3
GR_{DX}	Dexamethasone	*FKBP5*	Agonist	-36.54	-36.09	377.5	411.8
GR_{HC}	Hydrocortisone	*FKBP5*	Agonist	-33.27	-33.11	272.5	326.4
GR_{PN}	Prednisolone	*FKBP5*	Agonist	-34.69	-33.78	312.3	93.70
GR_{BD}	Budesonide	*FKBP5*	Agonist	-37.62	-37.92	323.9	493.6
GR_{FF_FKBP5}	Fluticasone Furoate	*FKBP5*	Agonist	-37.53	-42.67	N/A	422.6
GR_{FF_SGK1}	Fluticasone Furoate	*SGK1*	Agonist	-40.81	-41.13	N/A	N/A
7PRV	Fluticasone Furoate	*SGK1*	Agonist	-45.17	-43.62	364.4	287.7
GR_{MPS}	Mifepristone	*FKBP5*	Antagonist	-42.51	-44.35	502.1	437.1
GR_{CT}	CORT125281	*FKBP5*	Antagonist	-44.34	-44.63	357.7	335.7

values were calculated using a 1.4 Å probe. The relationship between pocket volume and potency was only moderately consistent. For example, the average LBP volume for GR_{PN} was the smallest at 203.0 $Å^3$, while GR_{MPS} was the largest at 469.6 $Å^3$. Both GR_{FF_FKBP5} and GR_{FF_SGK1} were unsuccessfully probed with either too large of pockets observed (>1500 $Å^3$), or no pocket observed in the correct space. The probe size was thus altered for these complexes between 1.2 Å and 1.6 Å in an attempt to successfully identify the pocket volume. Despite these efforts, no change was observed. Regardless, the least potent GCs hydrocortisone and prednisolone created the smallest LBPs, while more potent dexamethasone and budesonide created the largest LBP among agonists. Altogether, this data illustrates that pocket volume is loosely correlated with binding free energy, but is not a strong predictor of ligand influence.

3.4.4 – PROTEIN-PROTEIN INTERACTIONS AND TRENDS

Amino acid residues that contributed the most to interdomain interactions were identified using the hydrogen bond analysis tool within VMD.[50] This method provided detailed information about which amino acids formed a hydrogen bond within 3.5 Å between chain A and chain B throughout the simulation and how frequently they occurred. We chose to only focus on the interactions if they were present at least 5% of the 100 ns simulation (ex. > 5% occupancy). Some interactions between DBDA and DBDB were present in all simulations, regardless of the ligand docked. For example, Arg460 and Asp462 displayed a H-bond occupancy close to 100% for all complexes (**Figure 3.9**). However, most agonistic complexes produced interdomain interactions outside of those present between DBDs. For instance, dexamethasone induces a unique ionic interaction between Arg479 and Glu537 with a H-bond occupancy of 59.1% (**Figure 3.9A**). This bond persisted through 200 ns and is likely stabilized because the opposite charges lead to an electrostatic interaction between the two amino acids. GR_{HC} displayed a unique interaction between Lys695 and Glu631 with 26.9% occupancy while the only new interaction for GR_{PN} was between Thr529 and Pro526 with 5.19% occupancy (**Figure 3.9B-C**). LBDB of GR_{BD} and GR_{FF_FKBP5} interacted with DNA, not

Figure 0.118 – Hydrogen bond occupancy between Chain A and Chain B for all MD simulations following ligand binding.

LBDA, and therefore, no interactions beyond those between DBDs were observed for these systems (**Figure 3.9D-E**). Similar results were observed for antagonistic systems GR_{MPS} and GR_{CT} (Figure 3.9G-H). 7prv displayed the most interdomain interactions, partially since the system began in a low energy conformation from the start of the simulation. By contrast, GR_{FF_SGK1} had one interdomain interaction between Gly706 and Asp466 with 18.1% occupancy (**Figure 3.9F**). This interaction was not observed in 7prv (**Figure 3.9I**).

3.4 – DISCUSSION

The GR remains one of the most well studied NRs due to the substantial number of genes it can influence through either its activation or inhibition.[105] Despite over seventy years of research, little is known about how different agonists selectively drive transcriptional output. With only a few quaternary structures of the GR crystallized to date, there is a need to rapidly and accurately understand how different ligands and GBSs influence GR activity. A GR complex consisting of the DBD, HR, and LBD on a classic GBS was thus modeled *in silico* with both agonists and antagonists to observe how these ligands allosterically drive the dimer's conformation.

Herein, we present an *in silico* study to model how different agonists produce unique, stabilizing interdomain interactions. Agonists hydrocortisone and prednisolone differ only by the presence of a double bond between C1 and C2 on the steroidal A-ring, while dexamethasone contains a fluorine at C9 and a methyl group at C16. These minor changes dramatically impact potency with hydrocortisone requiring four and 26-times higher dose-equivalency than prednisolone and dexamethasone, respectively.[106] In the presence of these three ligands, LBDA and LBDB of the GR formed different stabilizing interactions that were unique to each agonist. Furthermore, the average binding free-energy of these three compounds correlated with their biological potency. Additionally, agonists budesonide and fluticasone furoate in the dimer complex on FKBP5 resulted in each LBDA forming a stabilizing interaction with the DNA itself. In addition to containing either an ester or acetal group instead of an alcohol on C17, these compounds have both been shown to be more potent in vitro than dexamethasone and here have, on average, a higher binding free-energy than dexamethasone by approximately 1

kcal/mol.[71] This suggests that the potency of various agonists bound to the same GBS may result not only from their binding affinity for the protein, but also from the overall conformation of the dimer complex.

Antagonists mifepristone and CORT125281 produced no interdomain interactions even through 200 ns and had, on average, higher protein-ligand binding free-energies on FKBP5 than any of the simulated agonists by at least 3 kcal/mol. This higher binding affinity of antagonists for the GR has been previously observed, but specific energetic contributions have not yet been reported.[11] For example, it is noteworthy that endothermic interactions with GLY570 and PRO750 exist between both antagonists and the GR, but are absent among agonistic ligands. Further testing will reveal which specific amino acid interactions may allosterically prevent dimerization.

3.5 – CONCLUSION

The development of improved GR agonists and antagonists has been an active area since the discovery of cortisol to treat inflammation.[25] Historically, this work has largely focused on developing GCs with increased potency, but has been stifled due to challenges in producing complete crystal structures of the GR to guide innovation . We propose that interdomain interactions, produced allosterically by specific endergonic or exergonic contacts between the ligand and active site residues, are a better guide for the future development of more selective GCs.

APPENDIX

3.5.1 – RMSD AND RMSF PLOTS THROUGH 100NS

Figure 0.119 – Agonist alpha carbon protein backbone root mean square deviation values.

Figure 0.120 – Antagonist and apo state alpha carbon protein backbone root mean square deviation values.

Figure 0.121 – Agonist ligands root mean square deviation values.

Figure 0.122 – Antagonist ligands root mean square deviation values.

Figure 0.123 – Agonist root mean square fluctuation values.

Figure 0.124 – Antagonist and apo state root mean square fluctuation values.

3.5.2 – RMSD AND RMSF PLOTS THROUGH 200 NS

Figure 0.125 – Alpha carbon protein backbone root mean square deviation values for 200 ns simulations.

Figure 0.126 – Ligand root mean square deviation values for 200 ns simulations.

Table 0.23 – Agonist's Raw Decomposition Values

Residue	DXA	DXB	HCA	HCB	PNA	PNB	BDA	BDB
ILE:559	0	0	0	0	0	0	-0.06	-0.08
MET:560	-1.58	-1.82	-1.38	-1.39	-1.43	-1.41	-1.83	-1.58
LEU:563	-1.84	-2.23	-1.47	-1.44	-1.72	-1.78	-2.54	-1.99
ASN:564	-2.73	-2.99	-2.21	-2.13	-2.25	-2.41	-2.48	-2.2
LEU:566	-0.72	-0.75	-1.02	-0.95	-0.74	-0.76	-0.73	-0.74
GLY:567	-0.73	-0.59	-1.02	-1.08	-0.97	-0.98	-0.74	-0.95
GLY:568	0	0	0	0	0	0	0	0
GLN:570	-1.05	-0.91	-0.89	-0.79	-1.21	-1.13	-0.96	-0.83
VAL:571	0	0	0	0	0	0	0	0
TRP:600	-0.49	-0.52	-0.17	-0.2	-0.07	-0.11	-0.3	-0.11
MET:601	-1.79	-1.84	-1.35	-1.44	-1.36	-1.34	-1.35	-1.3
LEU:603	0	0	0	0	0	0	0	0
MET:604	-1.65	-1.83	-1.87	-1.83	-1.78	-1.8	-1.81	-1.86
ALA:605	-0.59	-0.46	-0.5	-0.48	-0.61	-0.57	-0.41	-0.56
ALA:607	0	0	0	0	0	0	0	0
LEU:608	-0.81	-0.81	-0.9	-0.77	-0.85	-0.78	-0.65	-0.94
ARG:611	-0.69	-0.62	-0.18	-0.15	-0.83	-0.53	-0.07	-0.29
LEU:621	0	0	0	0	0	0	0	0
PHE:623	-1.19	-1.13	-0.54	-1.06	-1.1	-1.01	-0.8	-1.08
ILE:629	0	0	0	0	0	0	0.03	0.07
MET:634	0	0	0	0	0	0	0	0
MET:639	-0.09	0	0	0	0	0	-0.44	-0.71
GLN:642	-1.26	-0.16	-0.49	-1.26	-1.08	-1.1	-1.18	-1.31
CYS:643	0	0	0	0	0	0	-0.36	-0.52
MET:646	-0.97	-1.21	-0.63	-0.78	-1.15	-1.06	-0.98	-0.77
LEU:732	-1.43	-1.32	-1.14	-1.13	-1.22	-1.19	-1.23	-1.43
TYR:735	-1.41	-1.46	-1.17	-0.97	-1.24	-1	-1.49	-1.58
CYS:736	-1.58	-1.41	-1.41	-1.46	-1.38	-1.43	-1.37	-1.4
THR:739	-0.62	-1.29	-0.96	-0.57	-0.76	-0.89	-1.16	-0.89
ILE:747	-0.35	-0.38	-0.32	-0.36	-0.31	-0.31	-0.32	-0.25
PHE:749	-0.4	-0.29	-0.36	-0.32	-0.31	-0.29	-0.25	-0.26
PRO:750	0	0	0	0	0	0	0	0
MET:752	0	0	0	0	0	0	0	0
LEU:753	-0.2	-0.4	-0.2	-0.16	-0.02	-0.12	-0.27	-0.02
ILE:757	0	0	0	0	0	0	0	0

Table 3.2 – Cont.

Residue	FFA_FKBP5	FFB_FKBP5	FFA_SGK1	FFB_SGK1	FFA_7prv	FFB_7prv
ILE:559	-0.48	0	-0.68	-0.48	-0.33	0
MET:560	-2.49	-2.46	-2.85	-2.68	-2.53	-2.55
LEU:563	-2.34	-2.3	-2.47	-2.27	-2.35	-2.02
ASN:564	-2.9	-2.69	-2.84	-2.86	-2.64	-2.77
LEU:566	-0.74	-0.7	-0.7	-0.73	-0.75	-0.64
GLY:567	-0.73	-0.71	-0.65	-0.76	-0.73	-0.69
GLY:568	0	0	0	0	0	0
GLN:570	-0.78	-0.6	-0.5	-0.58	-1.26	-0.53
VAL:571	0	0	0	0	0	0
TRP:600	-0.64	-0.71	-0.74	-0.61	-0.61	-0.69
MET:601	-1.82	-2.04	-2.17	-2.07	-2.08	-2.03
LEU:603	0	0	0	0	0	0
MET:604	-2.06	-1.9	-2.1	-2	-1.94	-2.02
ALA:605	-0.36	-0.58	-0.44	-0.47	-0.52	-0.54
ALA:607	0	0	0	0	0	0
LEU:608	-0.69	-0.88	-0.96	-0.9	-1.07	-1.11
ARG:611	-0.09	-0.06	-0.11	-0.05	-1.25	-0.4
LEU:621	0	0	0	-0.17	0	0
PHE:623	-1.52	-1.63	-1.34	-1.58	-1.95	-1.43
ILE:629	-0.24	-0.36	-0.14	-0.28	-0.16	-0.07
MET:634	0	0	0	0	0	-0.43
MET:639	-0.83	-1.3	-0.81	-0.66	-0.7	-1.56
GLN:642	-0.89	-0.43	-0.82	-1	-1.16	-0.88
CYS:643	-0.49	-0.46	-0.45	-0.51	-0.37	-0.33
MET:646	-1.32	-1.63	-1.56	-1.43	-2.14	-1.79
LEU:732	-1.25	-1.78	-1.6	-1.63	-1.64	-1.76
TYR:735	-0.9	-1.28	-1.25	-1.25	-1.5	-1.77
CYS:736	-1.4	-1.46	-1.51	-1.4	-1.77	-1.73
THR:739	-0.52	-0.37	-0.33	-0.32	-0.33	-0.3
ILE:747	-0.52	-0.4	-0.49	-0.56	-0.49	-0.53
PHE:749	-0.85	-0.65	-0.7	-0.66	-0.62	-0.68
PRO:750	0	0	0	0	0	0
MET:752	0	0	0	0	0	0
LEU:753	-0.71	-0.29	-0.52	-0.39	-0.3	-0.32
ILE:757	0	0	0	0	0	0

Table 0.24 – Antagonist's Raw Decomposition Values

Residue	MPA	MPB	CTA
ILE:559	-0.27	-0.09	-0.1
MET:560	-1.21	-0.73	-0.83
LEU:563	-1.96	-1.89	-2.25
ASN:564	0.01	-0.19	-0.19
LEU:566	-0.79	-1.08	-1.04
GLY:567	-1.01	-1.69	-0.73
GLY:568	0.08	0.11	0.05
GLN:570	-0.9	-1.22	-1.71
VAL:571	-0.09	-0.2	0
TRP:600	0.06	0.01	-0.13
MET:601	-0.79	-1.3	-1.77
LEU:603	0	0	-0.22
MET:604	-2.08	-2.69	-3.68
ALA:605	-0.47	-0.71	-0.62
ALA:607	0	0	-0.84
LEU:608	-1	-1.01	-2.34
ARG:611	-0.1	-0.08	-0.67
LEU:621	0	0	0
PHE:623	-1.75	-1.68	-2.32
ILE:629	0	0	-0.21
MET:634	0	0	0
MET:639	-1.19	-0.46	-0.48
GLN:642	-0.87	-1.73	-1.4
CYS:643	-0.71	-0.26	-0.58
MET:646	-0.95	-0.83	-1.06
LEU:732	-0.94	-1	-0.92
TYR:735	-0.95	-0.98	-0.93
CYS:736	-1.55	-1.61	-1.48
THR:739	0	0	0
ILE:747	0	0	0
PHE:749	-0.43	-0.34	-0.21
PRO:750	0.08	0.11	0
MET:752	-0.07	-0.09	0
LEU:753	-0.27	-0.44	-0.63
ILE:757	0	0	-0.29

CONCLUSION

Glucocorticoids (GCs) are the primary choice for treating debilitating illnesses like rheumatoid arthritis, asthma, multiple sclerosis, and allograft rejection in solid organ transplants. Despite being in use for over 70 years, the most common GCs still exhibit detrimental effects, particularly for patients using them for extended periods of time. Even so, extensive research has been performed to develop a GC with a dissociative and highly selective profile. This work probes the flexibility of the glucocorticoid receptor (GR) ligand binding pocket (LBP) through the derivatization and expansion of clinical GCs, producing a series of compounds with unique activity that can be rationalized through molecular dynamic (MD) simulations.

The development of steroid induced diabetes following long-term GC use may be resolved through the synthesis of a compound with reduced transactivation. In the first study, 6 GC scaffolds were modified with a mercaptobenzothiazole moiety and all displayed selective GR modulation. The top performing compound, **DX1**, demonstrated an 87% reduction in transactivation, while maintaining 90% of the anti-inflammatory potential compared with dexamethasone. Surprisingly, two molecules, **DX4** and **PN4**, modified with thiomethyl and furoyl ester substituents, elicited activity at attomolar concentrations, possibly due to the formation of an unoccupied channel that expanded the volume of the LBP.

The second study capitalized on the GR's ability to accommodate ligands of varying sizes through the systematic modification of a hydrocortisone scaffold. Notably, the introduction of a single aryl pyrazole moiety significantly enhanced hydrocortisone's potency and conferred exclusive selectivity for the GR. Remarkably, ligands with three modification sites and double the molecular weight of hydrocortisone still exhibited agonistic activity. Like **DX4** and **PN4** in study 1, the two aryl pyrazole compounds expanded the LBP, accounting for the increase in potency. Additionally, these GCs displayed a 30% lower free-binding energy with active site residue N564, implying that a strong interaction reduces selectivity for the GR.

Generating ligands with different transcriptional outputs and analyzing their active site interactions proved unsatisfactory as a method to fully explain their selectivity

and potency. Indeed, due to difficulties in crystallizing the GR, little information exists in the literature explaining how the overall protein conformation changes in response to even the most well studied GC agonists and antagonists. To address this fundamental gap in knowledge, a GR dimer consisting of a DBD, HR, and LBD was built and placed on glucocorticoid binding sequences (GBS). Molecular docking of five agonists and two antagonists revealed that agonists produce stabilizing interactions either between the two monomer domains, or between the monomers and the DNA segment. In contrast, antagonists drive the monomers apart allosterically. These results suggest that binding affinity and active site interactions together influence the arrangement of the dimer complex and its subsequent activity.

Together, this work highlights recent advancements in understanding how an intricate system like the GR functions. An interdisciplinary approach utilizing organic chemistry to synthesize new ligands, biological chemistry to observe their activity, and computational chemistry to predict the atomic level interactions that drives their structure-activity relationship is necessary to drive innovation. A better understanding of the allosteric regulation associated with GC binding may help guide future research. The *in silico* addition of the N-terminal domain (NTD) to the GR would provide a more accurate depiction of the complex interprotein interactions that occur upon ligand binding. Furthermore, insights from the enthalpic calculations described in the MD simulations provide a unique platform for the computer-aided drug design of new ligands. Taking risks in collaborative spaces will undoubtedly lead to the eventual development of a GC with high therapeutic efficacy.

REFERENCES

(1) Lim, H.-W.; Uhlenhaut, N. H.; Rauch, A.; Weiner, J.; Hübner, S.; Hübner, N.; Won, K.-J.; Lazar, M. A.; Tuckermann, J.; Steger, D. J. Genomic redistribution of GR monomers and dimers mediates transcriptional response to exogenous glucocorticoid in vivo. *Genome research* **2015**, *25* (6), 836-844.

(2) Espinosa-Cantú, A.; Cruz-Bonilla, E.; Noda-Garcia, L.; DeLuna, A. Multiple forms of multifunctional proteins in health and disease. *Frontiers in Cell and Developmental Biology* **2020**, *8*, 451.

(3) Li, D.; Ji, B. Protein conformational transitions coupling with ligand interactions: Simulations from molecules to medicine. *Medicine in Novel Technology and Devices* **2019**, *3*, 100026.

(4) Timmermans, S.; Souffriau, J.; Libert, C. A general introduction to glucocorticoid biology. *Frontiers in immunology* **2019**, *10*, 1545.

(5) Conn, D. L. The story behind the use of glucocorticoids in the treatment of rheumatoid arthritis. In *Seminars in Arthritis and Rheumatism*, 2021; Elsevier: Vol. 51, pp 15-19.

(6) Ora, J.; Calzetta, L.; Matera, M. G.; Cazzola, M.; Rogliani, P. Advances with glucocorticoids in the treatment of asthma: state of the art. *Expert Opinion on Pharmacotherapy* **2020**, *21* (18), 2305-2316.

(7) Goodin, D. S. Glucocorticoid treatment of multiple sclerosis. *Handbook of clinical neurology* **2014**, *122*, 455-464.

(8) Ronchetti, S.; Ayroldi, E.; Ricci, E.; Gentili, M.; Migliorati, G.; Riccardi, C. A glance at the use of glucocorticoids in rare inflammatory and autoimmune diseases: still an indispensable pharmacological tool? *Frontiers in Immunology* **2021**, *11*, 613435.

(9) Koorneef, L. L.; Kroon, J.; Viho, E. M.; Wahl, L. F.; Heckmans, K. M.; van Dorst, M. M.; Hoekstra, M.; Houtman, R.; Hunt, H.; Meijer, O. C. The selective glucocorticoid receptor antagonist CORT125281 has tissue-specific activity. *Journal of Endocrinology* **2020**, *246* (1), 79-92.

(10) Burke, S. J.; May, A. L.; Noland, R. C.; Lu, D.; Brissova, M.; Powers, A. C.; Sherrill, E. M.; Karlstad, M. D.; Campagna, S. R.; Stephens, J. M.; et al.

Thiobenzothiazole-modified Hydrocortisones Display Anti-inflammatory Activity with Reduced Impact on Islet β-Cell Function. *J Biol Chem* **2015**, *290* (21), 13401-13416. DOI: 10.1074/jbc.M114.632190 From NLM.
(11) Fleseriu, M.; Biller, B. M.; Findling, J. W.; Molitch, M. E.; Schteingart, D. E.; Gross, C.; Investigators, S. S.; include, S. S. I. Mifepristone, a glucocorticoid receptor antagonist, produces clinical and metabolic benefits in patients with Cushing's syndrome. *The Journal of Clinical Endocrinology & Metabolism* **2012**, *97* (6), 2039-2049.
(12) Zhang, T.; Liang, Y.; Zhang, J. Natural and synthetic compounds as dissociated agonists of glucocorticoid receptor. *Pharmacological Research* **2020**, *156*, 104802.
(13) Lesovaya, E. A.; Chudakova, D.; Baida, G.; Zhidkova, E. M.; Kirsanov, K. I.; Yakubovskaya, M. G.; Budunova, I. V. The long winding road to the safer glucocorticoid receptor (GR) targeting therapies. *Oncotarget* **2022**, *13*, 408.
(14) Postel, S.; Wissler, L.; Johansson, C. A.; Gunnarsson, A.; Gordon, E.; Collins, B.; Castaldo, M.; Köhler, C.; Öling, D.; Johansson, P. Quaternary glucocorticoid receptor structure highlights allosteric interdomain communication. *Nature Structural & Molecular Biology* **2023**, *30* (3), 286-295.
(15) De Bosscher, K.; Beck, I. M.; Dejager, L.; Bougarne, N.; Gaigneaux, A.; Chateauvieux, S.; Ratman, D.; Bracke, M.; Tavernier, J.; Vanden Berghe, W. Selective modulation of the glucocorticoid receptor can distinguish between transrepression of NF-κB and AP-1. *Cellular and molecular life sciences* **2014**, *71*, 143-163.
(16) Kennedy, B. J.; Lato, A. M.; Fisch, A. R.; Burke, S. J.; Kirkland, J. K.; Prevatte, C. W.; Dunlap, L. E.; Smith, R. T.; Vogiatzis, K. D.; Collier, J. J. Potent anti-inflammatory, arylpyrazole-based glucocorticoid receptor agonists that do not impair insulin secretion. *ACS Medicinal Chemistry Letters* **2021**, *12* (10), 1568-1577.
(17) Zhang, X.; Lv, H.; Mei, J.; Ji, B.; Huang, S.; Li, X. The Potential Role of R4 Regulators of G Protein Signaling (RGS) Proteins in Type 2 Diabetes Mellitus. *Cells* **2022**, *11* (23), 3897.
(18) Álvarez, L. D.; Presman, D. M.; Pecci, A. Molecular dynamics simulations of the glucocorticoid receptor DNA-binding domain suggest a role of the lever-arm mobility in transcriptional output. *PLoS One* **2017**, *12* (12), e0189588.

(19) Reichardt, H. M.; Tuckermann, J. P.; Göttlicher, M.; Vujic, M.; Weih, F.; Angel, P.; Herrlich, P.; Schütz, G. Repression of inflammatory responses in the absence of DNA binding by the glucocorticoid receptor. *The EMBO journal* **2001**, *20* (24), 7168-7173.
(20) Burke, S. J.; Goff, M. R.; Updegraff, B. L.; Lu, D.; Brown, P. L.; Minkin Jr, S. C.; Biggerstaff, J. P.; Zhao, L.; Karlstad, M. D.; Collier, J. J. Regulation of the CCL2 gene in pancreatic β-cells by IL-1β and glucocorticoids: role of MKP-1. *PLoS One* **2012**, *7*, e46986.
(21) Altonsy, M. O.; Sasse, S. K.; Phang, T. L.; Gerber, A. N. Context-dependent cooperation between nuclear factor κB (NF-κB) and the glucocorticoid receptor at a TNFAIP3 intronic enhancer: a mechanism to maintain negative feedback control of inflammation. *Journal of Biological Chemistry* **2014**, *289* (12), 8231-8239.
(22) Suino-Powell, K.; Xu, Y.; Zhang, C.; Tao, Y.-g.; Tolbert, W. D.; SimonsJr, S. S.; Xu, H. E. Doubling the size of the glucocorticoid receptor ligand binding pocket by deacylcortivazol. *Molecular and Cellular Biology* **2008**.
(23) He, Y.; Shi, J.; Yi, W.; Ren, X.; Gao, X.; Li, J.; Wu, N.; Weaver, K.; Xie, Q.; Khoo, S. K. Discovery of a highly potent glucocorticoid for asthma treatment. *Cell discovery* **2015**, *1* (1), 1-13.
(24) Autry, B. M.; Wadhwa, R. Mifepristone. In *StatPearls [Internet]*, StatPearls Publishing, 2024.
(25) Rodriguez, A. C. I.; Epel, E. S.; White, M. L.; Standen, E. C.; Seckl, J. R.; Tomiyama, A. J. Hypothalamic-pituitary-adrenal axis dysregulation and cortisol activity in obesity: a systematic review. *Psychoneuroendocrinology* **2015**, *62*, 301-318.
(26) Hwang, J. L.; Weiss, R. E. Steroid-induced diabetes: a clinical and molecular approach to understanding and treatment. *Diabetes/Metabolism Research and Reviews* **2014**, *30* (2), 96-102, https://doi.org/10.1002/dmrr.2486. DOI: https://doi.org/10.1002/dmrr.2486 (acccessed 2022/05/16).
(27) Van Staa T.P., L. H. G., Abenhaim L., et al. . Use of Oral Corticosteroids in the United Kingdom. *QJM : monthly journal of the Association of Physicians* **2000**, *93*, 105-111.

(28) Ramamoorthy, S.; Cidlowski, J. A. Corticosteroids: mechanisms of action in health and disease. *Rheumatic Disease Clinics* **2016**, *42* (1), 15-31.
(29) Schäcke, H.; Döcke, W.-D.; Asadullah, K. Mechanisms involved in the side effects of glucocorticoids. *Pharmacology & therapeutics* **2002**, *96* (1), 23-43.
(30) Overman, R. A.; Yeh, J. Y.; Deal, C. L. Prevalence of oral glucocorticoid usage in the United States: a general population perspective. *Arthritis care & research* **2013**, *65* (2), 294-298.
(31) Onwubalili, J.; Obineche, E. High incidence of post-transplant diabetes mellitus in a single-centre study. *Nephrology Dialysis Transplantation* **1992**, *7* (4), 346-349.
(32) Kuo, T.; McQueen, A.; Chen, T.-C.; Wang, J.-C. Regulation of glucose homeostasis by glucocorticoids. *Glucocorticoid signaling* **2015**, *872*, 99-126.
(33) Steiner, R. W.; Awdishu, L. Steroids in kidney transplant patients. In *Seminars in Immunopathology*, 2011; Springer: Vol. 33, pp 157-167.
(34) Holden, N. S.; Bell, M. J.; Rider, C. F.; King, E. M.; Gaunt, D. D.; Leigh, R.; Johnson, M.; Siderovski, D. P.; Heximer, S. P.; Giembycz, M. A. β2-Adrenoceptor agonist-induced RGS2 expression is a genomic mechanism of bronchoprotection that is enhanced by glucocorticoids. *Proceedings of the National Academy of Sciences* **2011**, *108* (49), 19713-19718.
(35) Flamini, S.; Sergeev, P.; Viana de Barros, Z.; Mello, T.; Biagioli, M.; Paglialunga, M.; Fiorucci, C.; Prikazchikova, T.; Pagano, S.; Gagliardi, A. Glucocorticoid-induced leucine zipper regulates liver fibrosis by suppressing CCL2-mediated leukocyte recruitment. *Cell Death & Disease* **2021**, *12* (5), 421.
(36) Burke, S. J.; May, A. L.; Noland, R. C.; Lu, D.; Brissova, M.; Powers, A. C.; Sherrill, E. M.; Karlstad, M. D.; Campagna, S. R.; Stephens, J. M.; et al. Thiobenzothiazole-modified Hydrocortisones Display Anti-inflammatory Activity with Reduced Impact on Islet beta-Cell Function. *J Biol Chem* **2015**, *290* (21), 13401-13416. DOI: 10.1074/jbc.M114.632190.
(37) Biju, P.; McCormick, K.; Aslanian, R.; Berlin, M.; Solomon, D.; Chapman, R.; McLeod, R.; Prelusky, D.; Eckel, S.; Kelly, G. Steroidal C-21 mercapto derivatives as

dissociated steroids: discovery of an inhaled dissociated steroid. *Bioorganic & medicinal chemistry letters* **2011**, *21* (21), 6343-6347.
(38) Wuest, F.; Carlson, K. E.; Katzenellenbogen, J. A. Expeditious synthesis of steroids containing a 2-methylsulfanyl-acetyl side chain as potential glucocorticoid receptor imaging agents. *Steroids* **2008**, *73* (1), 69-76.
(39) Hohmeier, H. E.; Mulder, H.; Chen, G.; Henkel-Rieger, R.; Prentki, M.; Newgard, C. B. Isolation of INS-1-derived cell lines with robust ATP-sensitive K+ channel-dependent and-independent glucose-stimulated insulin secretion. *Diabetes* **2000**, *49* (3), 424-430.
(40) Smoak, P.; Burke, S. J.; Martin, T. M.; Batdorf, H. M.; Floyd, Z. E.; Collier, J. J. Artemisia dracunculus L. Ethanolic Extract and an Isolated Component, DMC2, Ameliorate Inflammatory Signaling in Pancreatic β-Cells via Inhibition of p38 MAPK. *Biomolecules* **2022**, *12* (5), 708.
(41) Burke, S. J.; Karlstad, M. D.; Regal, K. M.; Sparer, T. E.; Lu, D.; Elks, C. M.; Grant, R. W.; Stephens, J. M.; Burk, D. H.; Collier, J. J. CCL20 is elevated during obesity and differentially regulated by NF-κB subunits in pancreatic β-cells. *Biochimica et Biophysica Acta (BBA)-Gene Regulatory Mechanisms* **2015**, *1849* (6), 637-652.
(42) Collier, J. J.; Batdorf, H. M.; Merrifield, K. L.; Martin, T. M.; White, U.; Ravussin, E.; Burk, D. H.; Cooley, C. R.; Karlstad, M. D.; Burke, S. J. Pioglitazone reverses markers of islet beta-cell de-differentiation in db/db mice while modulating expression of genes controlling inflammation and browning in white adipose tissue from insulin-resistant mice and humans. *Biomedicines* **2021**, *9* (9), 1189.
(43) Schrödinger, L. The PyMOL Molecular Graphics System, Version 2.0 Schrödinger, LLC (2017). *Google Scholar There is no corresponding record for this reference*.
(44) Trott, O.; Olson, A. J. AutoDock Vina: improving the speed and accuracy of docking with a new scoring function, efficient optimization, and multithreading. *Journal of computational chemistry* **2010**, *31* (2), 455-461.
(45) Laskowski, R. A.; Swindells, M. B. LigPlot+: multiple ligand–protein interaction diagrams for drug discovery. ACS Publications: 2011.

(46) Abraham, M. J.; Murtola, T.; Schulz, R.; Páll, S.; Smith, J. C.; Hess, B.; Lindahl, E. GROMACS: High performance molecular simulations through multi-level parallelism from laptops to supercomputers. *SoftwareX* **2015**, *1*, 19-25.
(47) Yu, Y.; Kramer, A.; Venable, R. M.; Simmonett, A. C.; MacKerell Jr, A. D.; Klauda, J. B.; Pastor, R. W.; Brooks, B. R. Semi-automated optimization of the CHARMM36 lipid force field to include explicit treatment of long-range dispersion. *Journal of Chemical Theory and Computation* **2021**, *17* (3), 1562-1580.
(48) Jorgensen, W. L.; Chandrasekhar, J.; Madura, J. D.; Impey, R. W.; Klein, M. L. Comparison of simple potential functions for simulating liquid water. *The Journal of chemical physics* **1983**, *79* (2), 926-935.
(49) M., M. A. A. A. C. B. C. B. E. B. M. D. S. F. V. G. G. G. S. G. G. G. A. G. GROMACS 2023.2 Manual. **2023**. DOI: https://doi.org/10.5281/zenodo.8134388.
(50) Humphrey, W.; Dalke, A.; Schulten, K. VMD: visual molecular dynamics. *Journal of molecular graphics* **1996**, *14* (1), 33-38.
(51) Biggadike, K.; Bledsoe, R. K.; Hassell, A. M.; Kirk, B. E.; McLay, I. M.; Shewchuk, L. M.; Stewart, E. L. X-ray crystal structure of the novel enhanced-affinity glucocorticoid agonist fluticasone furoate in the glucocorticoid receptor− ligand binding domain. *Journal of medicinal chemistry* **2008**, *51* (12), 3349-3352.
(52) Tian, W.; Chen, C.; Lei, X.; Zhao, J.; Liang, J. CASTp 3.0: computed atlas of surface topography of proteins. *Nucleic acids research* **2018**, *46* (W1), W363-W367.
(53) Roma, L. P.; Oliveira, C. A.; Carneiro, E. M.; Albuquerque, G. G.; Boschero, A. C.; Souza, K. L. N-acetylcysteine protects pancreatic islet against glucocorticoid toxicity. *Redox Report* **2011**, *16* (4), 173-180.
(54) Ullrich, S.; Berchtold, S.; Ranta, F.; Seebohm, G.; Henke, G.; Lupescu, A.; Mack, A. F.; Chao, C.-M.; Su, J.; Nitschke, R. Serum-and glucocorticoid-inducible kinase 1 (SGK1) mediates glucocorticoid-induced inhibition of insulin secretion. *Diabetes* **2005**, *54* (4), 1090-1099.
(55) Mishra, V.; Yadav, N.; Saraogi, G. K.; Tambuwala, M. M.; Giri, N. Dendrimer based nanoarchitectures in diabetes management: An overview. *Current Pharmaceutical Design* **2019**, *25* (23), 2569-2583.

(56) Cardozo, A. K.; Proost, P.; Gysemans, C.; Chen, M.-C.; Mathieu, C.; Eizirik, D. L. IL-1β and IFN-γ induce the expression of diverse chemokines and IL-15 in human and rat pancreatic islet cells, and in islets from pre-diabetic NOD mice. *Diabetologia* **2003**, *46* (2), 255-266.
(57) Stojceski, F.; Buetti-Dinh, A.; Stoddart, M. J.; Danani, A.; Della Bella, E.; Grasso, G. Influence of dexamethasone on the interaction between glucocorticoid receptor and SOX9: A molecular dynamics study. *Journal of Molecular Graphics and Modelling* **2023**, *125*, 108587.
(58) Bridgham, J. T.; Ortlund, E. A.; Thornton, J. W. An epistatic ratchet constrains the direction of glucocorticoid receptor evolution. *Nature* **2009**, *461* (7263), 515-519.
(59) Veleiro, A. S.; Alvarez, L. D.; Eduardo, S. L.; Burton, G. Structure of the glucocorticoid receptor, a flexible protein that can adapt to different ligands. *ChemMedChem* **2010**, *5* (5), 649-659.
(60) Frank, F.; Ortlund, E. A.; Liu, X. Structural insights into glucocorticoid receptor function. *Biochemical Society Transactions* **2021**, *49* (5), 2333-2343.
(61) Liu, X.; Wang, Y.; Gutierrez, J. S.; Damsker, J. M.; Nagaraju, K.; Hoffman, E. P.; Ortlund, E. A. Disruption of a key ligand-H-bond network drives dissociative properties in vamorolone for Duchenne muscular dystrophy treatment. *Proceedings of the National Academy of Sciences* **2020**, *117* (39), 24285-24293.
(62) Vandevyver, S.; Dejager, L.; Tuckermann, J.; Libert, C. New insights into the anti-inflammatory mechanisms of glucocorticoids: an emerging role for glucocorticoid-receptor-mediated transactivation. *Endocrinology* **2013**, *154* (3), 993-1007.
(63) Biddie, S. C.; Conway-Campbell, B. L.; Lightman, S. L. Dynamic regulation of glucocorticoid signalling in health and disease. *Rheumatology* **2012**, *51* (3), 403-412.
(64) Kuo, T.; McQueen, A.; Chen, T.-C.; Wang, J.-C. Regulation of glucose homeostasis by glucocorticoids. *Glucocorticoid Signaling: From Molecules to Mice to Man* **2015**, 99-126.
(65) Burke, S. J.; Goff, M. R.; Updegraff, B. L.; Lu, D.; Brown, P. L.; Minkin Jr, S. C.; Biggerstaff, J. P.; Zhao, L.; Karlstad, M. D.; Collier, J. J. Regulation of the CCL2 gene in pancreatic β-cells by IL-1β and glucocorticoids: role of MKP-1. **2012**.

(66) Lato, A. M. Aryl Pyrazole Glucocorticoid Receptor Agonists: Probing Structure Activity Relationships in the Expanded Ligand Binding Pocket. **2022**.
(67) Burke, S. J.; May, A. L.; Noland, R. C.; Lu, D.; Brissova, M.; Powers, A. C.; Sherrill, E. M.; Karlstad, M. D.; Campagna, S. R.; Stephens, J. M. Thiobenzothiazole-modified hydrocortisones display anti-inflammatory activity with reduced impact on islet β-cell function. *Journal of Biological Chemistry* **2015**, *290* (21), 13401-13416.
(68) Van Moortel, L.; Gevaert, K.; De Bosscher, K. Improved glucocorticoid receptor ligands: fantastic beasts, but how to find them? *Frontiers in Endocrinology* **2020**, *11*, 559673.
(69) Quax, R.; Peeters, R.; Feelders, R. Selective glucocorticoid receptor modulators: future of glucocorticoid immunosuppressive therapy? Oxford University Press: 2011.
(70) Humphrey, E.; Williams, J. H.; Davie, M. W.; Marshall, M. J. Effects of dissociated glucocorticoids on OPG and RANKL in osteoblastic cells. *Bone* **2006**, *38* (5), 652-661.
(71) Seaton, W. B.; Burke, S. J.; Fisch, A. R.; Schilletter, W. A.; Beck, M. G. A.; Cassagne, G. A.; Harvey, I.; Fontenot, M. S.; Collier, J. J.; Campagna, S. R. Channel Expansion in the Ligand-Binding Domain of the Glucocorticoid Receptor Contributes to the Activity of Highly Potent Glucocorticoid Analogues. *Molecules* **2024**, *29* (7), 1546.
(72) Zimmerman, J. A.; Fang, M.; Doumbia, B.; Neyman, A.; Cha, J. H.; Thomas, M.; Hall, B.; Wu, M.; Wilson, A. M.; Pufall, M. A. Deacylcortivazol-like pyrazole regioisomers reveal a more accommodating expanded binding pocket for the glucocorticoid receptor. *RSC Medicinal Chemistry* **2021**, *12* (2), 203-212.
(73) Biju, P.; Wang, H.; Anthes, J.; McCormick, K.; Aslanian, R.; Berlin, M.; Bitar, R.; Lim, Y.-H.; Lee, Y. J.; Prelusky, D. Steroidal C-21 heteroaryl thioethers. Part 3: pregn-4-eno-[3, 2-c] pyrazole fused A ring modified steroids as selective glucocorticoid receptor modulators (dissociated steroids). *Bioorganic & medicinal chemistry letters* **2012**, *22* (9), 3291-3295.
(74) Wüst, F.; Carlson, K. E.; Katzenellenbogen, J. A. Synthesis of novel arylpyrazolo corticosteroids as potential ligands for imaging brain glucocorticoid receptors. *Steroids* **2003**, *68* (2), 177-191.

(75) Valdés-Tresanco, M. S.; Valdés-Tresanco, M. E.; Valiente, P. A.; Moreno, E. gmx_MMPBSA: a new tool to perform end-state free energy calculations with GROMACS. *Journal of chemical theory and computation* **2021**, *17* (10), 6281-6291.
(76) Wang, E.; Sun, H.; Wang, J.; Wang, Z.; Liu, H.; Zhang, J. Z.; Hou, T. End-point binding free energy calculation with MM/PBSA and MM/GBSA: strategies and applications in drug design. *Chemical reviews* **2019**, *119* (16), 9478-9508.
(77) Scherholz, M. L.; Schlesinger, N.; Androulakis, I. P. Chronopharmacology of glucocorticoids. *Advanced drug delivery reviews* **2019**, *151*, 245-261.
(78) Kliewer, S. A.; Moore, J. T.; Wade, L.; Staudinger, J. L.; Watson, M. A.; Jones, S. A.; McKee, D. D.; Oliver, B. B.; Willson, T. M.; Zetterström, R. H. An orphan nuclear receptor activated by pregnanes defines a novel steroid signaling pathway. *Cell* **1998**, *92* (1), 73-82.
(79) Zhai, Y.; Pai, H. V.; Zhou, J.; Amico, J. A.; Vollmer, R. R.; Xie, W. Activation of pregnane X receptor disrupts glucocorticoid and mineralocorticoid homeostasis. *Molecular endocrinology* **2007**, *21* (1), 138-147.
(80) Mao, L.; Wei, W.; Chen, J. Biased regulation of glucocorticoid receptors signaling. *Biomedicine & Pharmacotherapy* **2023**, *165*, 115145.
(81) Reeves, E. K.; Hoffman, E. P.; Nagaraju, K.; Damsker, J. M.; McCall, J. M. VBP15: preclinical characterization of a novel anti-inflammatory delta 9, 11 steroid. *Bioorganic & medicinal chemistry* **2013**, *21* (8), 2241-2249.
(82) Dashti-Khavidaki, S.; Saidi, R.; Lu, H. Current status of glucocorticoid usage in solid organ transplantation. *World journal of transplantation* **2021**, *11* (11), 443.
(83) Oasa, S.; Mikuni, S.; Yamamoto, J.; Kurosaki, T.; Yamashita, D.; Kinjo, M. Relationship between homodimeric glucocorticoid receptor and transcriptional regulation assessed via an in vitro fluorescence correlation spectroscopy-microwell system. *Scientific Reports* **2018**, *8* (1), 7488.
(84) Weikum, E. R.; Knuesel, M. T.; Ortlund, E. A.; Yamamoto, K. R. Glucocorticoid receptor control of transcription: precision and plasticity via allostery. *Nature reviews Molecular cell biology* **2017**, *18* (3), 159-174.

(85) Timmermans, S.; Vandewalle, J.; Libert, C. Dimerization of the glucocorticoid receptor and its importance in (patho) physiology: a primer. *Cells* **2022**, *11* (4), 683.
(86) Alves, N. R. C.; Pecci, A.; Alvarez, L. D. Structural Insights into the Ligand Binding Domain of the Glucocorticoid Receptor: A Molecular Dynamics Study. *Journal of Chemical Information and Modeling* **2020**, *60* (2), 794-804. DOI: 10.1021/acs.jcim.9b00776.
(87) Jumper, J.; Evans, R.; Pritzel, A.; Green, T.; Figurnov, M.; Ronneberger, O.; Tunyasuvunakool, K.; Bates, R.; Žídek, A.; Potapenko, A. Highly accurate protein structure prediction with AlphaFold. *Nature* **2021**, *596* (7873), 583-589.
(88) Meijsing, S. H.; Pufall, M. A.; So, A. Y.; Bates, D. L.; Chen, L.; Yamamoto, K. R. DNA binding site sequence directs glucocorticoid receptor structure and activity. *Science* **2009**, *324* (5925), 407-410.
(89) Schrödinger, L. *The PyMOL Molecular Graphics System, Version 2.0*. 2017. (accessed.
(90) Jo, S.; Kim, T.; Iyer, V. G.; Im, W. CHARMM-GUI: a web-based graphical user interface for CHARMM. *Journal of computational chemistry* **2008**, *29* (11), 1859-1865.
(91) Lee, J.; Cheng, X.; Jo, S.; MacKerell, A. D.; Klauda, J. B.; Im, W. CHARMM-GUI input generator for NAMD, GROMACS, AMBER, OpenMM, and CHARMM/OpenMM simulations using the CHARMM36 additive force field. *Biophysical journal* **2016**, *110* (3), 641a.
(92) Vanommeslaeghe, K.; Hatcher, E.; Acharya, C.; Kundu, S.; Zhong, S.; Shim, J.; Darian, E.; Guvench, O.; Lopes, P.; Vorobyov, I. CHARMM general force field: A force field for drug-like molecules compatible with the CHARMM all-atom additive biological force fields. *Journal of computational chemistry* **2010**, *31* (4), 671-690.
(93) Huang, J.; Rauscher, S.; Nawrocki, G.; Ran, T.; Feig, M.; De Groot, B. L.; Grubmüller, H.; MacKerell Jr, A. D. CHARMM36m: an improved force field for folded and intrinsically disordered proteins. *Nature methods* **2017**, *14* (1), 71-73.
(94) Boonstra, S.; Onck, P. R.; van der Giessen, E. CHARMM TIP3P water model suppresses peptide folding by solvating the unfolded state. *The journal of physical chemistry B* **2016**, *120* (15), 3692-3698.

(95) Deploey, N.; Van Moortel, L.; Rogatsky, I.; Peelman, F.; De Bosscher, K. The biologist's guide to the glucocorticoid receptor's structure. *Cells* **2023**, *12* (12), 1636.
(96) Schoch, G. A.; D'Arcy, B.; Stihle, M.; Burger, D.; Bär, D.; Benz, J.; Thoma, R.; Ruf, A. Molecular switch in the glucocorticoid receptor: active and passive antagonist conformations. *Journal of molecular biology* **2010**, *395* (3), 568-577.
(97) Hu, X.; Pang, J.; Zhang, J.; Shen, C.; Chai, X.; Wang, E.; Chen, H.; Wang, X.; Duan, M.; Fu, W. Discovery of novel GR ligands toward druggable GR antagonist conformations identified by MD simulations and Markov state model analysis. *Advanced Science* **2022**, *9* (3), 2102435.
(98) Johanssen, S.; Allolio, B. Mifepristone (RU 486) in Cushing's syndrome. *European Journal of Endocrinology* **2007**, *157* (5), 561-569.
(99) Nicolaides, N. C.; Pavlaki, A. N.; Alexandra, M.; Chrousos, G. P. Glucocorticoid therapy and adrenal suppression. **2015**.
(100) Namkung-Matthai, H.; Seale, J.; Brown, K.; Mason, R. Comparative effects of anti-inflammatory corticosteroids in human bone-derived osteoblast-like cells. *European Respiratory Journal* **1998**, *12* (6), 1327-1333.
(101) Heikinheimo, O.; Kekkonen, R.; Lähteenmäki, P. The pharmacokinetics of mifepristone in humans reveal insights into differential mechanisms of antiprogestin action. *Contraception* **2003**, *68* (6), 421-426.
(102) Kroon, J.; Koorneef, L. L.; van den Heuvel, J. K.; Verzijl, C. R.; van de Velde, N. M.; Mol, I. M.; Sips, H. C.; Hunt, H.; Rensen, P. C.; Meijer, O. C. Selective glucocorticoid receptor antagonist CORT125281 activates brown adipose tissue and alters lipid distribution in male mice. *Endocrinology* **2018**, *159* (1), 535-546.
(103) Lato, A. M.; Burke, S. J.; Ducote, M. P.; Kennedy, B. J.; Collier, J. J.; Campagna, S. R. Stereoisomers of an Aryl Pyrazole Glucocorticoid Receptor Agonist Scaffold Elicit Differing Anti-inflammatory Responses. *ACS Medicinal Chemistry Letters* **2022**, *13* (9), 1493-1499.
(104) Suino-Powell, K.; Xu, Y.; Zhang, C.; Tao, Y.-g.; Tolbert, W. D.; Simons Jr, S. S.; Xu, H. E. Doubling the size of the glucocorticoid receptor ligand binding pocket by deacylcortivazol. *Molecular and cellular biology* **2008**.

(105) Hudson, W. H.; Kossmann, B. R.; de Vera, I. M. S.; Chuo, S.-W.; Weikum, E. R.; Eick, G. N.; Thornton, J. W.; Ivanov, I. N.; Kojetin, D. J.; Ortlund, E. A. Distal substitutions drive divergent DNA specificity among paralogous transcription factors through subdivision of conformational space. *Proceedings of the National Academy of Sciences* **2016**, *113* (2), 326-331.
(106) Gensler, L. S. Glucocorticoids: complications to anticipate and prevent. *The Neurohospitalist* **2013**, *3* (2), 92-97.

VITA

Wesley Benjamin Seaton was born on June 4th, 1994, in Knoxville, TN and grew up in Las Cruces, NM. While completing his undergraduate degree in Biology at the University of New Mexico, he qualified to travel with a small group of students and his organic chemistry instructor to Germany to take a medicinal chemistry class and visit multiple pharmaceutical companies, including Merck. This experience, combined with two years of teaching high school physical science and biology in Memphis, deepened his appreciation for both organic chemistry and teaching, prompting him to pursue a PhD at the University of Tennessee. Wesley joined Dr. Shawn Campagna's research group at UT in 2019 where he studied synthetic organic chemistry, focusing on the synthesis of novel glucocorticoid analogues with reduced impact on insulin secretion.